102

-TR-83-006

CROPHY ..CS OF SNOW CRYSTAL
ROWFLAK MELTING

Mike Fukuta
Savage
Donovan
L. Liu

ADA129030

Dec 1982

Approved for public release; distribution unlimited

AIR FORCE GEOPHYSICS LABORATORY
AIR FORCE SYSTEMS COMMAND
UNITED STATES AIR FORCE
HANSCOM AFB, MASSACHUSETTS 01731

Unclassified

SECURITY CLASSIFICATION OF THIS PAGE (When Data Entered)

REPORT DOCUMENTATION PAGE		READ INSTRUCTIONS BEFORE COMPLETING FORM
1. REPORT NUMBER AFGL-TR-83-0066	2. GOVT ACCESSION NO. AD-A129030	3. RECIPIENT'S CATALOG NUMBER
4. TITLE (and Subtitle) THE MICROPHYSICS OF SNOW CRYSTAL AND SNOWFLAKE MELTING		5. TYPE OF REPORT & PERIOD COVERED Final Report 1 Sept 1980 - 31 Dec 1982
		6. PERFORMING ORG. REPORT NUMBER
7. AUTHOR(s) Norihiko Fukuta, R. C. Savage, G. J. Donovan and C.-M. Liu		8. CONTRACT OR GRANT NUMBER(s) F19628 ~~F19268~~-81-K-0021
9. PERFORMING ORGANIZATION NAME AND ADDRESS University of Utah Salt Lake City, Utah 84112		10. PROGRAM ELEMENT, PROJECT, TASK AREA & WORK UNIT NUMBERS 61102F 2310G5BA
11. CONTROLLING OFFICE NAME AND ADDRESS Air Force Geophysics Laboratory Hanscom AFB, Massachusetts 01731 Monitor/ Capt Ian D. Cohen/LYC		12. REPORT DATE December 1982
		13. NUMBER OF PAGES 109
14. MONITORING AGENCY NAME & ADDRESS(if different from Controlling Office)		15. SECURITY CLASS. (of this report) Unclassified
		15a. DECLASSIFICATION/DOWNGRADING SCHEDULE

16. DISTRIBUTION STATEMENT (of this Report)

Approved for public release; distribution unlimited

17. DISTRIBUTION ST[ATEM]ENT (of [the] abstract entered in Block 20, if different from Report)

18. SUPPLEMENTARY [NO]TES

19. KEY WORDS (Continue on reverse side if necessary and identify by block number)

Melting	Radar reflectivity
Ice crystal	Wind tunnel
Snow flake	Fall velocity
Bright band	Melting layer
Cloud physics	

20. ABSTRACT (Continue on reverse side if necessary and identify by block number)

A new portable, vertically-diverging wind tunnel was developed for studying melting of natural snowflakes and snow crystals during their free fall under controlled condition of the air stream. Using the tunnel, their size and fall velocity were measured and the regression equations were obtained. Their observed melting time depended only weakly with the size suggesting the possibility of internal melting due to air flow through their structure. Rotating and orbiting motions were commonly detected with snow crystals. Disruption was found

DD FORM 1 JAN 73 1473

Unclassified

SECURITY CLASSIFICATION OF THIS PAGE (When Data Entered)

frequently towards the end of melting of both snowflakes and ice crystals and resulted in instability in their suspension. A theoretical development was carried out for melting snowflakes and ice crystals considering their non-spherical shape. A new simple model of snowflake melting had been developed and was applied to a representative atmospheric condition. Comparison of the model with observed behaviors of radar bright bands suggested that the shape and its development as well as size during aggregation play important roles in the bright band mechanism. The model predicts that the higher the snowfall rate, the larger the reflectivity increase and the lower the altitude of the bright band center.

Accession For	
NTIS GRA&I	☑
DTIC TAB	☐
Unannounced	☐
Justification PER CALL JC	
By	
Distribution/	
Availability Codes	
Dist	Avail and/or Special
A	

TABLE OF CONTENTS

TABLE OF FIGURE CAPTIONS

Figure Number	Caption	Page

1. Introduction

When ice crystals fall through the 0°C isotherm in the atmosphere, they begin to melt. In this ice melting zone, it is known that radar echoes show the so-called "bright band" (Ryde, 1946). The bright band is believed to be due to microwave back scattering from melting ice crystals that are undergoing simultaneous microphysical changes and interactions.

The bright bands are generally observed from about 100 to 400 m below the 0°C isotherm (Austin and Bemis, 1950; Hooper and Kippax, 1950), with the ratio of the radar reflectivity in the center of the bright band to that at the 0°C isotherm being normally between 15 and 30. The ratio ranges as high as 100 and as low as 2 or 3. The ratio of the radar reflectivity in the brightest position of the band to that in the rain just below varies normally in the range from 4 to 9.

The main microphysical factors that are thought to affect the characteristics of the bright bands are (i) high radar reflectivity of water and its coating effect on ice, (ii) fall velocity variation, normally the increase, (iii) variation of aggregation process including possible disintegration and (iv) particle shape change particularly under partially melting condition (Battan, 1973).

The laboratory studies of ice melting in the past were mostly with spherical ice particles (Mason, 1956; Macklin, 1963; Drake and Mason, 1966; Bailey and Macklin, 1968) although different levels of ice density were sometimes chosen (Mason, 1956) and snow pellets were recently used (Matsuo and Sasyo; 1982). Matsuo and Sasyo (1981a) also reported melting of snowflakes that were supported on nylon nets and it is the only work of the kind known to date. The basic microphysical informations of ice crystal and snowflake melting are essential for

clarification of the bright band formation mechanism but they are presently far from sufficient for the purpose.

In our laboratory, an effort has recently been made to determine some of the needed microphysical data under simulated atmospheric conditions by developing and utilizing a new vertical wind tunnel. Applying the obtained data in the tunnel both to the existing and newly developed theories of ice crystal and snowflake melting under possible atmospheric conditions, the bright band formation mechanism was reexamined. We shall report results of the study below.

2. Experimental Method

In planning the measurement of ice crystal and snowflake melting, the degree of simulation to the natural melting layer was considered. Natural snow crystals and snowflakes melt while they are falling and due to melting the fall velocity changes. The velocity change in turn affects the melting rate. As discussed in the introduction, the fall behavior of melting hydrometeors is already known to be one of the main factors that influence the bright band characteristics. For this reason the vertical wind tunnel method was selected for measurements.

2.1 Vertical wind tunnel and the supporting devices

Vertical wind tunnels were originally developed to test aircraft spin characteristics using models. They are featured with (i) a saucer-shaped velocity profile with low turbulence in the test section which is about 5 - 10% lower at the centerline than at the side to keep the model near the center of the tunnel, and (ii) a fast response drive system to rapidly adjust the air velocity. Researchers have used various modifications of the vertical wind tunnel in cloud-

physical studies, drop suspension in particular (Kinzer and Gunn, 1951; Telford et al., 1955; Kinzer and Cobb, 1956 and 1958; Cotton and Gokhale, 1967; Iribarne and Klemes, 1970). Hoffer and Mallen (1968) developed a tunnel which was capable of suspending droplets smaller than 500 μm in diameter by incorporating a velocity profile creator and a diffuser. The most widely used vertical wind tunnel to date is that in the University of California at Los Angeles (UCLA) (Pruppacher and Neiburger, 1968; Beard and Pruppacher, 1969; Pruppacher and Beard, 1975; Pruppacher and Rasmussen, 1979). Ice particles were also studied in the wind tunnel with (List, 1959) or without (Pitter and Pruppacher, 1973; Pflaum and Pruppacher, 1979) support. Freely suspended, however, were only dense ice particles like frozen drops and graupel.

Suspension of snow crystals in the tunnel presents additional problems due to their non-spherical shapes. Indeed, Pruppacher and Neiburger (1968) felt that aerodynamic characteristics of a melting snow crystal or a snowflake may make it impracticable to freely suspend them. Fukuta et al. (1979) were among the first to freely suspend ice crystals, though small. The group later developed an upward converging tunnel to suspend larger crystals for longer periods of time (Kowa, 1981; Fukuta et al., 1982).

The design of the tunnel was decided considering (i) the available and proven technique of the vertical wind tunnel, (ii) the snow crystal fall velocity and the range, (iii) operator reaction for air speed adjustment, (iv) the mechanism to introduce the crystals into the tunnel and its feasibility in the selected design, and (v) data collection under outdoor operation. The vertical wind tunnel section consists of the vertical tunnel, the settling chamber, the honeycomb, screens, and the air exit box with snow introducing device. (See Fig. 1)

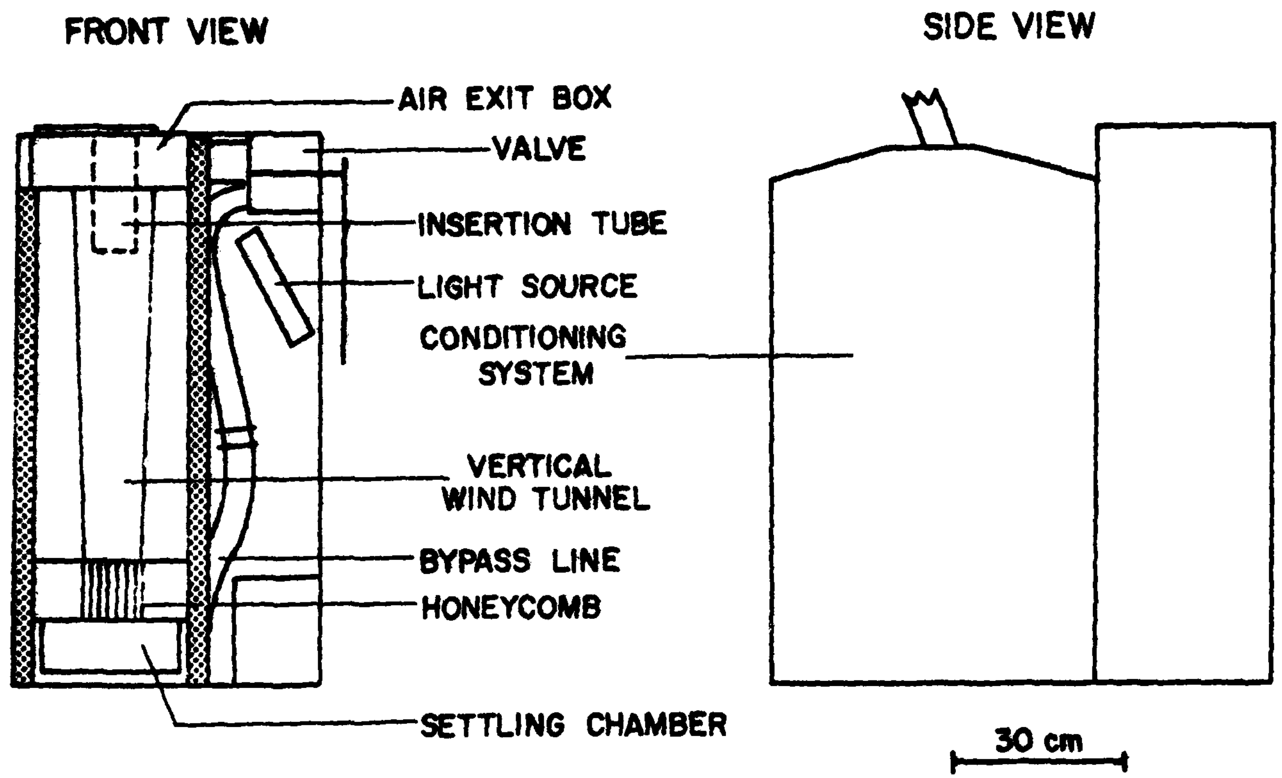

Fig. 1. Major sections of the experimental apparatus.

Vertical Wind Tunnel

A vertical wind tunnel employing an upward diverging design was built and tested independently for optimization using suspension of model snow crystals as the tunnel performance indicator. The model snow crystals were formed by placing a sheet of heavy duty aluminum foil over a piece of chamois and punching out disks. the result is a 5 mm diameter aluminum disk, curved upward slightly at the edge and weighing about 2 mg.

The diverging design would hold a velocity profile, increasing towards the bottom, and would allow the snowflake to automatically find a balancing position in the tunnel. Then, as it melted, and its fall velocity increased due to its smaller profile, it would slowly settle toward the bottom of the chamber. Depending on its size, an adjustment in the chamber airflow may not be necessary. Required adjustment, if any, would be small. In this way, the design of the tunnel would simplify the process of adjusting the airflow to hold the snowflake motionless. After testing different shapes including square cross section, it was found that a vertical wind tunnel with a round cross section and dimensions 60 cm high, 9.5 cm in diameter at the bottom and 13.6 cm at the top, giving a taper of less than 3 degrees in semi-vertical angle, was satisfactory for our purpose. The chamber was constructed by rolling a 24 mil cellulose acetate sheet and embedding at both ends in 6.5 mm thick acrylic plates. In between the top and bottom plates were two 3.2 mm thick acrylic rings which provided support approximately 10 cm from each end (see Fig. 2).

Settling Chamber

A settling chamber acts to constrict the flow through the tunnel, while

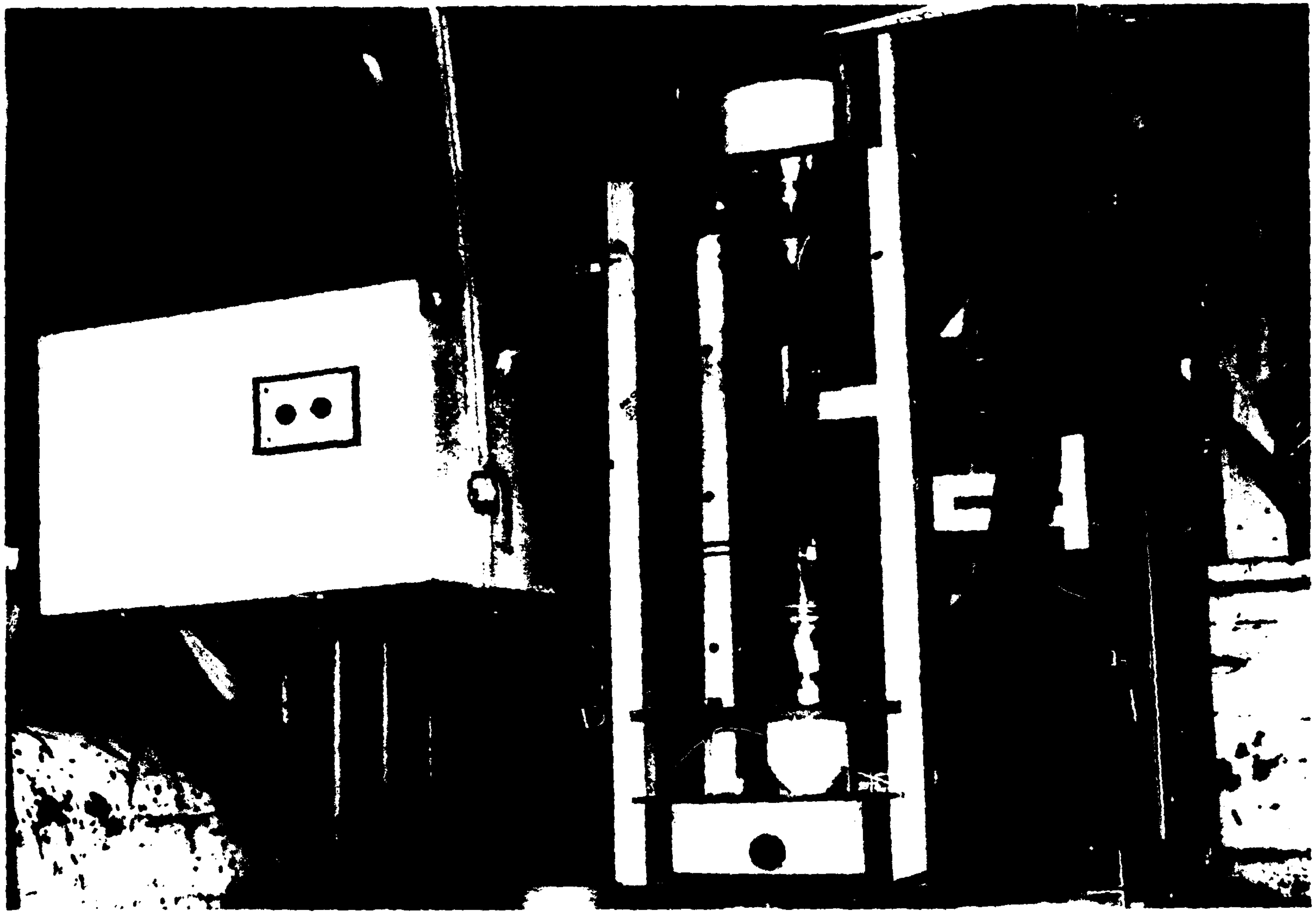

Fig. 2. Vertical wind tunnel and supporting equipments.

damping out some large scale turbulence. The settling chamber actually used measures 22 x 30.5 cm^2 and is 8 cm deep, and is made of 21 gauge galvanized sheet metal. However, it was found that disturbance in the settling chamber would not affect the tunnel performance due to excellent flow control by the honeycomb we adopted.

Honeycomb

After testing different honeycombs including Hexcel (Hexcel Corp., Dublin, Ca.), properly packed plastic straws of suitable diameter were found to be convenient, inexpensive, available and effective. It is said that in order to obtain a laminar flow, the length to diameter ratio of 10 is sufficient. Two new methods were developed with respect to the honeycomb application in the tunnel. The first is the scheme to produce the desired air velocity profile. The scheme of using straws of different diameters reported by Hoffer and Mallen (1967) was found to give too rapid velocity variation in the lateral direction. Against this problem, we developed a scheme of varying the length of straws. Since straws give resistance to the air flow, the longer the starws, the slower the air velocity after passing through them. To obtain the air velocity profile gently concave upward, the length of the straws has to be larger at the center (see Fig. 3). The second is the method to cut straws easily and after cutting to keep them together. An electrically heated wire mounted on a piece of plywood was pushed through the straws, melting them flush with the top of the honeycomb section and sealing them together. This allowed for easy removal of the honeycomb. The honeycomb used for measurement is 9.5 cm in diameter, made of 3.2 mm diameter plastic straws, arranged in 12 levels, with the straws verying in length from 6 to 9.4 cm. The straws were arranged in place in a 9.5 cm inside diameter (ID) clear acrylic tube, 10 cm

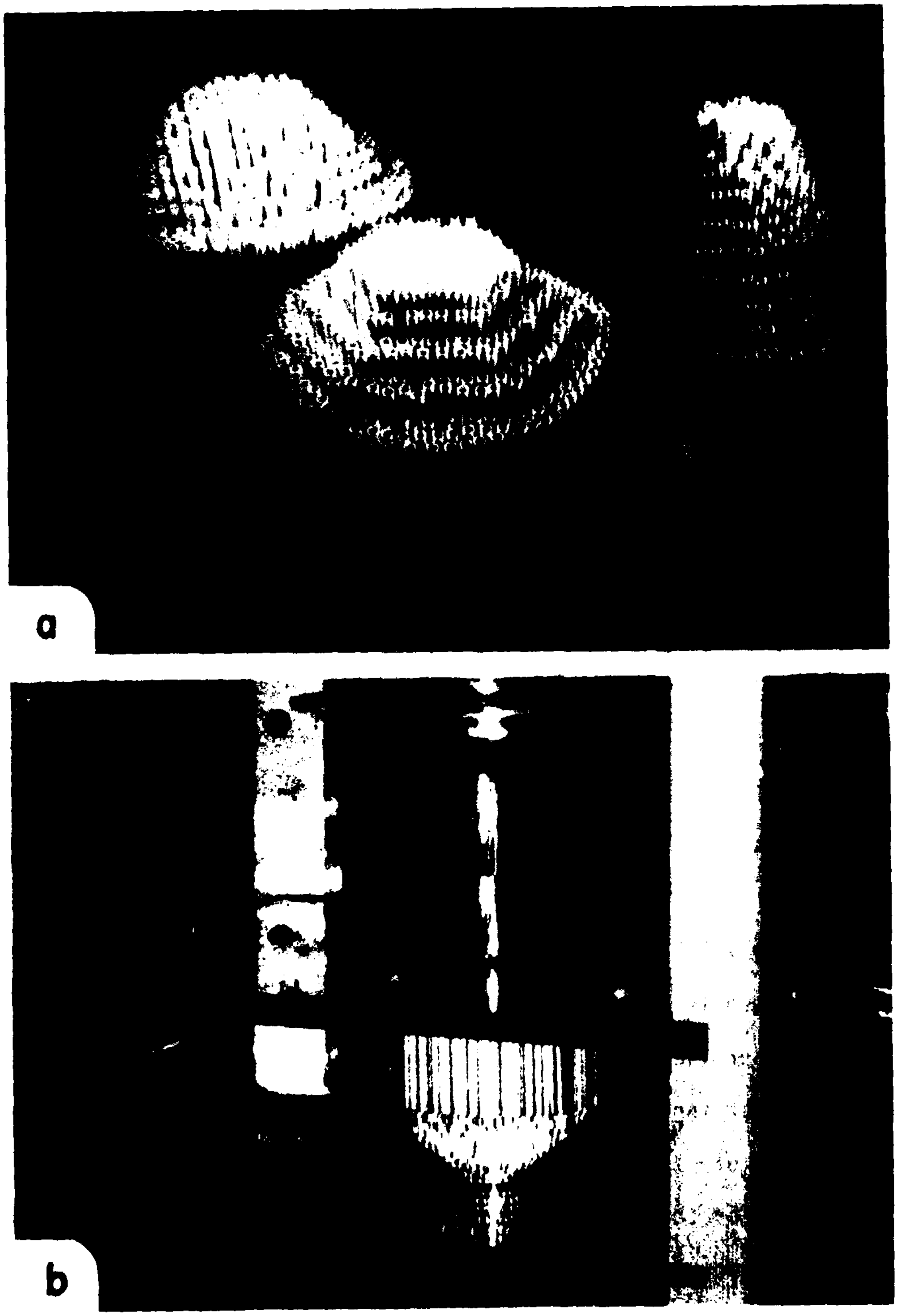

Fig 3. Honeycombs of different design (a) and a honeycomb positioned in the acrylic cylinder (b).

long, which was held at each end by a 30 cm square piece of 6.4 mm acrylic sheeting (see Fig. 3).

Screens

While the honeycomb was useful in approximating laminar flow, further refinement of the air stream was required to achieve the desired velocity profile. It was done with screens applying the trial and error method.

According to Pankhurst and Holder (1952), screens act to remove large-scale eddies at the expense of the introduction of a larger number of smaller eddies which decay rapidly. The screen thus decreases the turbulence at a sufficient distance downstream, although it may considerably increase it immediately after the screen. Pope and Harper (1966) state that screens are far more useful than honeycombs for adjusting airflow. Low turbulence wind tunnels may use six or more whereas a regular tunnel will only incorporate one or two. According to Pope (1954), the spacing between screens doesn't seem to make any difference as long as they don't touch each other. Our screens are made using 18 x 16 aluminum mesh, mounted on rings constructed of 20 gauge steel wire.

Three layers of screens were used, directly above the honeycomb in our tunnel. The desired velocity profile was made by using screens of higher resistence in the center. These screens were prepared by marking a circular center section on the mesh and then removing the excess wire strands. The remaining strands were arranged in the radial direction, evenly spaced and attached to the ring with epoxy glue. The rings and mesh were spray painted black and the rings further coated with polyurethane paint. A velocity profile whose center dip was too shallow allowed the artificial snow crystal to work its way up the slide until gravity pulled it down. It would cross the bottom of this

velocity "dish" and climb higher on the opposite side. By continuing this process, the artificial snowflake would soon climb over the side of the velocity "dish" and impact with the suspension chamber wall. If the velocity profile had been too deep, the artificial snow crystal drifted out of the bottom of the "dish" and tumbled instead of simply sliding back. Once the crystal began tumbling, it was impossible to hold it in the middle. Fig. 4 shows the screens used and their order of placement on the suspension chamber, beginning with the upper left. The height of the screens above the bottom of the tunnel is as follows:

first	0 cm
second	3.6
third	8.0
fourth	10.6
fifth	13.0
sixth	14.1
seventh	15.9

The best results were achieved by placing, bottom to top, the middle, small then large screen, and not the small, middle and large as one might expect.

Snow Introducing Device

To receive snow crystals during windy conditions, a chimney was erected based on experiences by Zikmunda and Vali (1972). It was a cylinder 24 cm in diameter, 91.4 cm high made of heavy wire mesh and covered with 1.5 mil plastic sheet. This cylinder was anchored to a wooden base, and positioned outside the shelter and above the vertical wind tunnel. The chimney was deep enough to enable a snowflake, to regain its vertical fall in the tunnel even if it had previously been travelling almost horizontally, thus allowing measurements on windy days. On the top of this tunnel, opening controls (3 removable covers with center holes 3 to 15 cm in diameter) can be attached.

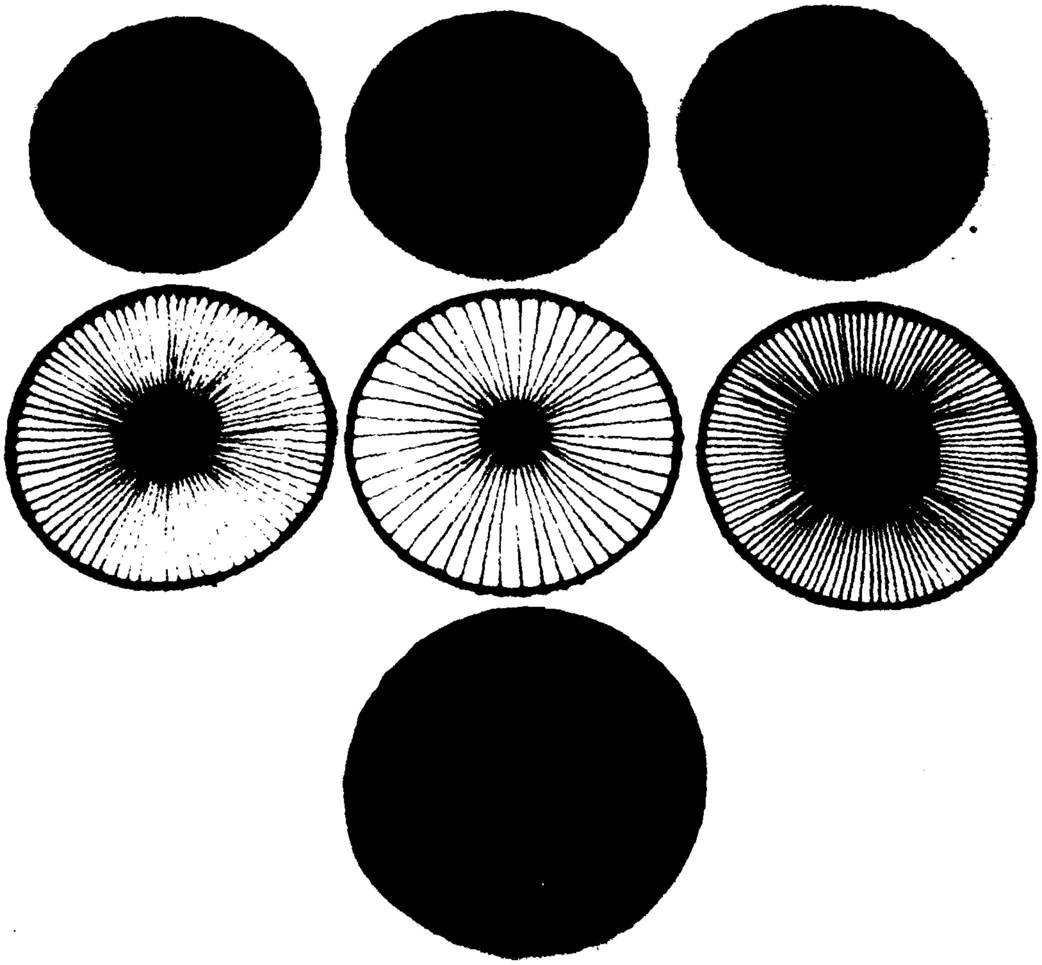

Fig. 4. Screens used in the vertical wind tunnel.

Depending on the intensity of the snowfall, these allow finer control on the number of snowflakes entering the tunnel.

The snowflake, after falling through the chimney, reaches the top of the tunnel, where the air exit chamber is located. This is an area of great turbulence, which could cause the snowflake to be thrown against the chamber wall and lost. To help the snowflake fall past this area, an insertion tube was designed and constructed. This consists of a 6.4 cm ID clear acrylic tube which extends 23 cm down into the tunnel space. This allows the snowflake to pass through the high turbulence area undisturbed. There is some turbulence at the bottom of this tube, but not enough to adversely affect the snowflake before it falls into the velocity profile and attains stability. The entrance to this insertion tube is a 2.5 cm diameter opening which acts to center the snowflake in the tube. The top opening has a spring-loaded cover which is opened by pulling a cable. As soon as a snowflake has entered the tunnel and achieved stability, the cable is released and the entrance closes.

Air Exit Box

An exit was designed and constructed for the air to exit smoothly from the tunnel. It is 30 cm square, 11 cm high and is connected with the valve by a 4.1 cm ID clear acrylic tube. Inside this box is a 15 cm diameter clear acrylic cylinder, which is sealed to the top and bottom of the box. The bottom of the box is cut away inside this cylinder and the top has a rubber seal through which the insertion tube fits. This 15 cm diameter cylinder has 500 3.8 mm diameter holes, spaced 6 mm apart, perforating it. To insure a symmetrical airflow, this 15 cm diameter cylinder is wrapped with a 1.3 cm thick foam rubber. This provides a resistance to the airflow, creating an area of lower pressure in the box, which in turn causes the air to be drawn from the suspension

chamber symmetrically, rather than favoring the area where the tube to the valve is located. This symmetrical exit of the air, combined with the center "dead spot" form the insertion tube tends to enhance the concave upward velocity profile in the tunnel (see Fig. 5).

2.2 Air suction system

Air Suction

The air suction for our apparatus is provided by 16 gallon (60 liter) Wet-Dry Shop Vac (Sears, Roebuck Co.). It provides more than adequate flow rates for this study and, is rugged enough to withstand cold temperatures for long periods of time. In addition, it met the portability requirements of our study and attachments and replacement parts are readily available. A variac was used to reduce the suction rate so that the airflow in the tunnel fell within the range suitable for suspending snowflakes. The power for our entire apparatus was provided by a portable alternator (Sears, Roebuck and Company, 2600 W). This unit provided ample power to meet our needs. It was easily handled by two people and operated well in the adverse weather conditions in which we carried out our measurements.

Valve

Direct control of the tunnel air velocity is provided by a valve designed and constructed in our laboratory (see Fig. 6). This valve is located directly outside the exit portion of the tunnel, thereby minimizing the lag time between valve adjustment and the corresponding air velocity change in the tunnel. The valve is constructed of a 10.8 cm section of clear acrylic tubing with ID of 14.6 cm and outside diameter (OD) 15.2 cm. The intake, i.e. exit for the tunnel,

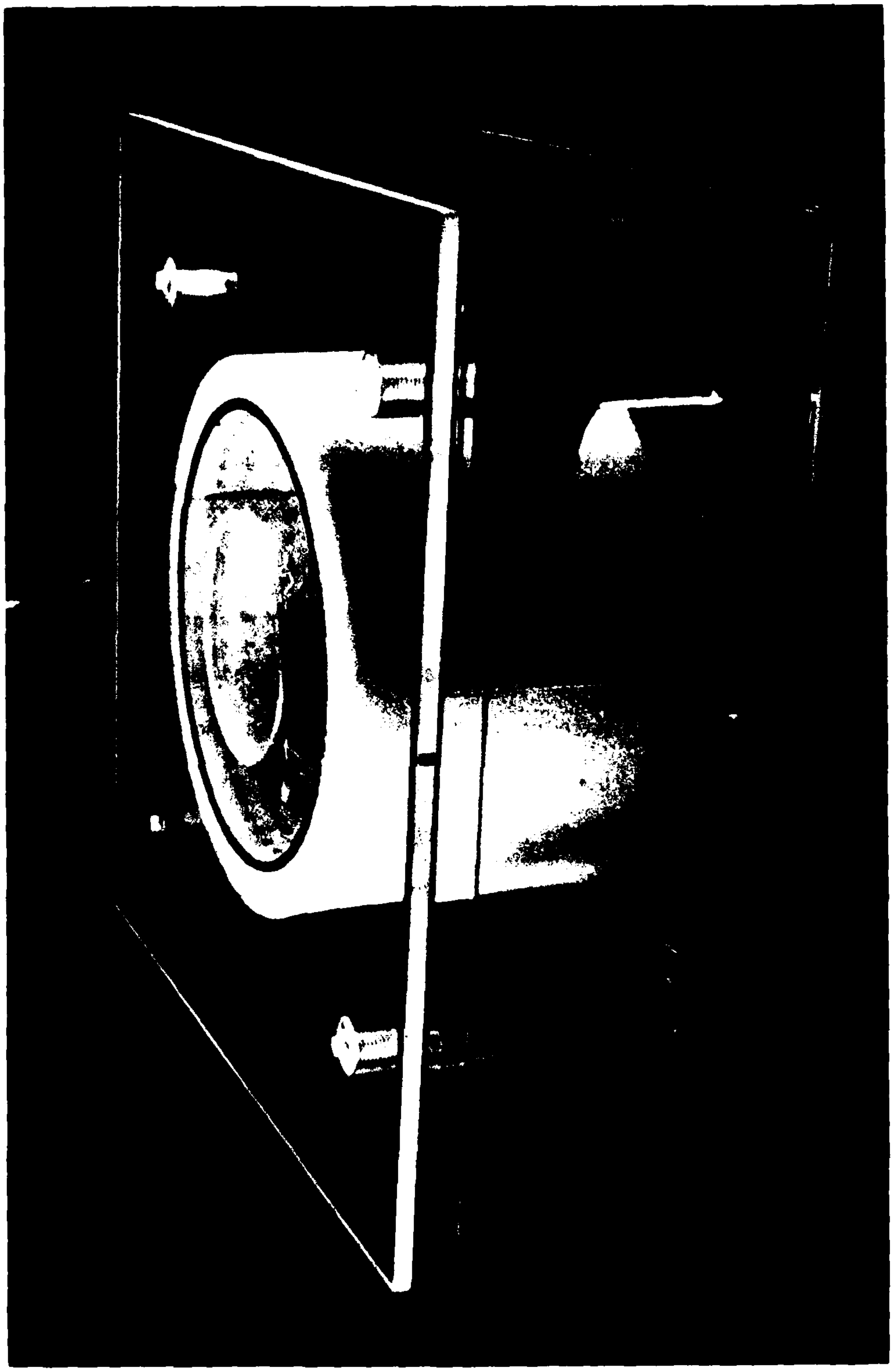

Fig. 5. Air exit box at the top of the vertical wind tunnel.

Fig. 6. Valve with anemometer probe.

is made of a 10 cm section of clear acrylic tubing with 5.7 cm OD. The bypass tubing, coming from the settling chamber, is a section of 6.4 cm diameter vacuum hose and connects to the valve next to the intake previously mentioned. The actual openings into the valve for both of these tubes are holes 3.3 cm in diameter. These holes are arranged so that as the cover plate, made of polyethylene to slide easily, inside the valve is rotated, the amount of air allowed to enter the valve remains constant, while one is opening the other closing. This ensures that Shop Vac is drawing a constant air flow rate at all times, and the flow rate of air drawn through the air conditioning system also remains constant which avoids variations in the relative humidity and temperature of the air. A steel shaft, attached to the cover plate, extends through the top of the valve and outside the enclosing box and is attached to the handle, 56 cm long. The valve was designed so that an upward movement of the handle results in increased airflow and a downward movement in reduced air flow, making the tunnel operation easier.

2.3 Air conditioning system

The original design of our apparatus called for the air to be recirculated, giving precise control over the relative humidity and temperature. Upon actually testing this system though, two serious problems appeared: vibration and heating, both caused by the suction system. So, it was decided to adapt an open system passing the air through the entire system one time only. Fortunately, the temperature of the environmental air remained constant over the time of observation, and under the condition a constant heating and airflow rate through a humidifier provided satisfactory control of air conditions in the tunnel.

Heater

The heater measures 44 x 55 cm^2 in a wooden frame. Thirty gauge alumel wire with a resistence of 11 ohms per meter is strung in the frame. The actual area spanned by the wire is 40 x 46 cm^2. To avoid heat loss from the heater by convection, a cover with holes whose cross-sectional areas combined to equal that at the bottom of the suspension chamber was placed over the heater (see Fig. 7). Over this cover is another box which draws outside air through a 6.4 cm diameter flexible tube. The metal walls of the conditioning system were insulated with 1.9 cm thick styrofoam sheeting.

Humidifier

The relative humidity of the air entering the suspension chamber was controlled by an evaporative cooler. Once the air sample has passed through the heater, it can be directed into the humidifier, bypass this and go directly to the settling chamber or any combination of these two. This allows the study of snowflake melting in different humidity conditions.

The humidifying section comprises the bulk of the conditioning system (see Fig. 7), which measures 44 x 55 cm^2 and is 79 cm high. It has three layers, each one composed of two layers of evaporative cooler batting. It holds 3.3 gallons (12.5 liters) of water. After running for several minutes (allowing time for the batting to become saturated), this leaves 8.6 cm of water standing in the bottom. The batting is held in place by 0.5 in. (1.3 cm) wire mesh, supported by wooden corner posts and plexiglass crossmembers.

The irrigation system is made up of a standard 115 V evaporative cooler pump, 20 cm in height. The water is distributed through an irrigation system comprised of 2.5 m of 6.4 mm diameter rubber hose, with holes 0.8 mm in

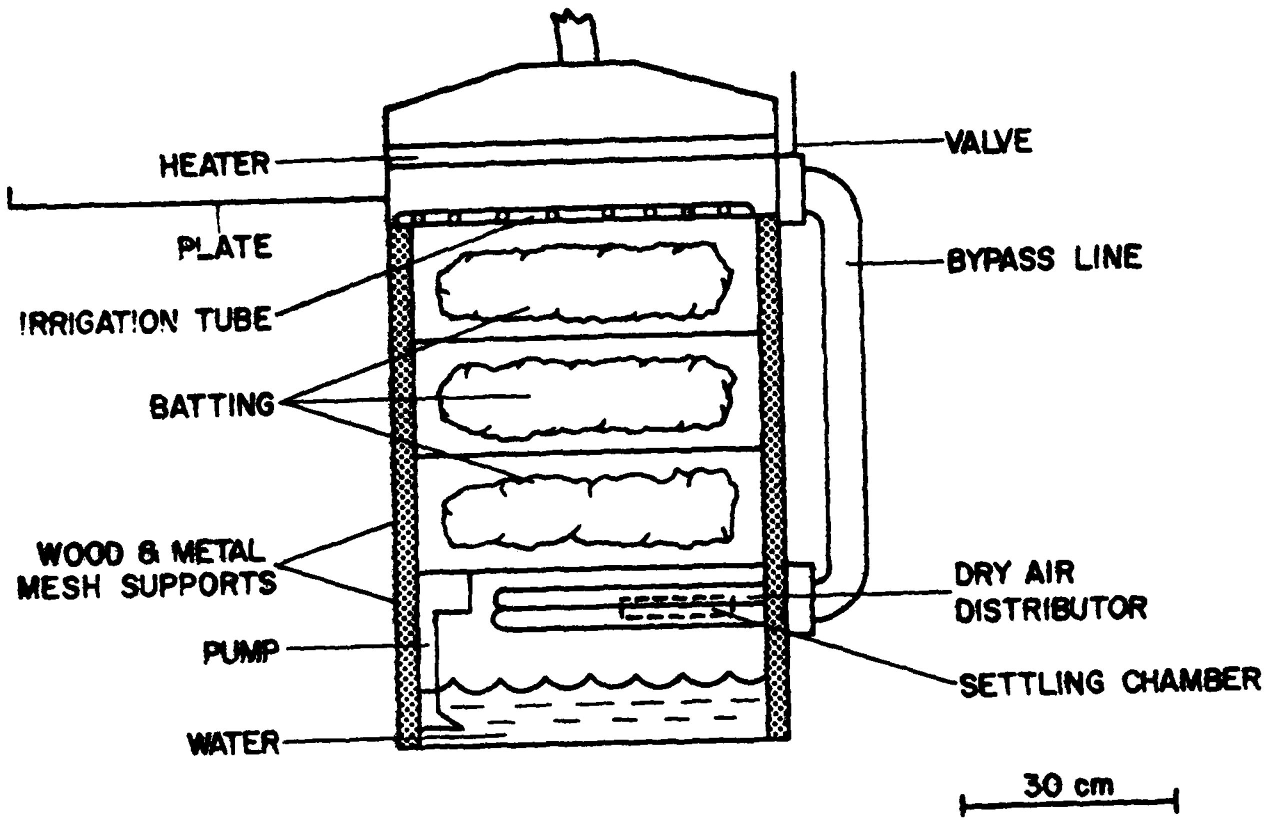

Fig. 7. Air conditioning system.

diameter, spaced every 3.8 cm. This system spreads the water evenly over the top layer of batting where gravity draws it back to the pump, wetting the batting in between. This system is very effective in helping achieve maximum practical relative humidity.

Above the irrigation system is a metal cover slide to control humidifying or bypassing the incoming air. The relative humidity of outdoor air is representative of that beneath a storm cloud just before or at the beginning of snowfall. As the snowfall continues, melting snow evaporates in the air, raising the relative humidity. Under the condition, simultaneous control of the metal cover and the bypass valve will permit the relative humidity adjustment to the desired level. To insure thorough mixing of this "dry" air with air passing through the humidifier, a device was built (see Fig. 7). The "dry" air exits the bypass line through ten 2.5 cm diameter polyvinyl chloride (PVC) pipes, each 38 cm long and containing thirty-six 3.2 mm diameter holes. The humidified air passes around these pipes prior to being drawn into the settling chamber and mixes with the dry air.

2.4 Photographic section

The photographic system used in the present study is shown in Figs. 8 and 9. Through the use of a common shutter release, both the cameras are activated and a timing mark is placed on the recorder chart simultaneously. This camera arrangement gives a top and side view of the snowflake at desired intervals throughout the melting process. The cameras are Olympus OM-2 35 mm cameras, equipped with Olympus Winder 2s. To provide further enlargement of the snowflake, the top camera uses a 14 mm extension tube and the bottom a 7 mm one. Ilford HP5, ASA 400 film is used in the cameras. The background

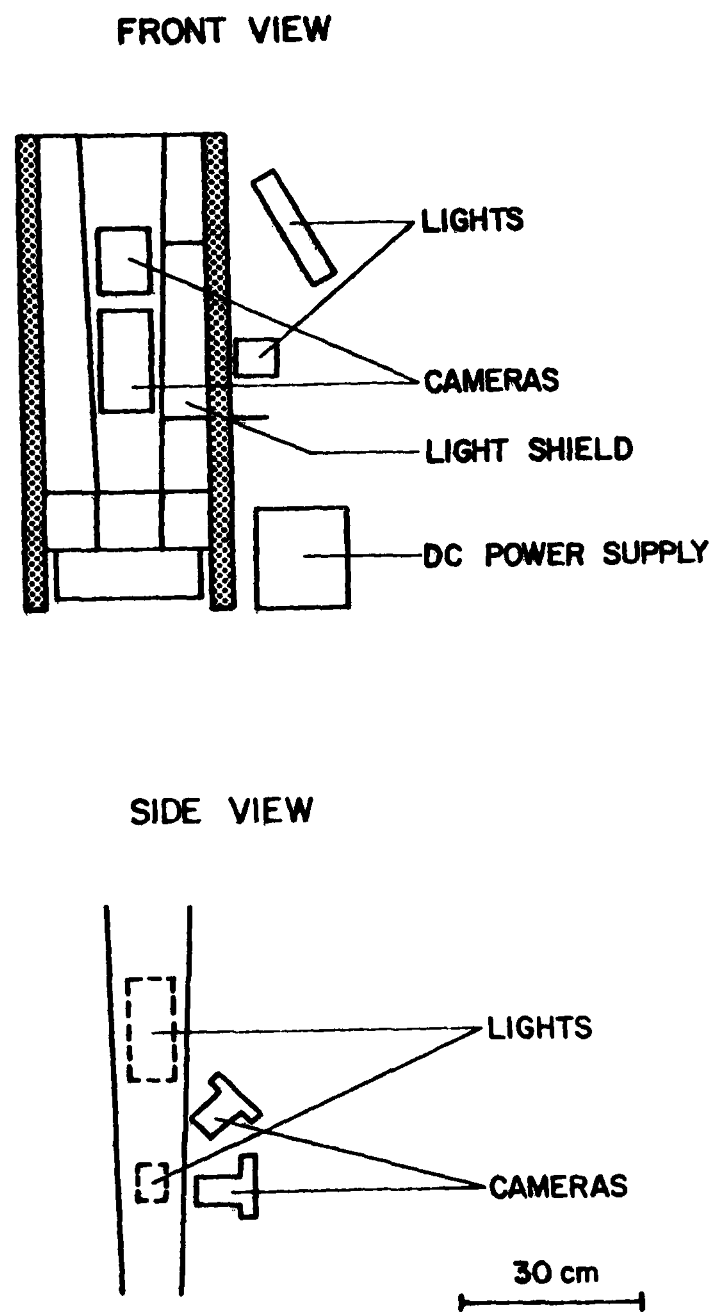

Fig. 8. Photographic section

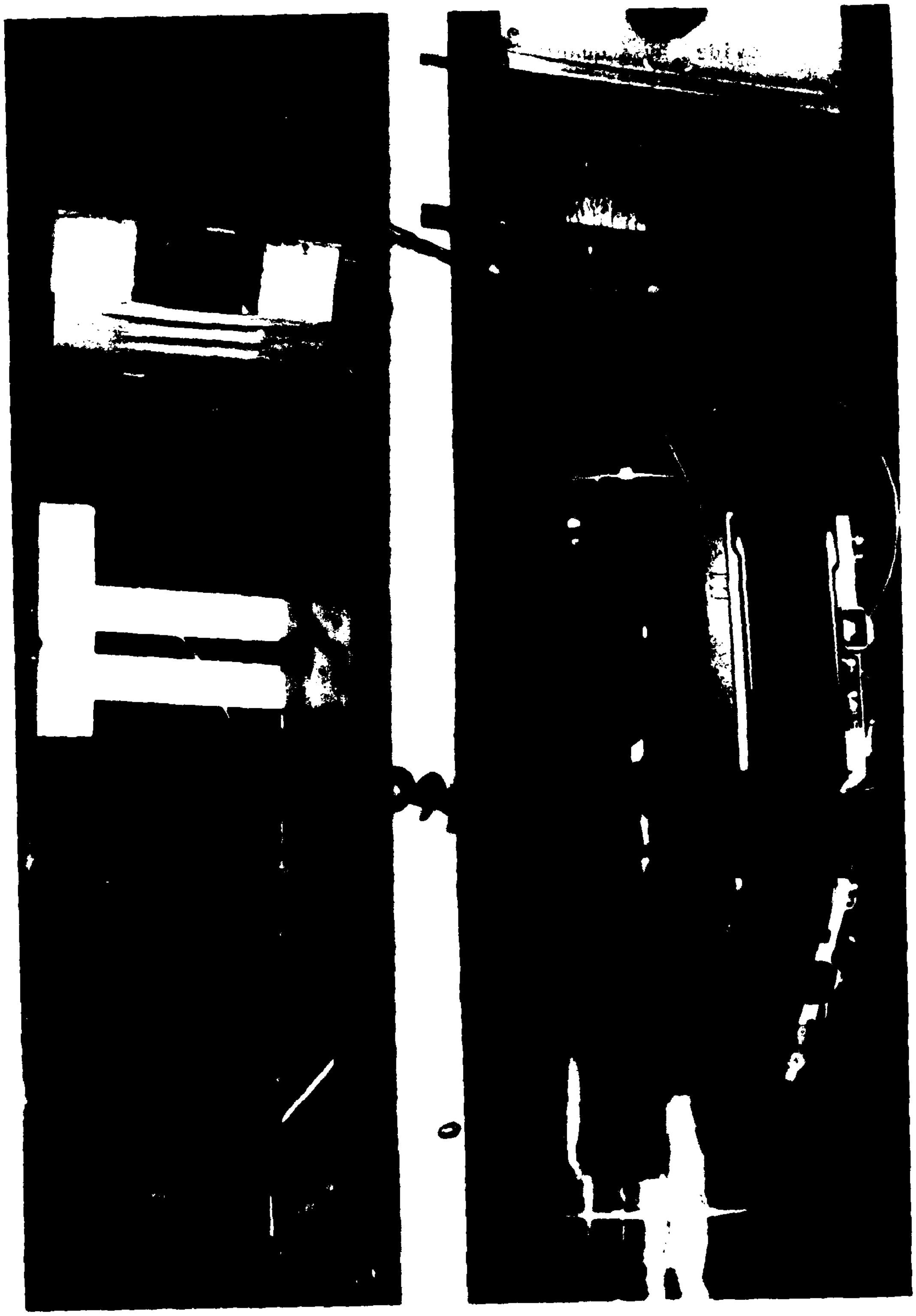

Fig. 9. Camera arrangement in front of the wind tunnel

lighting is provided by a quartz-halogen automobile driving light. Intermittent lighting is obtained by an Olympus T32 electronic flash, connected electrically to the top camera and positioned as shown in Figs. 8 and 9. To reduce glare from the tunnel wall, arrangements were made whenever necessary.

2.5 Supporting equipment

Recorder

To record the outside air temperature, the time the photographs were taken, the temperature and the velocity of the air in the wind tunnel a three-channel recorder (Cole-Parmer, model 8373-30) was used. By connecting the camera system to a temperature recording channel in such a way as to short circuit it when a photograph was taken, all the above parameters were recorded on it.

Anemometer

The probe of an anemometer (Kurz Instruments Inc., model 430 M-4) was mounted in the tube which led from the exit of the suspension chamber (Fig. 6), to utilize the sensitive zone of the meter for calibration. With the probe location we chose, calibrations were made to six horizontal reference lines in the wind tunnel, 2.5 cm apart, beginning 18.4 cm above the bottom of the chamber. These lines, in conjunction with a photograph, allowed an exact determination of the fall velocity. The error induced by the anemometer-recorder combination was 1.2%.

Hygrometer

The relative humidity of sample air was made using a dew point hygrometer designed and built in our laboratory. The mirrored container holding ether

was cooled by evaporation as the rubber bulb was squeezed, forcing air bubbling up through it. When the ether cooled the container to the dewpoint temperature, condensation would form on the mirrored surface. This was very noticeable with the aid of the uncooled mirrored fins on either side. The dewpoint and sample air temperatures were measured by two calibrated thermometers.

Air Temperature

The temperatures, both outside and inside the apparatus, were measured by two pre-calibrated thermocouples, constructed from type T, 20 gauge copper constantan wire. One thermocouple was located in the wind tunnel. The thermocouple measuring the outside air temperature extended through the shelter wall approximately 76 cm and was protected from falling snowflakes by a cover.

Shelter

A suitable shelter was necessary to protect both the equipment and the operators from the environment, as the observations were taken during snowstorms, often at night, with temperatures below 0°C, and lasted for several hours at a time. A shelter was made by building a wooden frame on the back of a 1968 Dodge 4-wheel drive Powerwagon. The framework was covered with two layers of plastic sheeting, and a layer of canvas, held in place by ropes. The equipment was mounted inside and access holes cut in the plastic. During experiments, the ropes were removed and the canvas folded back to expose the access holes (holes to allow the snowflake entrance to the chamber and an air intake for the air conditioning system). It offered the further advantage of being mobile, which allowed travel up into the mountains when snow was not expected in the valley. The shelter during an observation is shown in Fig. 10.

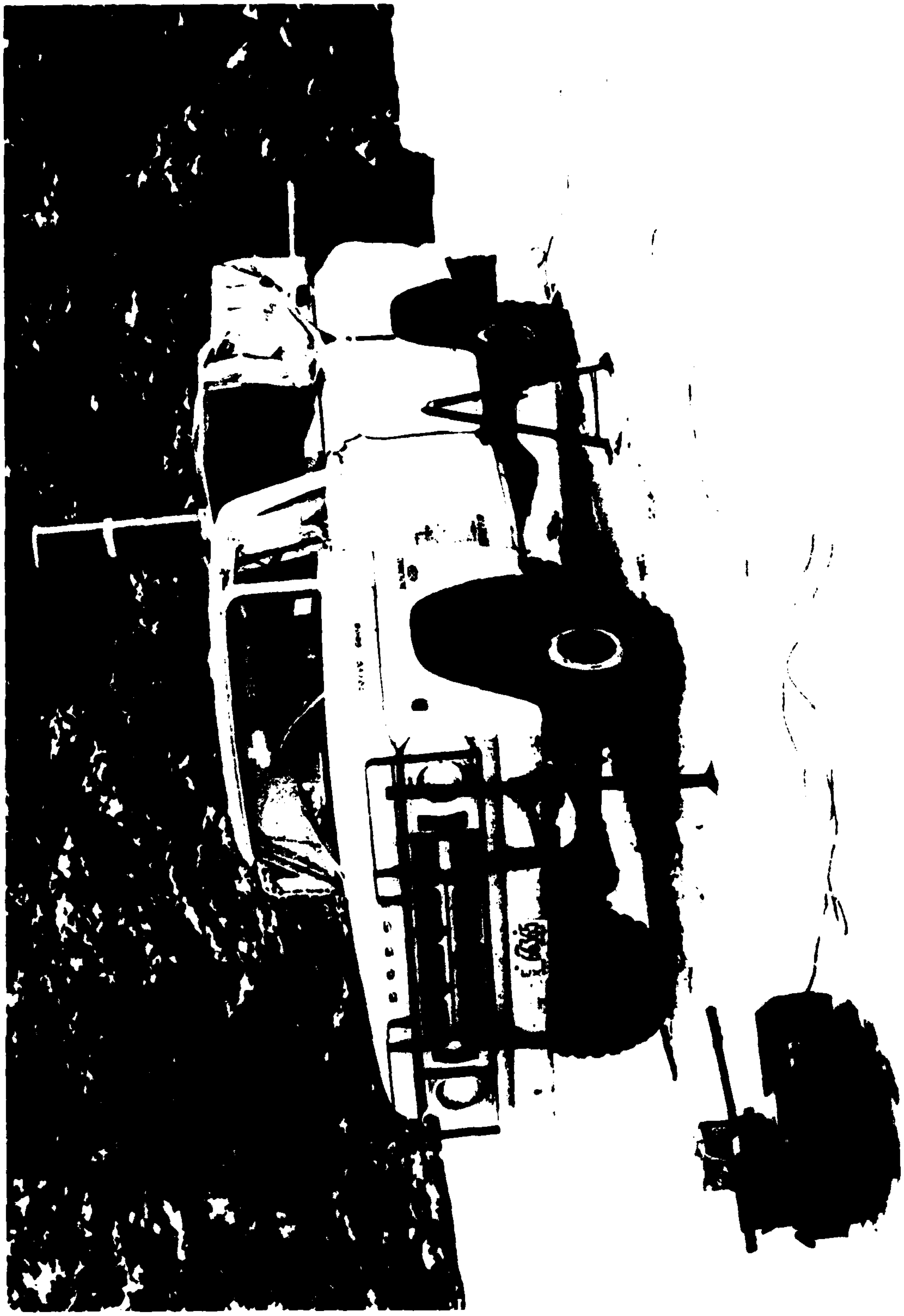

Fig. 10. Equipment under operation in the field

2.6 Experimental procedures

Preparation

Due to the limited snowfall during the winter, mobility was an important factor. With the eventual placement of the experimental apparatus in the bed of a 4-wheel drive truck, travel to the mountains, where snowfall frequently occurred, was possible. The majority of the equipment was stored on the truck. When it was determined that snowfall would occur in the mountains, a check list was used to insure everything required to collect data was loaded.

The problem of static electricity on the tunnel surface was noticed early in our equipment development. This was solved by wiping the surface with damp "Cling Free" antistatic cloth, drying for about 15 to 20 minutes, and polishing it with dry, clean cotton rag. It was found that this treatment of the chamber was not permanently effective. Therefore, we treated the equipment for static electricity prior to every storm and checked for its presence at the beginning of each data collection period.

Equipment Set Up

Upon arrival at the data gathering site, the truck was parked in the most level place available. After unloading the equipment, a decision was made as to whether or not to use the opening controls and/or entrance tunnel. This was based on the snowfall intensity and experience. The equipment worked best when about four to ten snowflakes entered the chamber every minute. With higher snowflake concentrations, it became difficult to concentrate on a single flake. Also, the others could interfere with its suspension and eventually land on the chamber walls or screens where they left water deposits. These water

deposits could disturb the air velocity profile or the photography, depending on their position. Once the equipment was unloaded, the work was divided between an outside and inside worker.

An important initial step was the tunnel stability test using the artificial snowflake. Experience showed that if the artificial snowflake could not be suspended, the chance of suspending natural snowflakes was very small. This test was very useful in identifying potential problems. After the suspension test, the snowflake was removed by suction.

The inside worker, like the outside, also had many tasks to complete. The two workers had to communicate as they set up and confirm the proper operation of the equipment. The camera with appropriate extension tubes were placed and made ready. The focal points of the cameras were in the center of the chamber, between the third and fourth reference lines. The recorder channels were zeroed. The checklists were reviewed just prior to data collection to confirm that all tasks had been completed.

Data Collection

As with setting up the apparatus, data collection was also a two-man job, with one person (hereafter called controller) operating the wind tunnel valve and the cable release/marker device and the other (the supporter) the opening to the insertion tube and taking notes.

Before data collection began, the controller measured the air and dewpoint temperatures of the tunnel while the supporter was recording relevant data. Data collection began with the supporter opening the entrance to the insertion tube. When a snowflake entered the suspension chamber, he immediately released the control cable, whereupon the spring loaded opening mechanism closed. Whereas before this operation, the air was being drawn both from the vertical wind

tunnel and from the outside, now it came solely from the wind tunnel. This gave an immediate velocity increase in the tunnel which was enough to cause most snowflakes to hesitate momentarily in their falling. During this hesitation, the controller increased the velocity and gained control of the snowflake suspension. When the snowflake was under control, approximately two seconds after entering the tunnel, the controller activated the camera release/marker device to record it. He also increased the airflow to keep the snowflake vertically stable as it melted and its fall velocity increased. This required practice to keep the snowflake in the optimum position for photographing. As the melting process progressed, both workers carefully observed the behavior of the snowflake. When the suspension was lost, the supporter recorded the information concerning that individual snowflake on the recorder strip. The number of pictures taken was also recorded. Then, the same procedure was repeated. Cleaning of the tunnel was carried out whenever it became necessary following the predetermined procedure.

Throughout our data collection the temperature inside the chamber ranged from 1.8 to 3.9°C, without operating the heater, due to the outside air temperature, body heat, the electric heater, and other equipment inside the shelter. This was rather convenient as these were some of the temperatures at which we desired to collect data. For other temperatures, the supporter must also control the heater through the on-off switch located on the front of the instrument box. By reading the temperature on the recorder and controlling the heater through its switch, temperature could be maintained at any level within ±0.2°C.

Shutting Down

The procedures for repacking the equipment were also divided between the inside and the outside worker, using a checklist prepared.

Upon returning to the university, the supply levels were checked. If data collection was expected within the next 24 hours, the wind tunnel was also serviced for static electricity as described earlier.

Post Experimental Maintenance

Thorough cleaning of the tunnel is crucial for the successful suspension of ice crystals. Unfortunately, cleaning of the equipment required the removal of the wind tunnel, the honeycomb device, and the top filter section. After the device was removed, water sitting in the tunnel was wiped off with a sponge or rag. Compressed air was used to remove any water that had settled inside the honeycomb device. The final procedure involved polishing the wind tunnel with the antistatic.

2.7 General remarks of measurement

The outdoor measurements of natural snow crystals provided us with some unusual and interesting experiences. It may be worthwhile to mention some of them here.

For thermocouple operation of temperature measurement, an ice bath of 0°C is commonly used. Crushed ice will normally melt to yield the condition. Under our operating conditions, though, the crushed ice was found sometimes not to melt due to low air temperatures. So, we had to flush the crushed ice with water and keep some water with it.

The position of a snowflake in the wind tunnel was important. Unless centered after entering the upper portion of the tunnel, they hit the wall. In the upper regions of the tunnel, the air velocity profile was flattened and the snowflake could impact with the wall. When centered, the velocity profile moved it away from the wall as it fell into the observing area and was suspended.

Snow crystals could be suspended almost anywhere in the tunnel depending upon their size. Very small ones, approximately one millimeter or less in diameter and appearing only as a sparkle of light, could even be suspended on the crest of the velocity profile.

It was found that our apparatus was not suitable for all types of ice particles. Graupel proved to be too dense to suspend and snow which was mostly melted was the same. Half melted snow often left water deposits which interfered with the tunnel airflow and our visibility. Best results were obtained by waiting until later in the storm when the surface temperature dropped and the snowflakes were not melting. Also, moderate snowfall was required to receive a significant number of snowflakes into the tunnel.

Large snowflakes, greater than ten millimeters in diameter, were seldom observed in the tunnel due to several reasons: The concentration of these size flakes during a storm was relatively low. Also, due to small entrance to the tunnel, only 2.5 cm in diameter, large snowflakes often struck the side of the entrance opening causing showers of small crystals. Once in the tunnel, the positioning of the snowflake became a factor.

3. Results of Measurement

In this section, we describe and discuss the results of our measurement, starting from our visual observation during the tunnel operation in the field.

3.1 Observation of melting behavior

The data collection for this study was performed during the three storms in January, 1982. During this time, nearly 400 photographs of ice crystals

and snowflakes were taken and over 100 sequences of their melting were analyzed. In addition, several experiments were conducted and ice crystal melting was observed although equipment malfunction prevented photographic data collection. In all, about 2,700 ice crystals and snowflakes were suspended and observed to melt. The data for single crystals were analyzed and reported by Savage (1982) and those for snowflakes by Donovan (1982). From these observations, several interesting patterns surfaced.

Rotation

Usually only in small crystals, from 1-3 mm in diameter, we observed that the crystals rotated around their vertical axes. We called this "helicoptering". As time progressed, the crystal began orbiting around the center of the chamber, rather than helicoptering. With each pass, the circle became wider and wider, until, just fractions of a second before melting, the crystal impacted with the chamber wall. This spiral was observed only at the end of the melting process, and only with this size crystal. The size of smaller crystals and their appearance as a sparkle of light prevented us from observing the helicoptering but larger ones did not show the rotation. The helicoptering movement did not affect our ability to suspend a crystal. Helicoptering was not observed in snowflakes.

Vertical Stability

The vertical stability of a suspended snowflake or an ice crystal was dependent upon its size and shape. The small crystals, less than one millimeter in diameter, were the easist to suspend. These weren't dependent upon the velocity profile to hold them. They could be suspended anywhere in the chamber

for one or two seconds, during which time they melted. Snowflakes and crystals became increasingly unstable with size, due to the way they melted. Also in our wind tunnel, we were able to suspend only the aerodynamically stable crystals. Although most of the ice crystals which entered in the wind tunnel appeared to be aerodynamically stable, we were able to suspend only roughly 10% of the crystals because the rest of them fell into the unstable zones. It still took much skill and luck to suspend even those crystals which fell within the stable zones of the tunnel.

Melting and Disruption

The surprising observation during this study was the way snowflakes and crystals melted. It is currently assumed that snowflakes have an ice skeleton which maintains its original shape during most of the melting process (Matsuo and Sasyo, 1981a). Fig. 11 shows a top and corresponding side view of a snowflake melting in our chamber. This ice skeleton can easily be seen. Matsuo and Sasyo postulate that this ice skeleton collapses to a water drop because of surface tension. We found that as these snowflakes and crystals melted, they frequently disrupted. Of course, caution must be taken in interpreting the disintegration process because the types of ice crystals we could catch were limited to dendrites, spatial crystals and snowflakes with no easily identifiable shape. The disintegration of ice crystals occurred rapidly in the final stages of melting and it was nearly impossible to photograph this process using the present camera set up. However, the visual observation during the final stages of melting clearly supports the existence of the disintegration process.

The size of the ice crystal affected the way it melted. Crystals less than 1 mm in diameter were easily suspended until the last fractions of a second of their crystal form. Then, instead of falling down toward the bottom of the

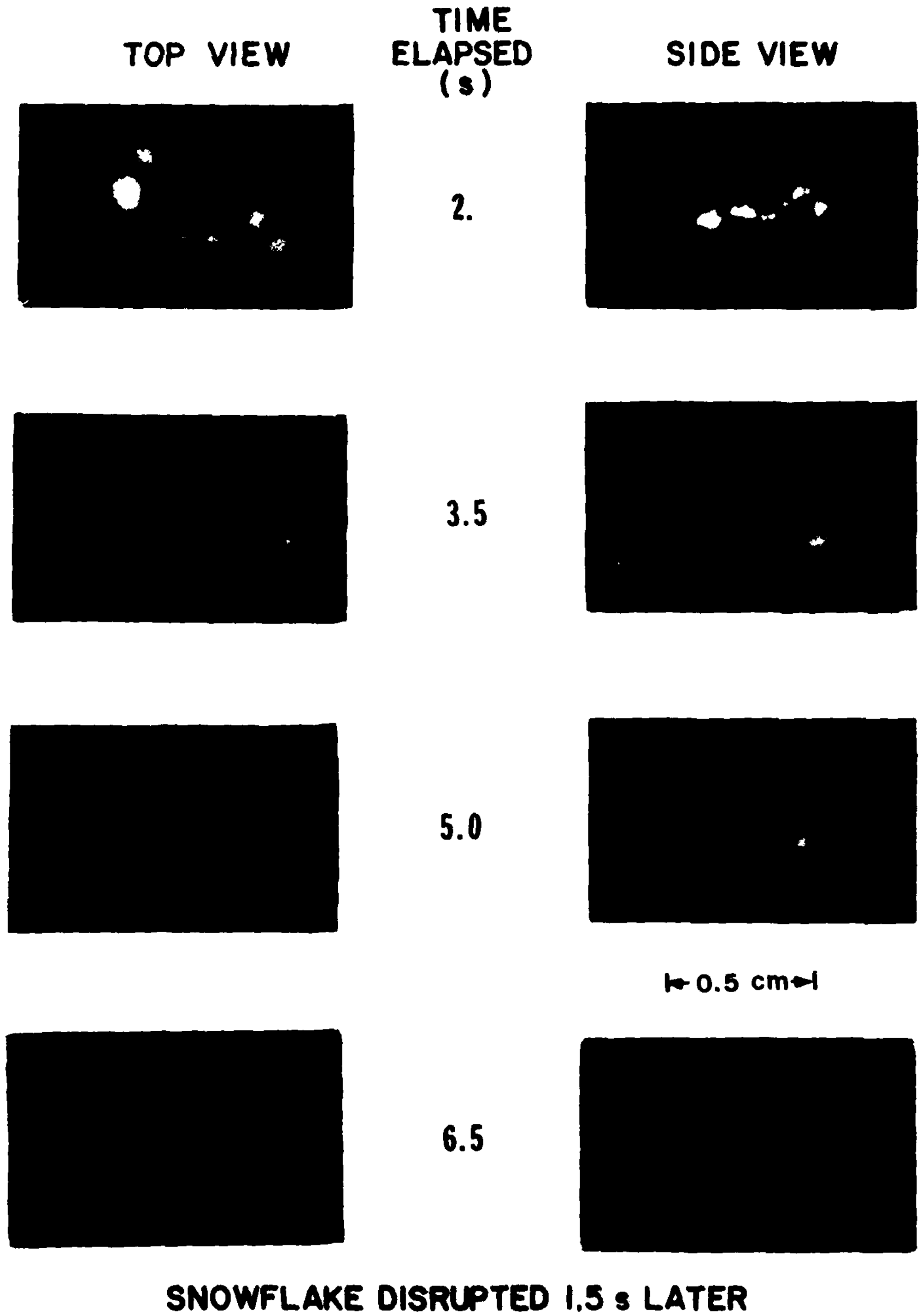

Fig 11. Snowflake melting sequence.

tunnel, these crystals were observed to take a violent jump. If these crystals had transformed into spheres, which having smaller cross-sectional areas, they should fall faster. In our observations, this downward fall, which should be a uniform increase in velocity, was the exception. These small crystals jumped sideways or straight up. A crystal suspended several centimeters from the tunnel wall often jumped over onto it and appeared instantly as a water droplet. Static electricity as the cause of this was ruled out because of our test with the artificial snow crystal, the violent nature of the crystal movement, and occurence only at the end of the melting process. A change in the aerodynamic condition of the crystal due to disruption, could cause this movement. Total disruption could also cause the pieces of the crystal to be swept straight up and out of the measurement area.

Disruption also offers the most reasonable explanation for the snowflake behavior in the final seconds of its melting process. The snowflake shown in Fig. 11 was easily suspended with a gradual increase in the tunnel airflow throughout the pictures taken. However, just after the fourth photograph, it broke up and fell to the bottom of the tunnel. This was the case with all the snowflakes we suspended. They were easily suspended, as they decreased in size by melting, up to a certain point (twenty seconds being the longest under the temperature and relative humidity ranges of this study), whereupon they broke into several pieces, with the larger pieces falling to the bottom of the tunnel and the smaller ones being swept up and out of the observation section. This occurred as if there were a small explosion in the snowflake. The larger drops behaved as if their wings, i.e., small droplets connected by the ice skeleton, were lost, falling out of the measuring section of the tunnel before the operator could react to increase the airflow and catch them.

Large, flat, symmetrical, dendritic crystals fell flat and were not affected by this disruption phenomenon. They melted slowly from the outer edges inwards as they drifted into the wall (see Fig. 12). No breakoff of a portion of the crystal was observed. This action of drifting into the wall after being stably suspended indicates that the velocity profile suitable for a snowflake or a crystal is not sufficient for a water droplet.

Environmental Conditions

Measurements were carried out under the following combinations of relative humidity (RH) and temperature T.

RH (%)	T (°C)
100	2
	3
	4
90	3
	4

3.2 Single crystal melting

3.2.1 Results of measurement and discussion

The experimental data were first reduced and plotted into the following 4 relationships: (i) initial diameter vs melting time, (ii) initial area vs melting time, (iii) diameter vs time, and (iv) velocity vs time.

In the data analysis, a clear change in the air velocity was always observed on the chart about two seconds before the first time mark of photographing. Based on this observation, it was assumed that the ice crystals were being suspended for two seconds before the first photograph was taken. We estimated the final melting time on the recorder chart based on the manner the stability of

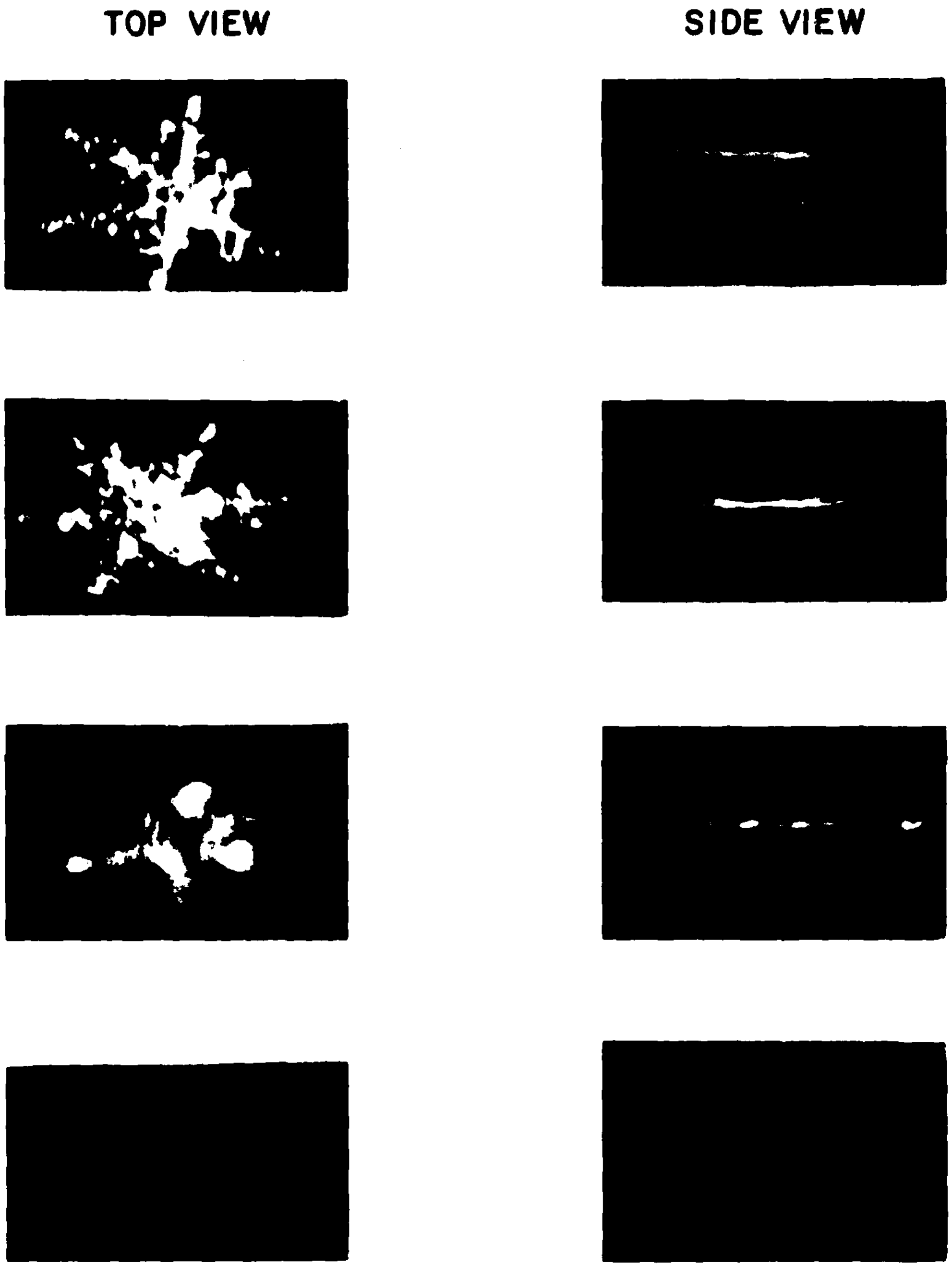

Fig. 12. Photographs of a dendritic ice crystal melting in the vertical wind tunnel.

the ice crystal was lost. Also the data for veloctiy and diameter changes with time were classified according to the average ice crystal size.

Initial Diameter and Area vs Melting Time

Figs. 13 and 14 show the observed relationships between the initial diameter d_o and melting time t_m, and that between the initial horizontal cross-section area A_o and t_m. The longest melting time occurred for non-dendritic ice crystals which had an initial diameter of about 3 mm or those which had an initial area of 7.5 mm^2. In the figures, the non-dendritic single crystals showed a convex upward tendency of melting. This is in agreement in tendency with the treatment for ice spheres by Mason (1956) and Drake and Mason (1966) and that which we have done for non-dendritic or plate crystals as we shall discuss later. However, they are different from dendrites and snowflakes, whose melting times do not vary appreciably depending on their sizes. It appears that the melting of dendrites and snowflakes is controlled mostly by heat conduction from the ventilating air through their structures. It also seems to be that dendritic ice crystals with initial diameters larger than 3 mm are affected more by ventilation than those smaller than 3 mm. The A_o vs t_m plots show the same tendency.

Diameter Change With Time

Figs. 15 through 18 show the observed diameter d vs time t relationships. In the figures, the diameters of the crystals are classified into seven different groups; they are 1 (0 to 1 mm), 2 (1 to 2 mm), 3 (2 to 3 mm), 4 (3 to 4 mm), 5 (4 to 5 mm), 6 (5 to 6 mm), and 7 (6 to 7 mm). It is natural to expect the larger the ice crystal, the longer it takes to melt. As can be seen in

the figures, a large ice crystal does show a quicker change in diameter than a small dense ice crystal. Fig. 15 gives slopes only for the groups 1, 2 and 3, but it suggests that the groups 1 and 2 melt slower than the group 3. Fig. 16 shows the slopes of the groups 2, 3 and 4 to be gentler than those of groups 5 and 7. This seems to suggest that ice crystals in the 0 to 3.0 mm diameter range melt slower than those in the 3.0 to 7.0 mm range. Fig. 18 shows clearly that the slope of the group 4 is steeper than either the group 2 or 3. Whereas, Fig. 17 shows an exception in the tendency of slope. The slope of the group 2 is smaller than those of groups 3 and 4. However, these data indicate generally that slower melting ice crystals do exist in small diameter ranges.

Fall Velocity Change With Time

Figs. 19 through 22 show the observed fall velocity v vs time t relationship. In these figures, it may be seen that the largest total change in fall velocity occurs in general for smaller crystals. It appears that large dendrites like the group 7 not only fall slowly but change the velocity relatively little during the melting.

Figs. 21 and 22 show the variation of fall velocity with time for ice crystals melting under relative humidity of 90%. Although the relative humidity in these cases is lower, suggesting slow-down effect of melting due to evaporation cooling, the initial ice crystal conditions are different compared with those in Figs. 19 and 20. Due to large variation of crystal conditions involved in the measurements, it is not possible to clearly isolate the effect of temperature or relative humidity on the fall velocity variation during the melting from the sample data analysis.

3.2.2 Regression analysis

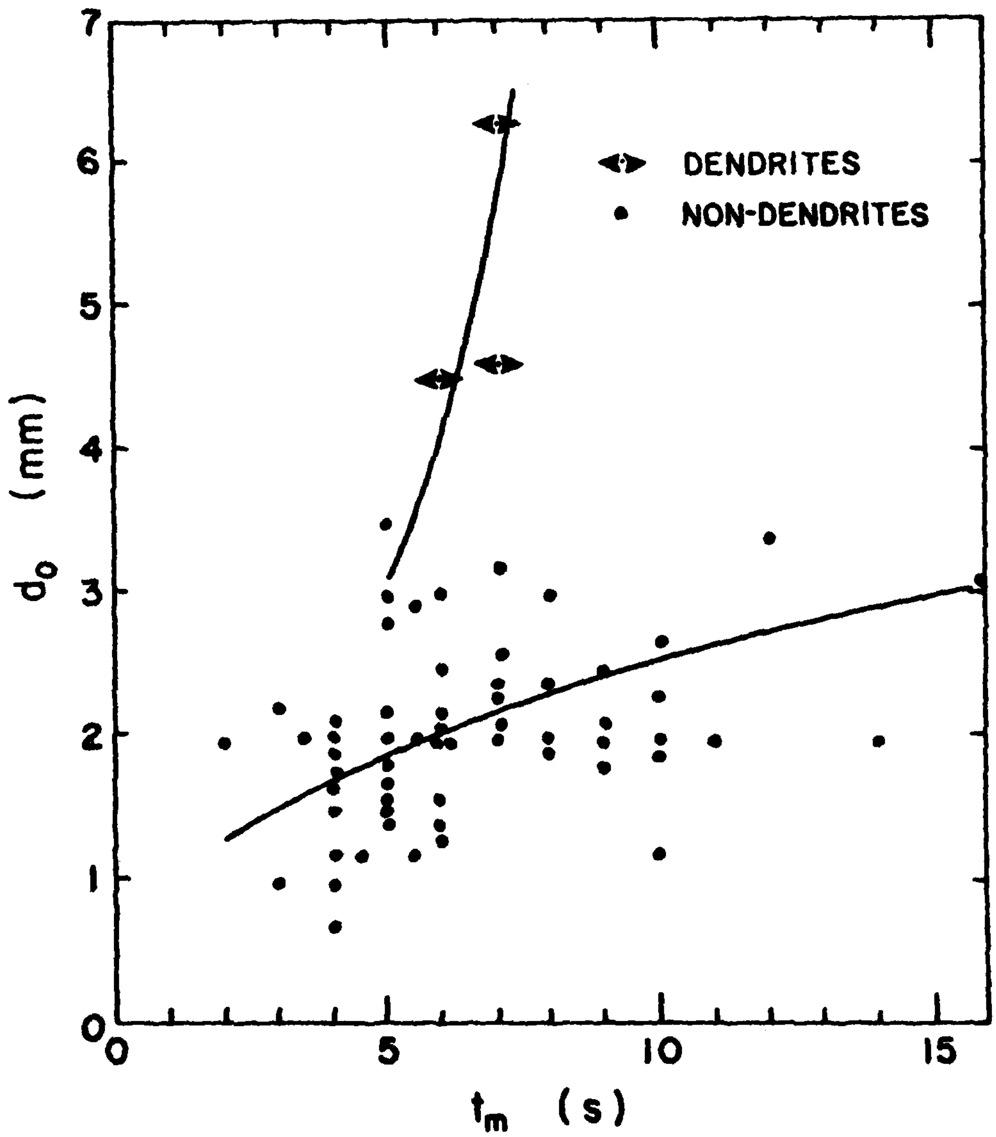

Fig. 13. Initial diameter of single ice crystals d_o vs melting time t_m for all the environmental conditions. Details of the environmental effects may be interpreted from the following figures.

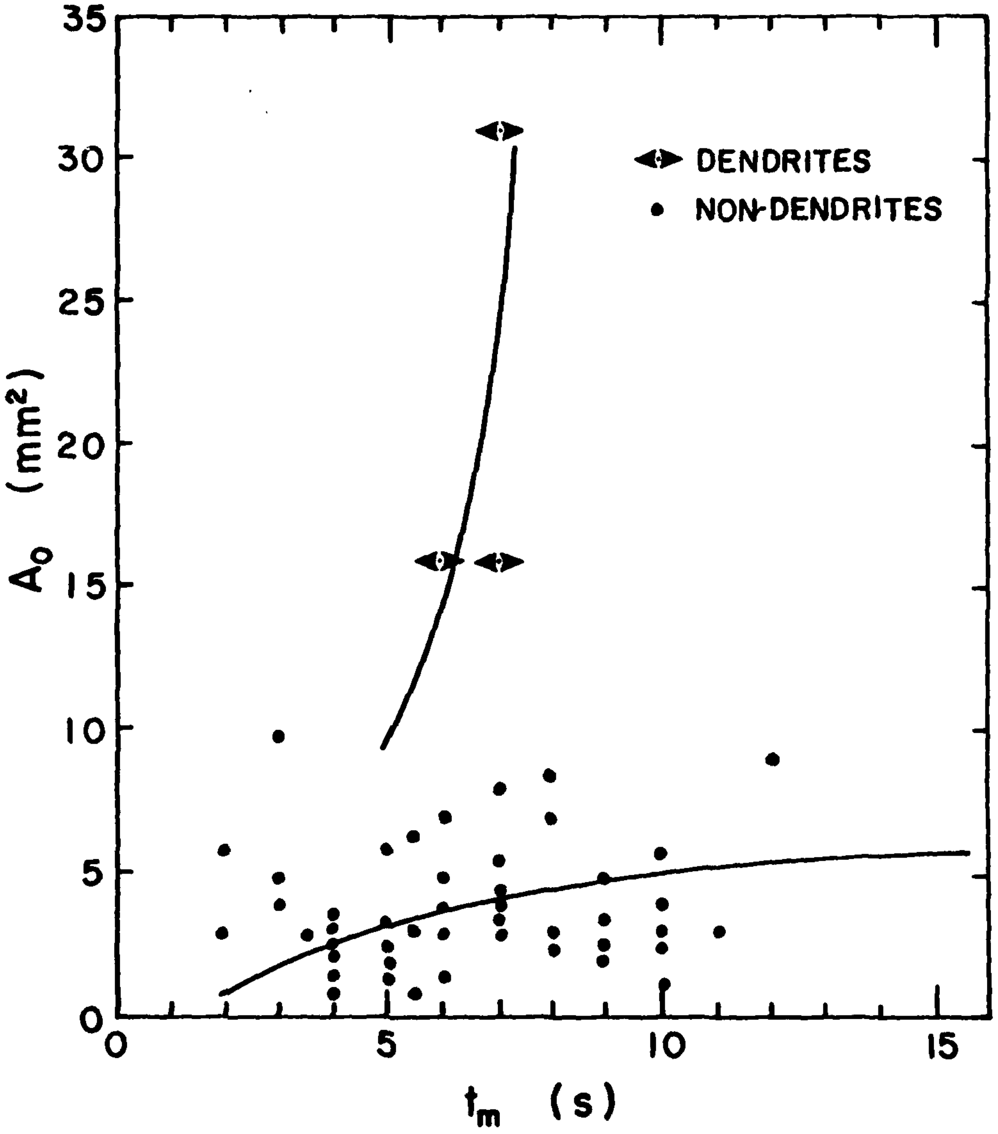

Fig. 14. Initial horizontal cross-sectional area of single ice crystals A_0 vs melting time t_m for all the environmental conditions. Details of the environmental effects may be interpreted from the following figures.

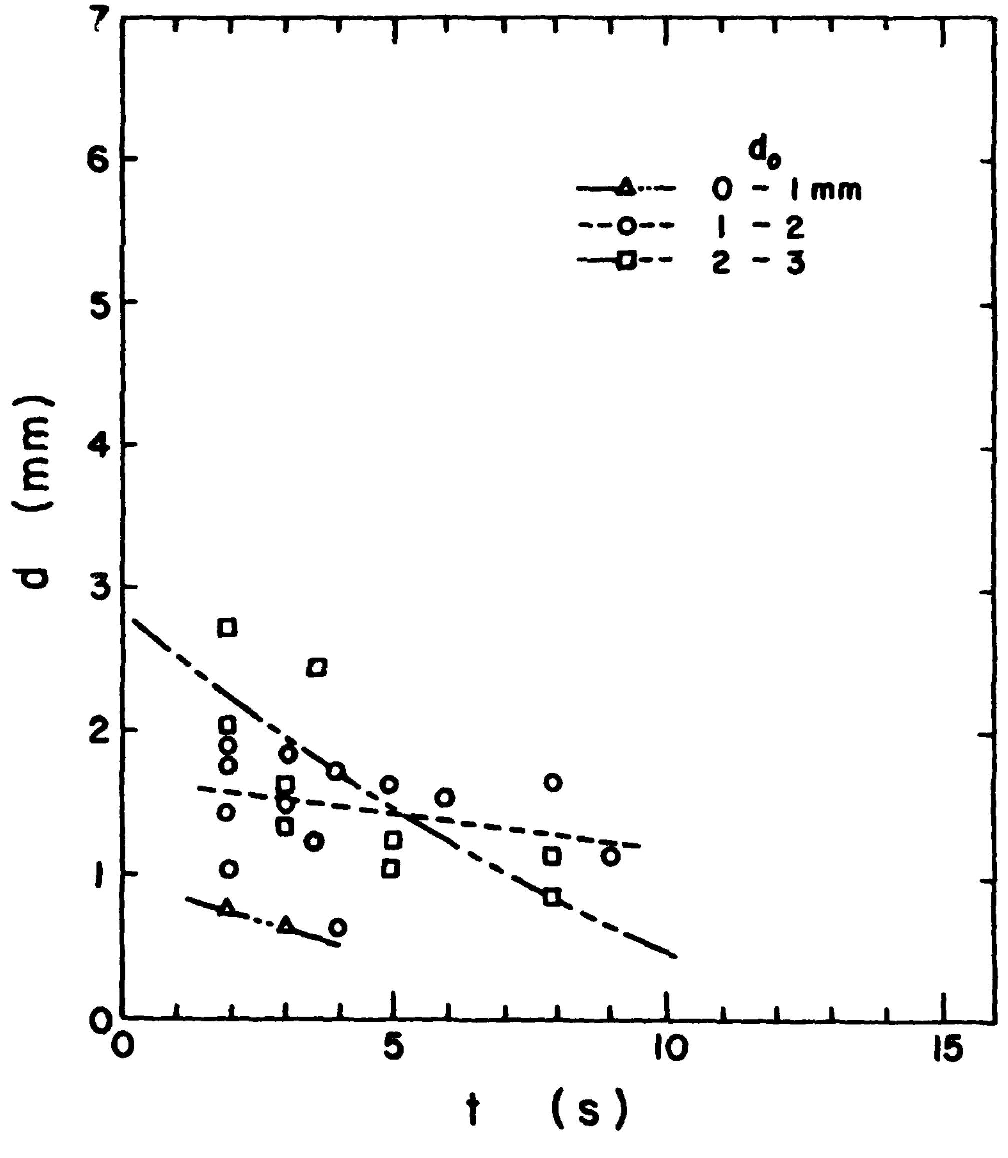

Fig. 15. Change of crystal diameter d with time t under a relative humidity of 100% and a temperature of 2°C.

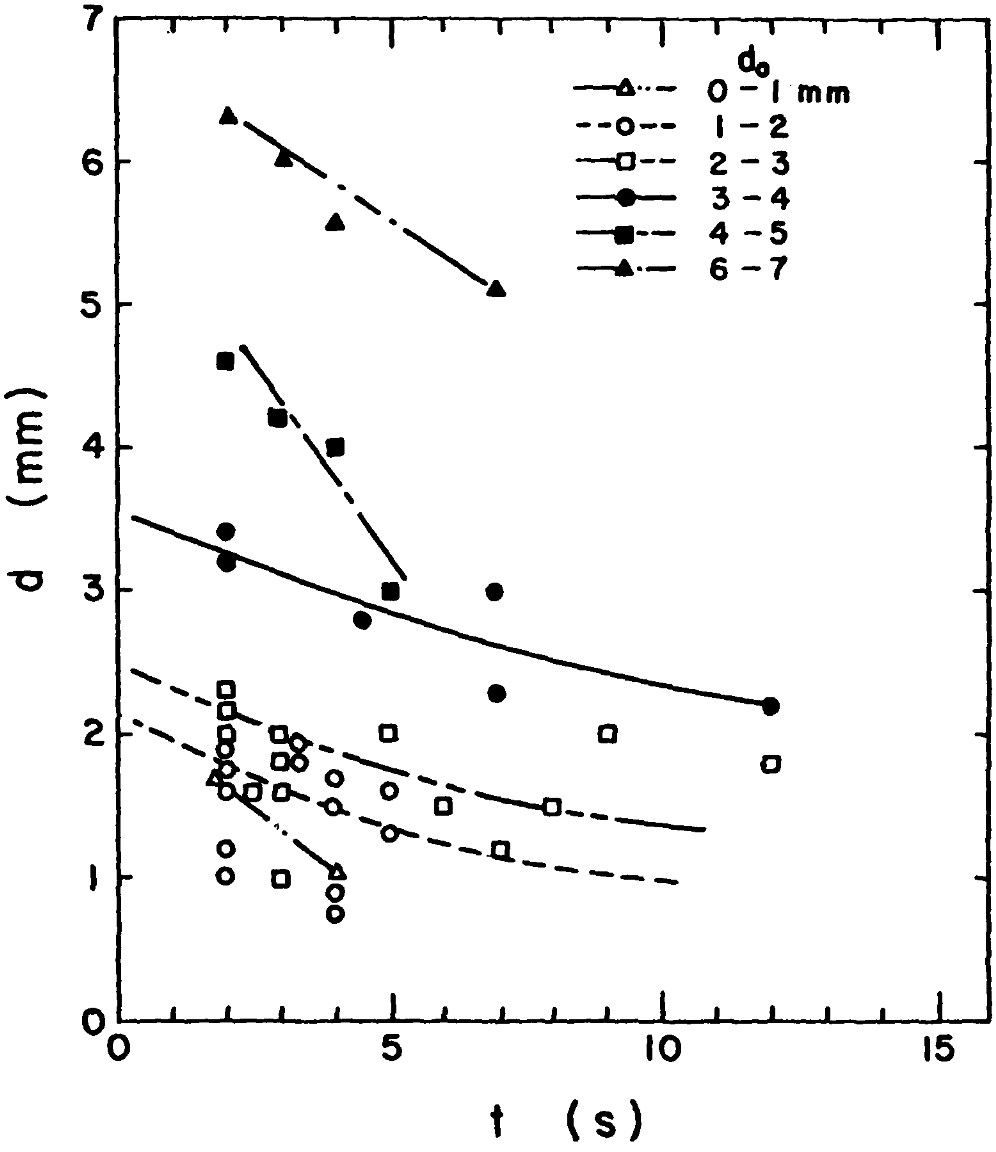

Fig. 16. Change of crystal diameter d with time t under a relative humidity of 100% and a temperature of $3^{o}C$.

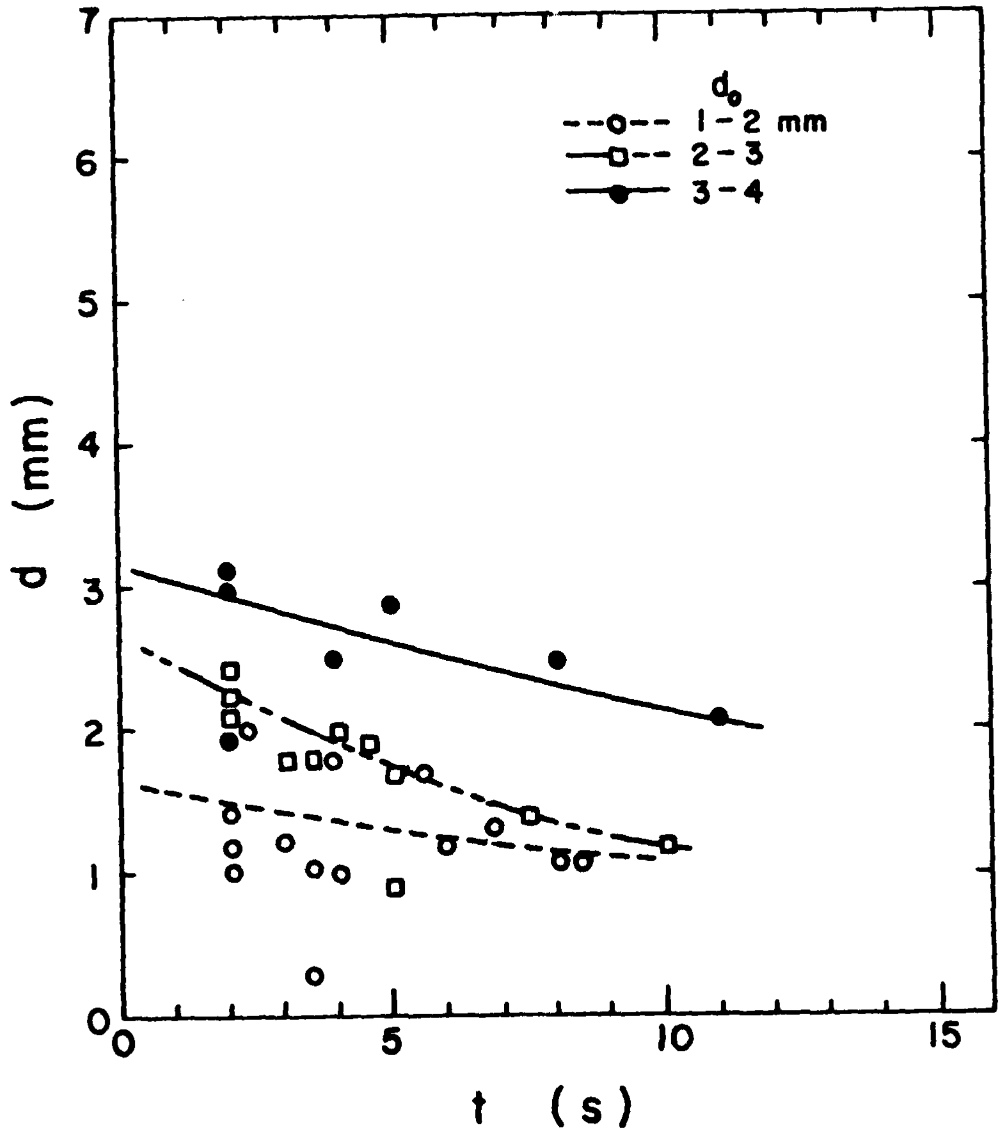

Fig. 17. Change of crystal diameter d with time t under a relative humidity of 90% and a temperature of 3°C.

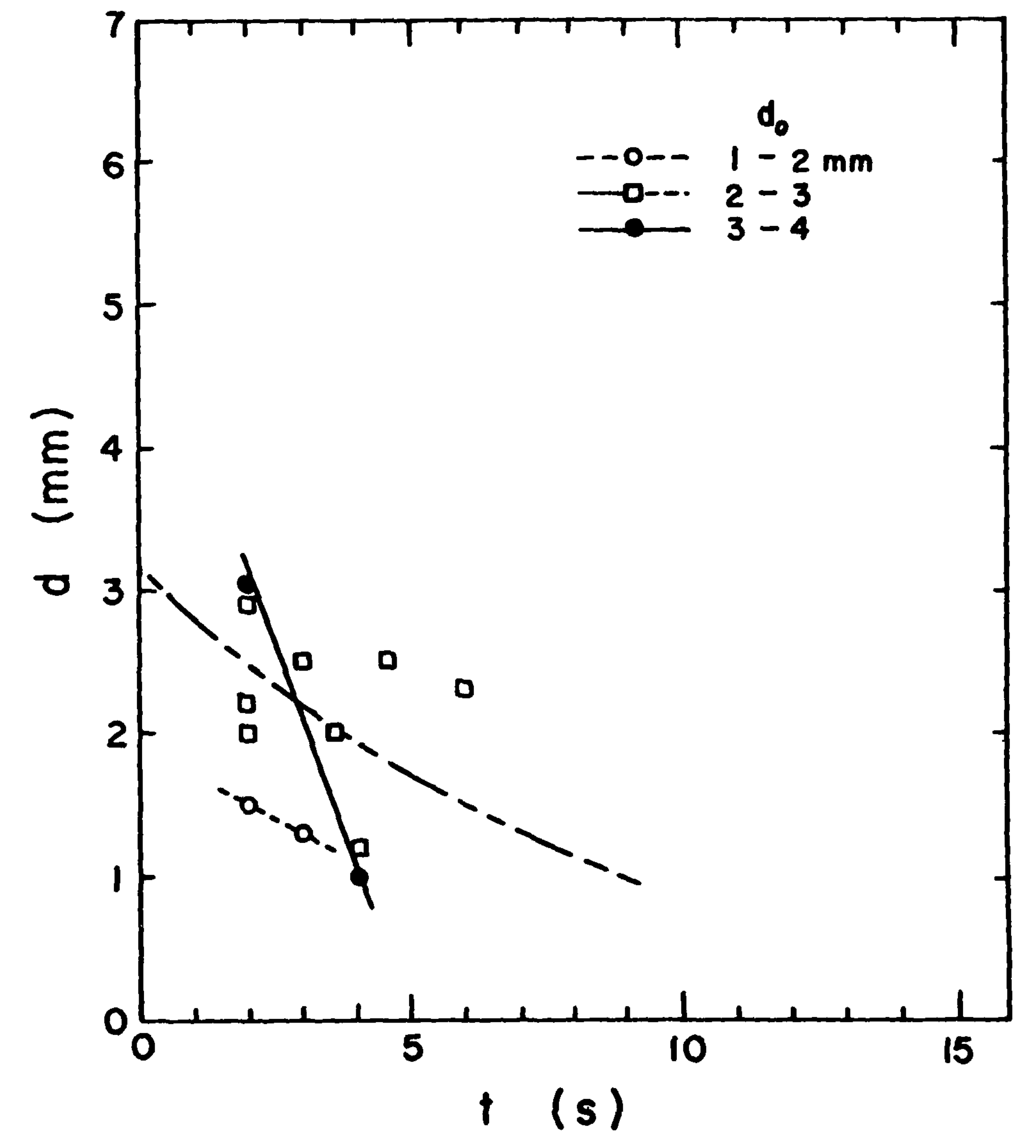

Fig. 18. Change of crystal diameter d with time t under a relative humidity of 90% and a temperature of 4°C.

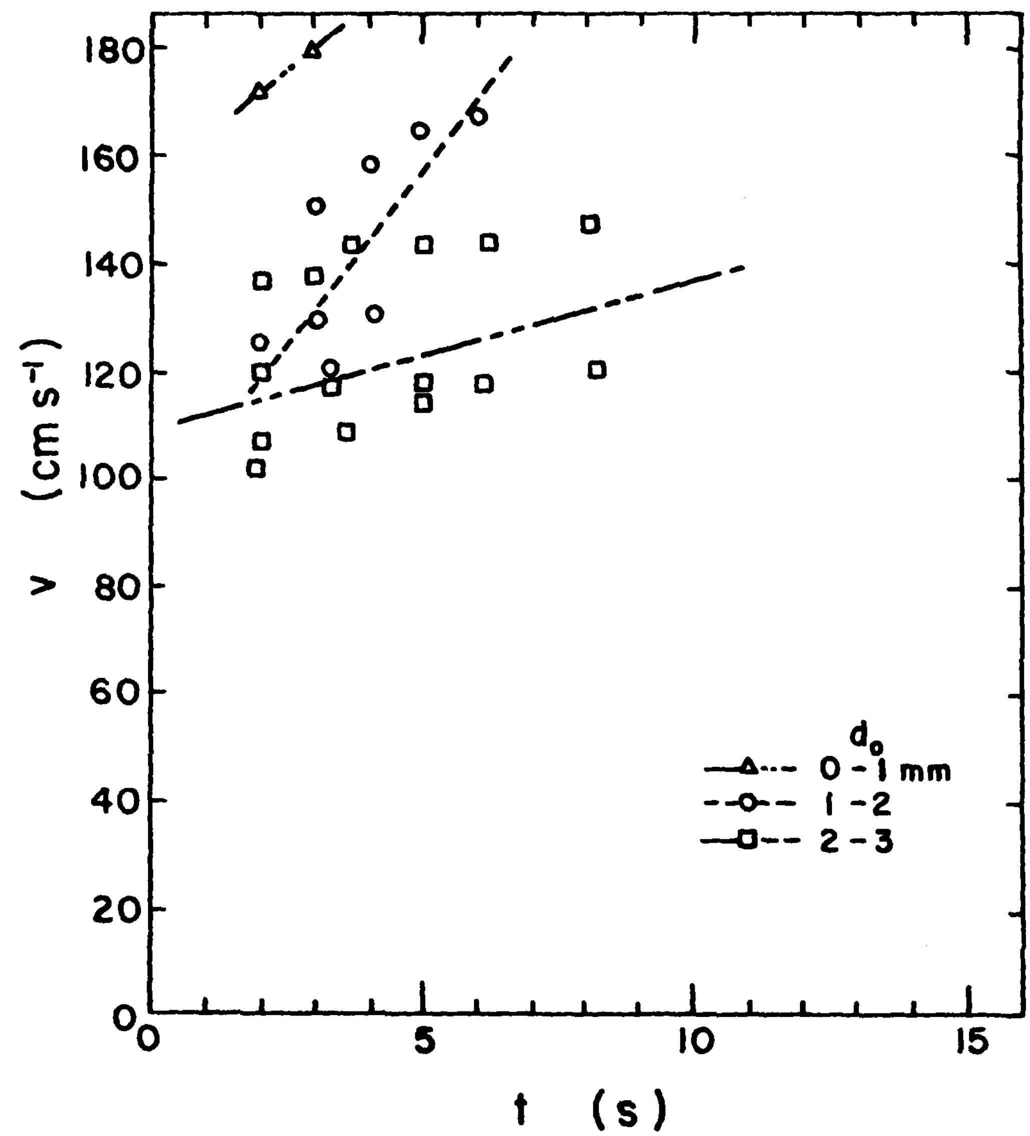

Fig. 19. Change of crystal fall velocity v with time t under a relative humidity of 100% and a temperature of 2^oC.

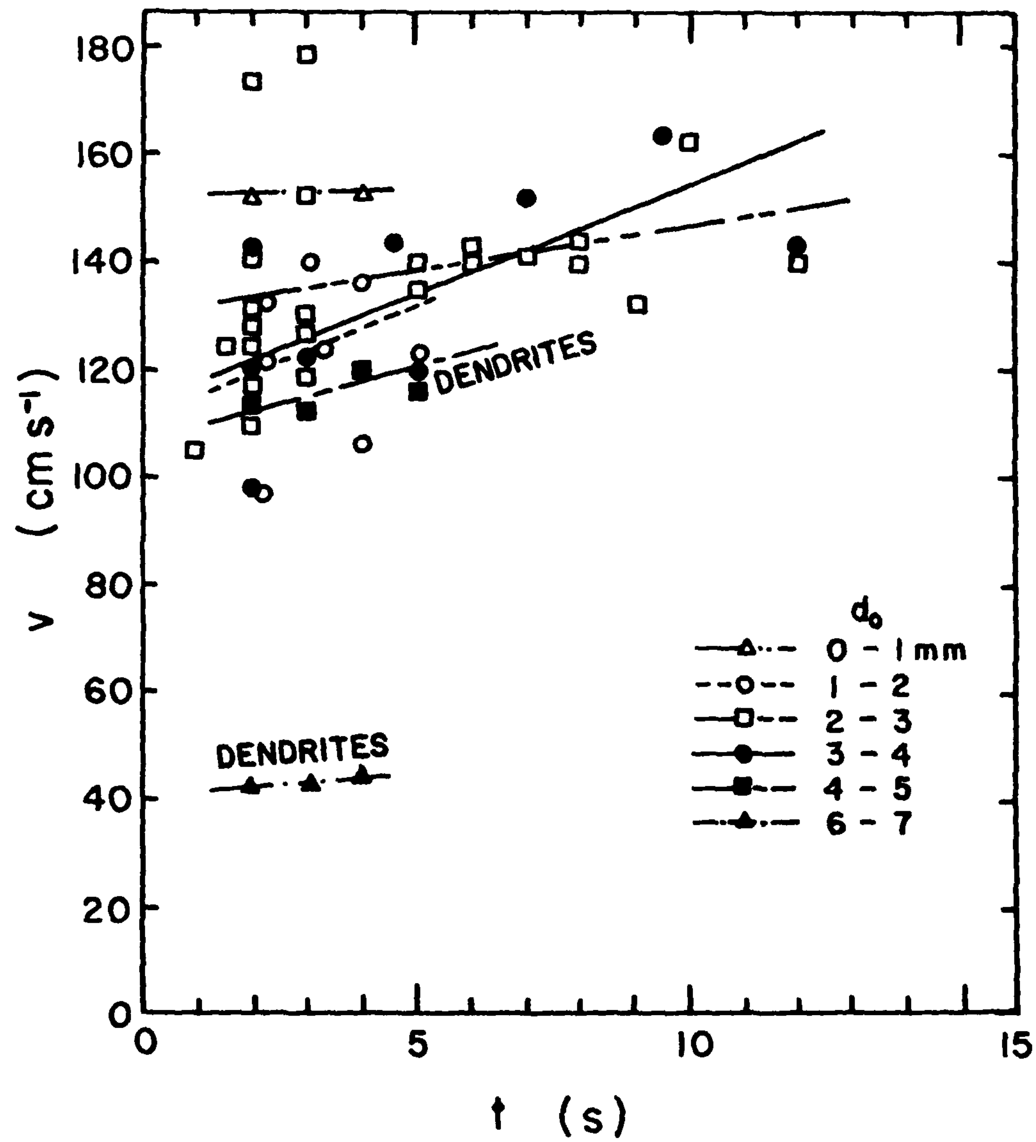

Fig. 20. Change of crystal fall velocity v with time t under a relative humidity of 100% and a temperature of 3°C.

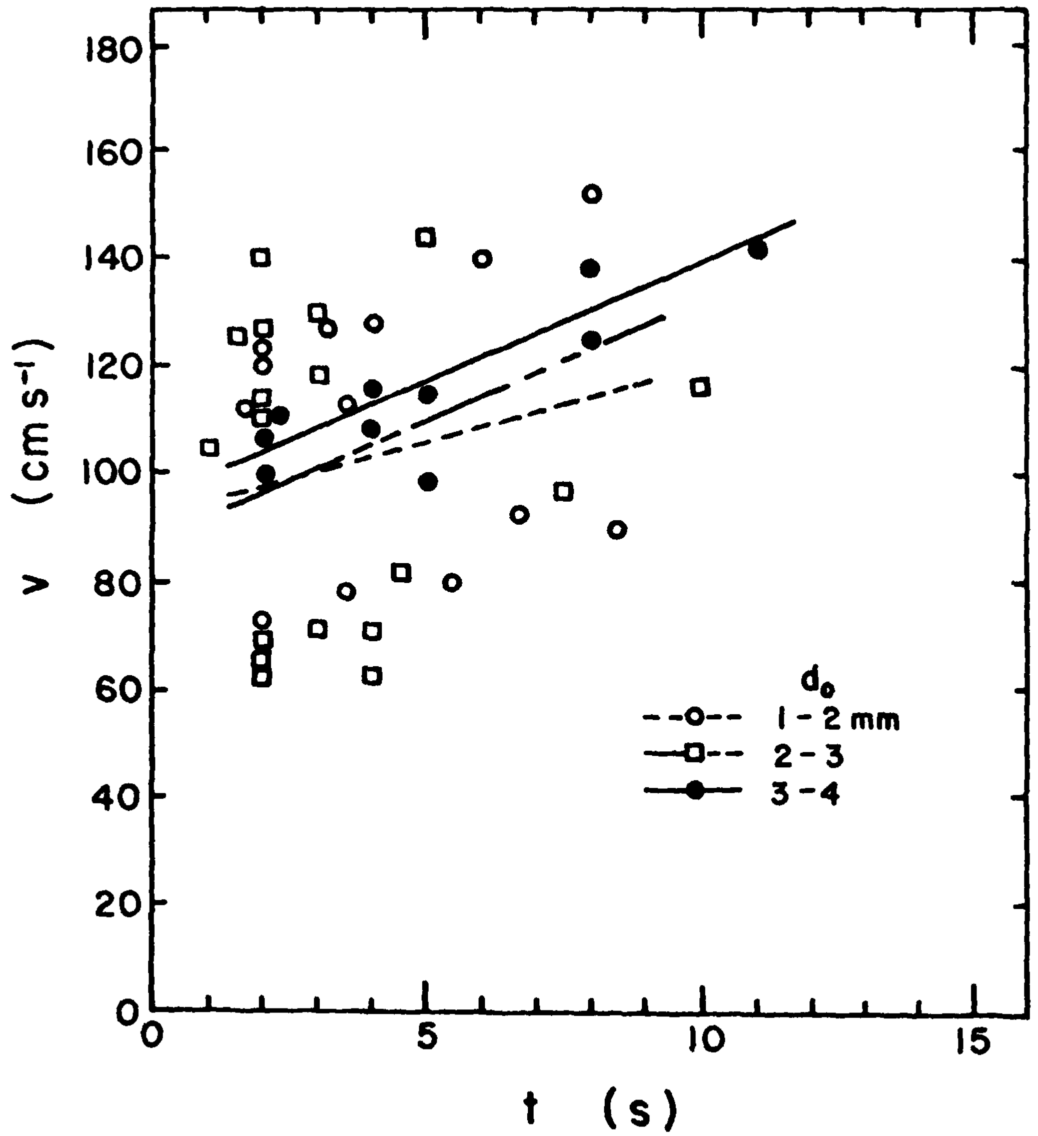

Fig. 21. Change of cry-+al fall velocity v with time t under a relative humidity of 90% and a temperature of 3^{o}C.

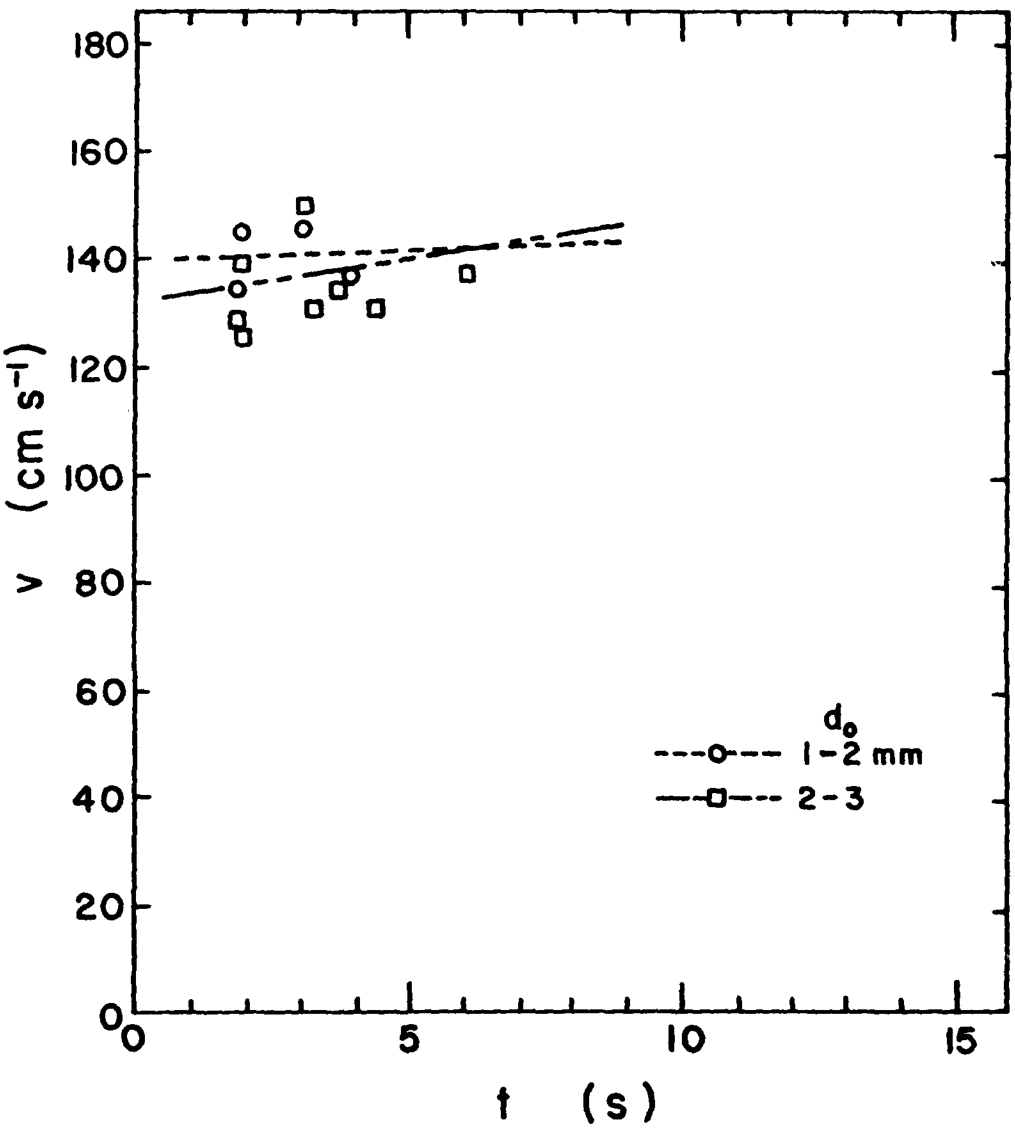

Fig. 22. Change of crystal fall velocity v with time t under a relative humidity of 90% and a temperature of 4°C.

Having analyzed the data for single ice crystal melting in a vertical wind tunnel under constant temperature and relative humidity, we found that there are eight groups of data which are useful to construct the regression equations for the time evolution of ice crystals. The conditions of the temperature and relative humidity of each group are listed in Table 1, along with the initial diameter.

Table 1 Environmental conditions and initial ice crystal diameter used for regression analysis of single crystal melting.

Group	Temperature (°C)	Relative humidity (%)	Initial Diameter (mm)
A	2	100	2.84
B	3	100	3.57
C	3	100	2.52
D	3	100	2.16
E	3	90	1.6
F	3	90	2.62
G	3	90	3.14
H	4	90	3.15

The regression equations constructed for each group of data are as follows for the diameter (mm)

$$d = d_0 + d_1 t + d_2 t^2 + d_3 t^3 + d_4 t^4 + d_5 t^5, \tag{1}$$

where d_0 through d_5 are constants.

For the fall velocity (cm s^{-1})

$$v = v_0 + v_1 t, \tag{2}$$

where v_0 and v_1 are constants. From the data of each group, we have determined

the coefficients in (1) and (2) used to draw regression lines in experimental data. For the group A, the regression lines for the diameter and the fall velocity as a function of time, are plotted respectively in Figs. 15 and 19. For groups B, C and D, the regression lines are plotted in Figs. 16 and 20, respectively. For groups E, F and G, they are plotted in Figs. 17 and 21 and for group H in Figs. 18 and 22.

The regression equations describing the change of diameter and fall velocity of the snow crystals can then be expressed on average as

$$d = d_o\ (1 + C_1 t + C_2 t^2 + C_3 t^3 + C_4 t^4 + C_5 t^5), \tag{3}$$

and

$$v = d_o\ (C_6 + C_7 t), \tag{4}$$

where d_o is the initial diameter. The constants in (3) and (4) are shown in Tables 2 and 3.

Table 2 Constants for the regression equation describing the diameter of snow crystals at different temperatures and relative humidities.

T (°C)	RH (%)	C_1 (s^{-1})	C_2 (s^{-2})	C_3 (s^{-3})	C_4 (s^{-4})	C_5 (s^{-5})
2	100	-0.12	5.27×10^{-3}	0.91×10^{-6}	-0.33×10^{-4}	0.22×10^{-5}
3	100	-0.07	0.96×10^{-2}	-0.24×10^{-2}	0.3×10^{-3}	-0.12×10^{-4}
3	90	-0.06	0.24×10^{-2}	0.41×10^{-3}	-0.1×10^{-3}	0.56×10^{-5}
4	90	-0.1	0.07×10^{-1}	0.3×10^{-2}	-0.035×10^{-2}	0.15×10^{-4}

Table 3 Constants for the regression equation describing the fall velocity of snow crystals at different temperatures and relative humidities.

Temperature (°C)	Relative Humidity (%)	C_6	C_7
2	100	38.66	1.17
3	100	40.25	1.27
3	90	35.19	1.45
4	90	41.74	0.6

Furthermore, we can generalize the equations considering the environmental temperature $T_\infty = T_o + \Delta T$, T_o being the melting point of ice,

$$d = d_o \ (1 + \alpha_1 \Delta Tt + \alpha_2 \Delta Tt^2 + \alpha_3 \Delta Tt^3 + \alpha_4 \Delta Tt^4 + \alpha_5 \Delta Tt^5), \tag{5}$$

and

$$v = d_o \ (\beta_o + \beta_1 \Delta T + \beta_2 \Delta Tt), \tag{6}$$

where β_o through β_2 are constants. The constants in (5) and (6) are given in Tables 4 and 5. We can notice that for $\Delta T = 0°C$, the snow crystal will keep its size with constant fall velocity.

Table 4 Constants for the generalized equation describing the diameter of snow crystals at different relative humidities.

RH (%)	α_1 ($°C^{-1}s^{-1}$)	α_2 ($°C^{-1}s^{-2}$)	α_3 ($°C^{-1}s^{-3}$)	α_4 ($°C^{-1}s^{-4}$)	α_5 ($°C^{-1}s^{-5}$)
100	-0.35×10^{-1}	0.3×10^{-2}	-0.56×10^{-3}	0.64×10^{-4}	-0.25×10^{-5}
90	-0.23	-0.89×10^{-3}	0.53×10^{-3}	-0.69×10^{-4}	0.31×10^{-5}

Table 5 Constants for the generalized equation describing the fall velocity of snow crystals at different relative humidities.

RH (%)	β_o (s^{-1})	β_1 ($°C^{-1}s^{-2}$)	β_2 ($°C^{-1}s^{-2}$)
100	39.45	0.06×10^{-1}	0.47
90	38.47	0.13	0.27

3.3 Snowflake melting

3.3.1 Results of measurement and discussion

The previously mentioned problems of suspending snowflakes reduced the number of cases observed to 42:

Relative Humidity (%)	Temperature (°C)	Number of Cases
90	3	1
	4	16
100	2	4
	3	15
	4	5

Snowflakes were initially identified from the photographs taken. From the observations, particles larger than 2.5 and 1.0 mm (a and c dimensions) were considered snowflakes and included in this study.

In analyzing the data, several assumptions were made. As mentioned above, an enveloping ellipsoid was used to represent the size of a snowflake. No attempt was made to compensate for the amount of the ellipsoid filled by the outer dimensions of the snowflake. Therefore, the snowflakes were all assumed to have been in the chamber environment for two seconds by the time the first photograph was taken as in the case of single crystals.

Finally, the melting time had to be estimated due to the disruption phenomenon, along with the apparent inability of our air velocity profile to suspend change of fall velocities for like groups under the same relative humidity conditions but different temperatures (Figs. 26 and 27). The velocity increase appears to be faster under the higher temperature (3°C) because the drop is melting faster, thus its cross-sectional area becomes smaller more rapidly.

Fall Velocity Change

Fig. 23 shows the fall velocity change with time for six area catagories of snowflakes. These areas represent maximum horizontal cross-sectional areas, perpendicular to the direction of fall. All conditions observed are included in the figure. With the exception of the 15-20 and 25-30 mm^2 area groups, flakes with larger areas seemed to fall faster than those with smaller areas. A comparison of the fall velocities of equal area groups under the same temperature but different relative humidities suggests some interesting information. Fig. 24 shows fall velocities under 90% relative humidity and temperature of 4°C. Fig. 25 gives fall velocities for the same temperature but with a relative humidity of 100%. The fall velocity increase for the same size snowflake appears to be faster in the 100% relative humidity environment than in the 90%. This may be explained by noting that in an environment of 90% relative humidity, evaporative cooling or lowered condensation heating reduces the rate of melting, therefore the rate of velocity increase. Whereas, in the saturated environment, melting occurs without this effect, so melting proceeds relatively rapidly causing faster velocity change. This tendency is seen also in the change of fall velocities for like groups under the same relative humidity conditions but different

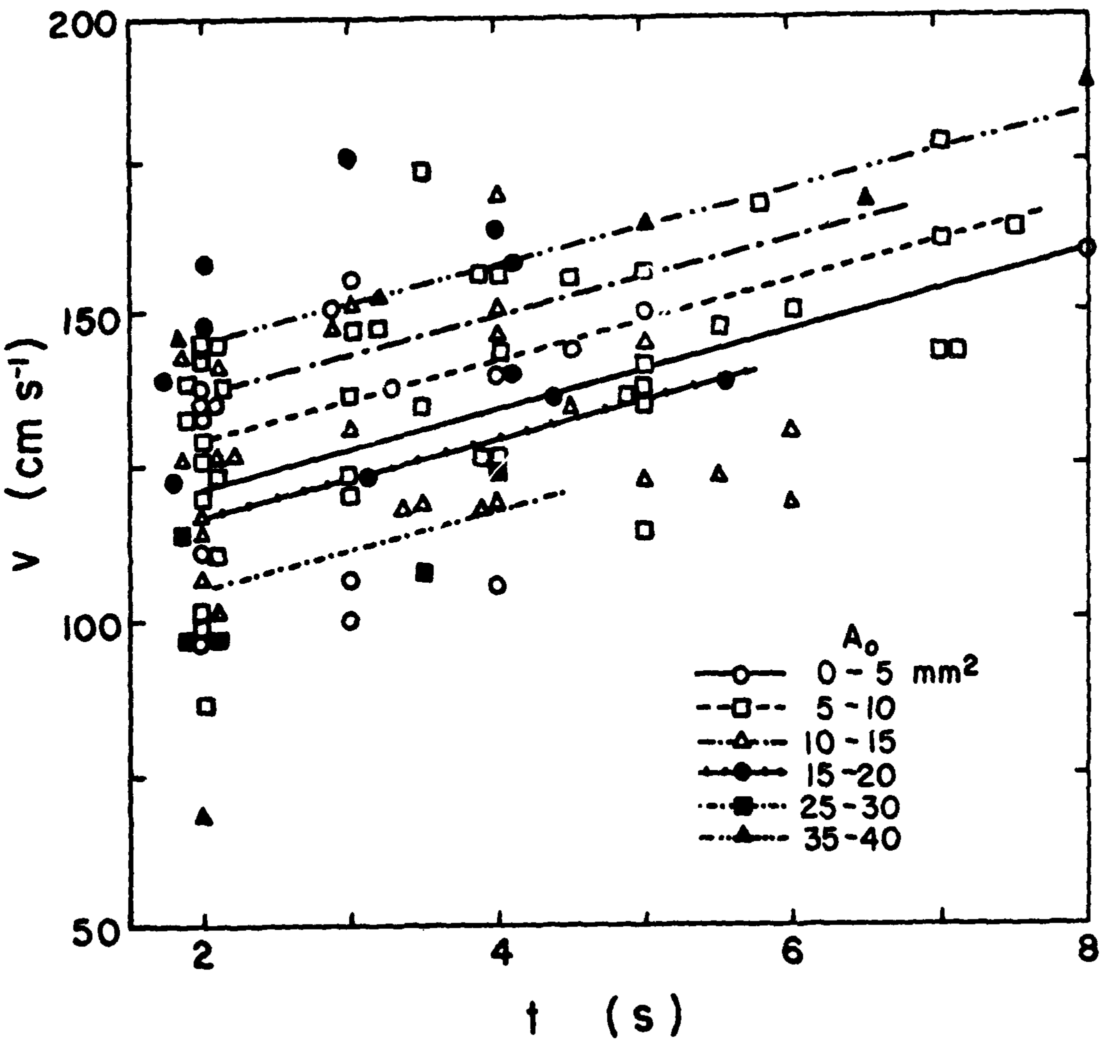

Fig. 23. Fall velocity vs time.

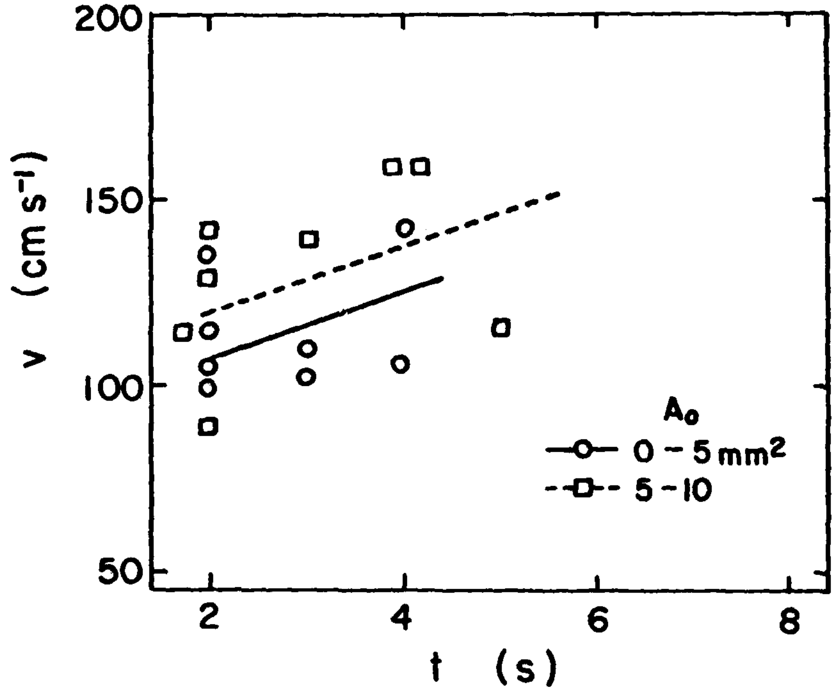

Fig. 24. Fall velocity vs time at $4^{o}C$, 90% RH.

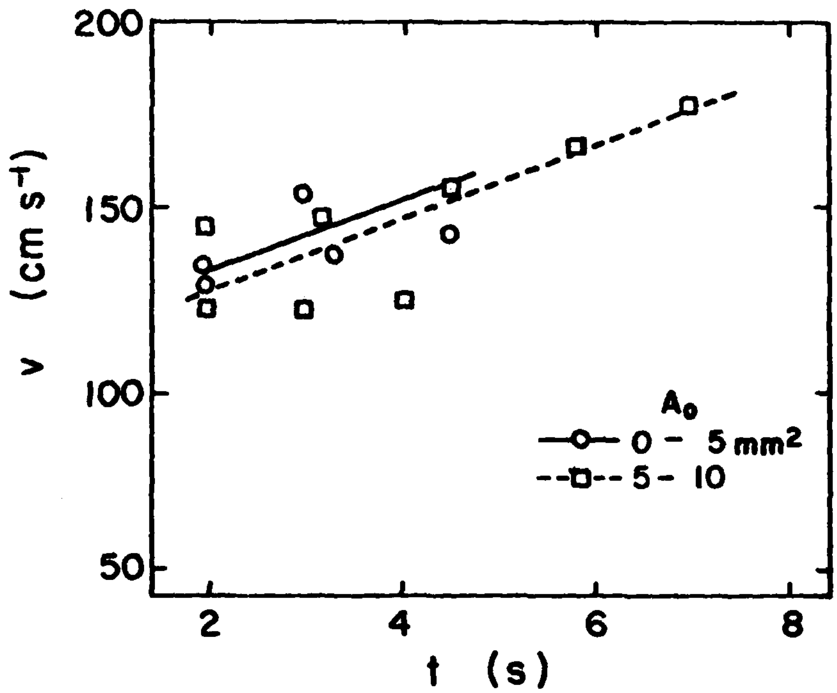

Fig. 25. Fall velocity vs time at $4^{o}C$, 100% RH.

temperatures (Figs. 26 and 27). The velocity increase appears to be faster under the higher temperature (3°C) because the drop is melting faster, thus its cross-sectional area becomes smaller more rapidly. This area should be studied further.

Shape Change

Fig. 28 shows the various area groups to be decreasing towards final values (the areas of the water droplets). Observations proved that snowflakes melted at such a rate that their suspension was controllable, until they disrupted. This disruption size was not predictable. Because this disruption occurred so quickly, a photograph could not be obtained for analysis. For analysis of the data shown in Figs. 28 thorugh 32, one must be cautious considering the disruption phenomenon that exists frequently at the end of the measurement.

Melting Rates

Examination of melting time versus the initial diameter of the snowflakes in Fig. 33 yields some interesting information. Current theory of snowflake melting (Matsuo and Sasyo, 1981a) predicts a curve which is concave upwards (by treating the snowflake as a solid object), while our data shows a convex curve. The melting time increases with the initial size, but there is no appreciable time difference between sizes. This may be because snowflakes are of a porous structure, not solid, thus allowing the air to pass through them. This air passing through the structure as it falls makes the heat transfer distance from the passing air nearly as small as that for a small ice crystal. Thus the crystals which make up the snowflake can melt somewhat independently of each other. The larger the snowflake, the larger the ice

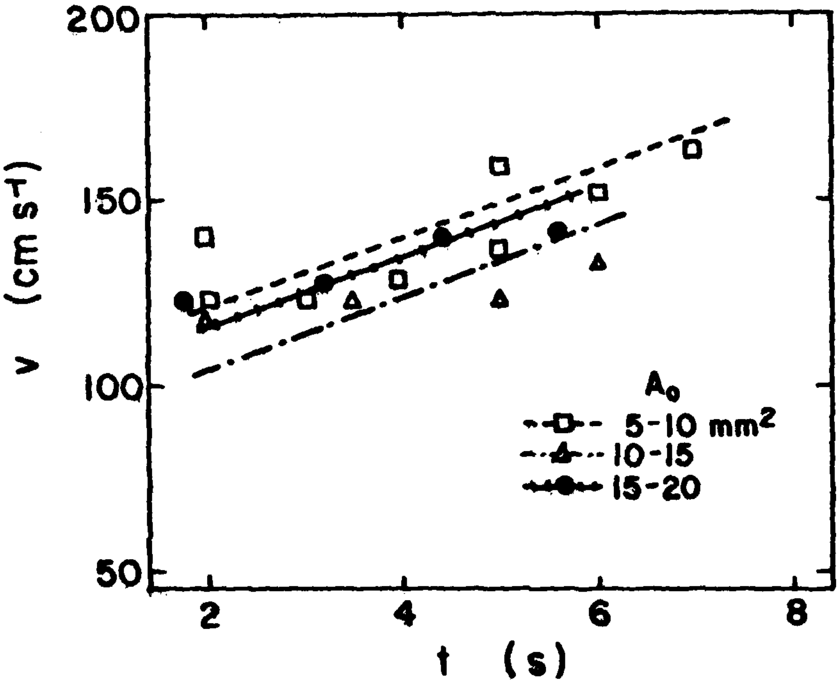

Fig. 26. Fall velocity v vs time t at 2°C, 100% RH.

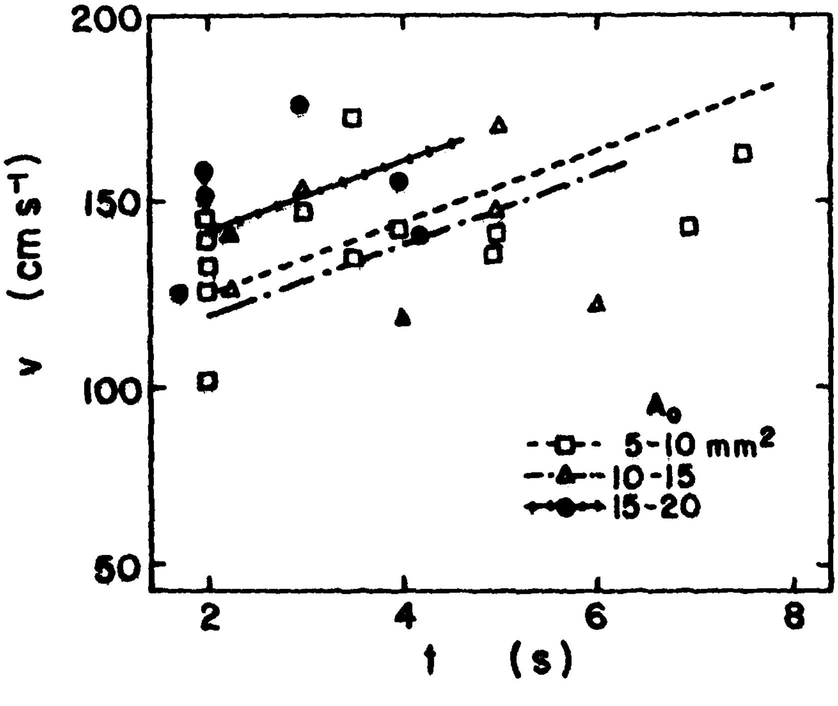

Fig. 27. Fall velocity v vs time t at 3°C, 100% RH.

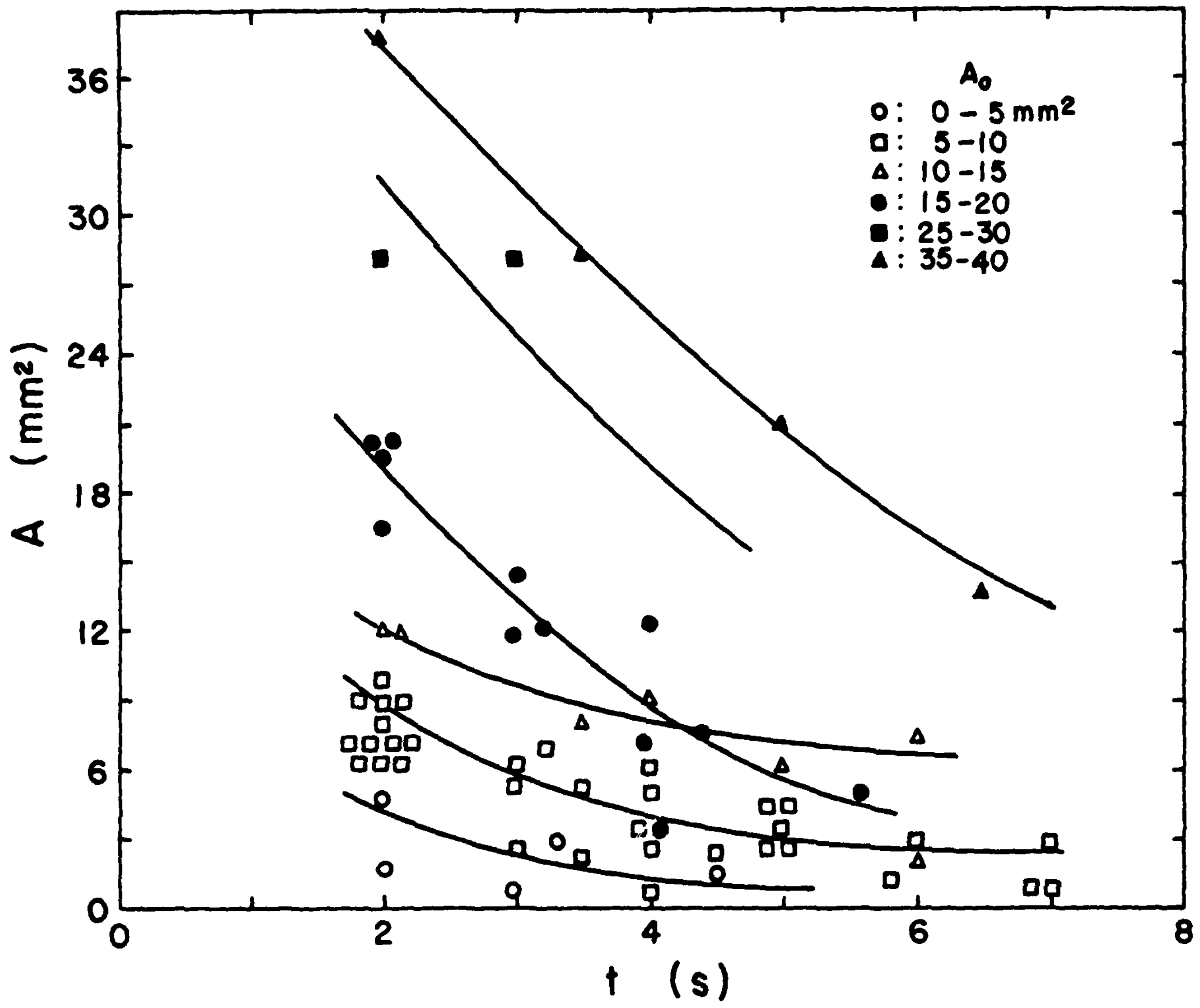

Fig. 28. Horizontal cross-sectional area A vs time t.

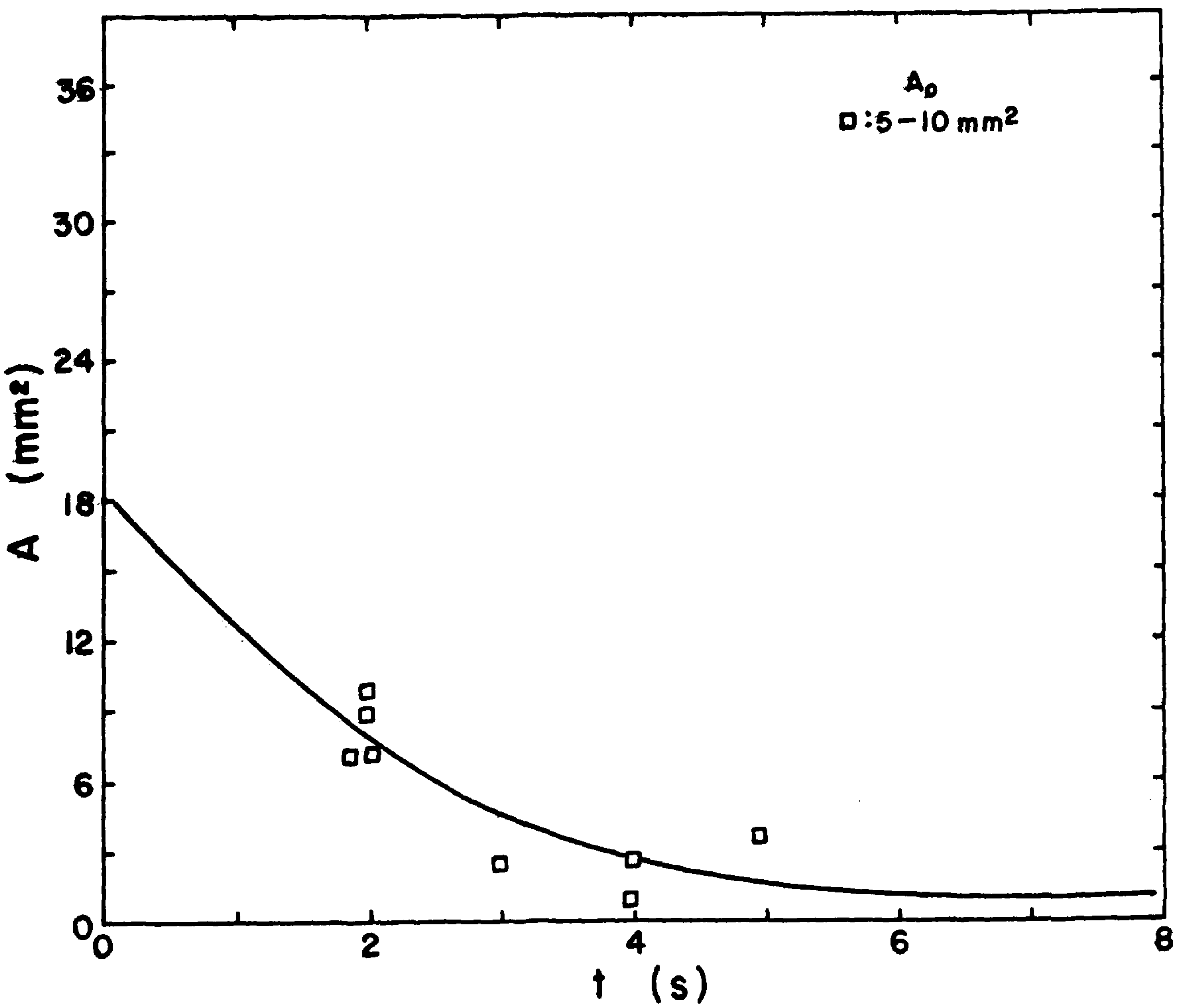

Fig. 29. Horizontal cross-sectional area A vs time t at 4^oC, 90% RH.

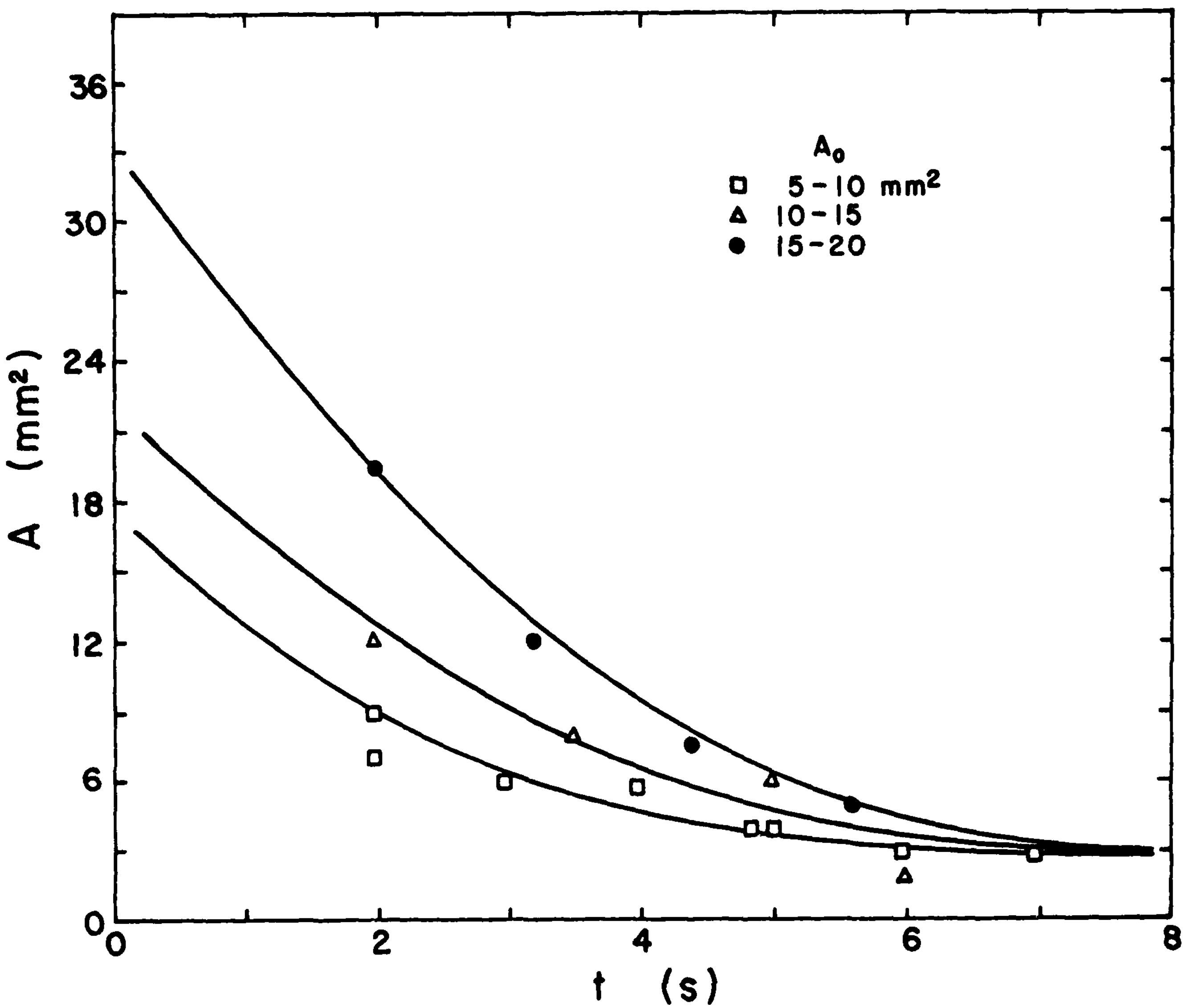

Fig. 30. Horizontal cross-sectional area A vs time t at $2^{O}C$, 100% RH.

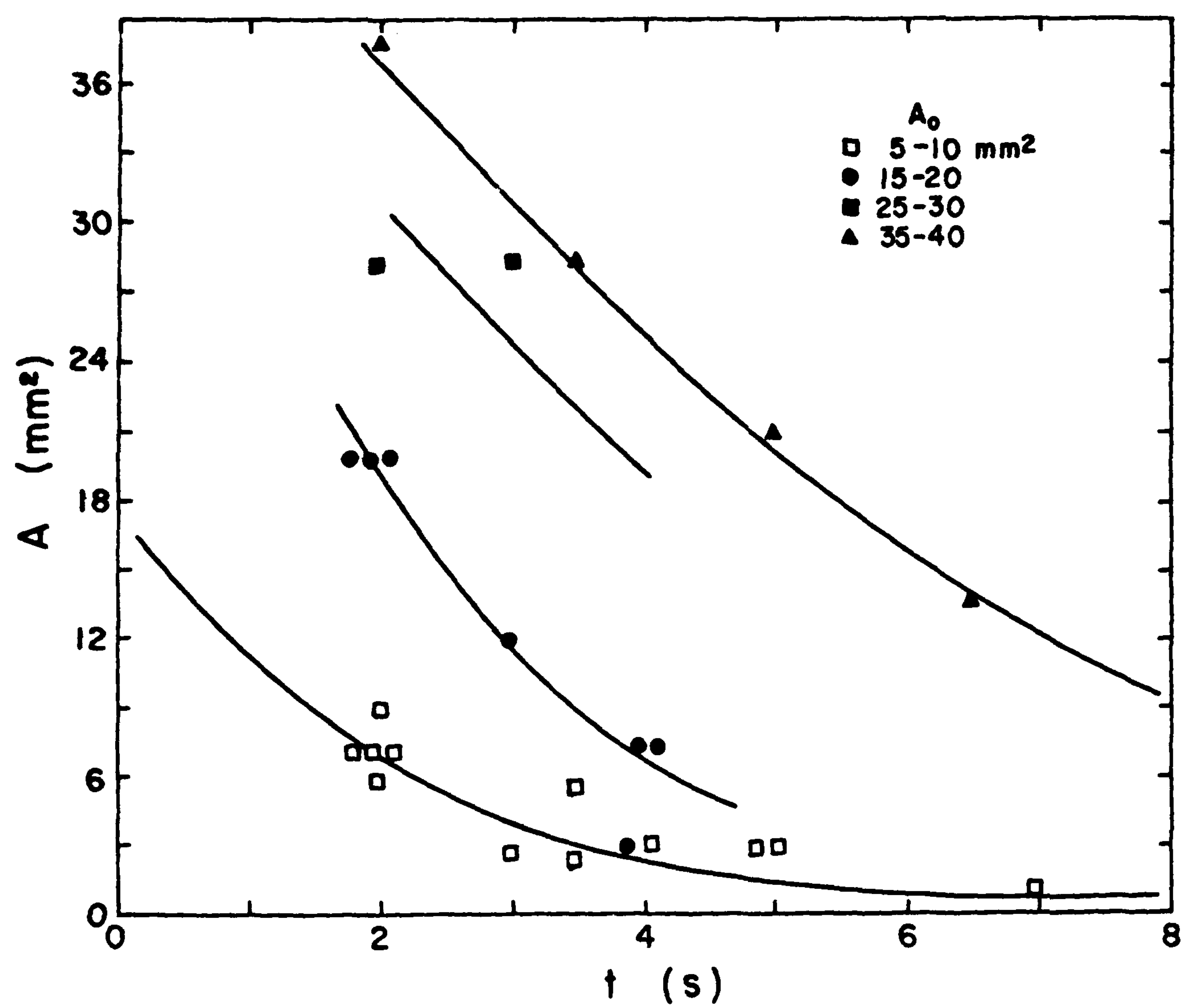

Fig. 31. Horizontal cross-sectional area A vs time t at 3°C, 100% RH.

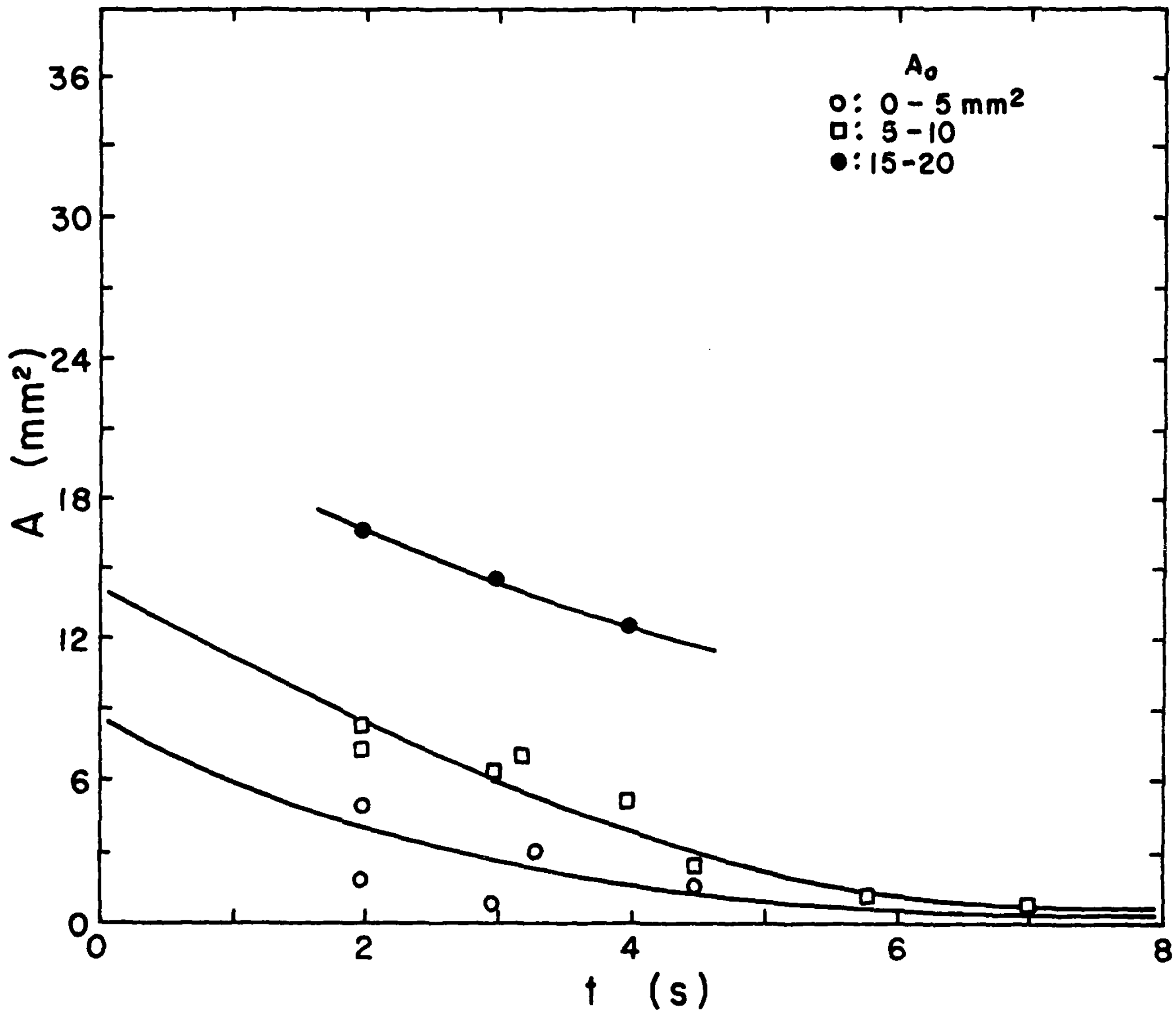

Fig. 32. Horizontal cross-sectional area A vs time t at 4^oC, 100% RH.

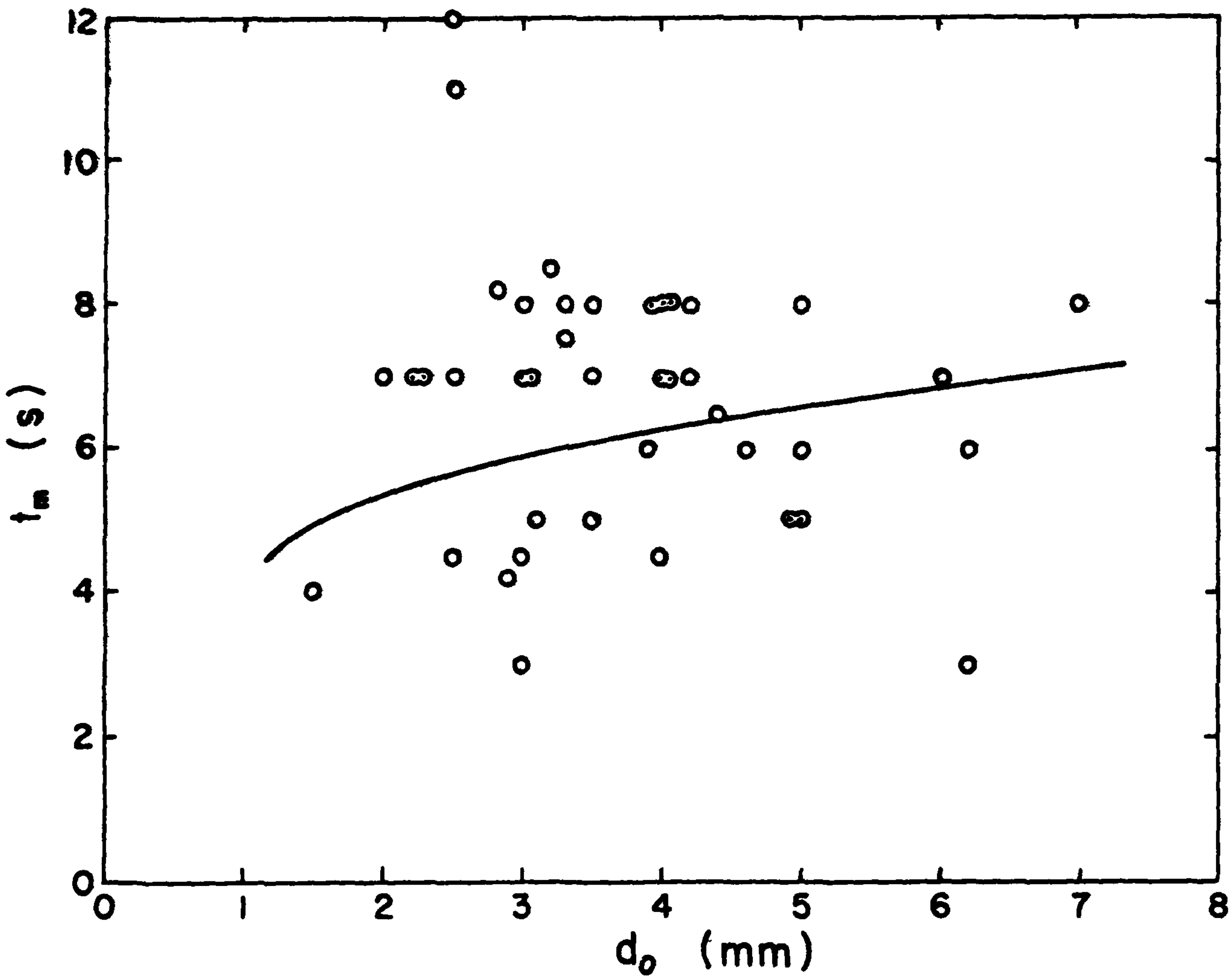

Fig. 33. Melting time t_m vs initial diameter d_o.

skeleton, which would make this process more inefficient thereby giving the slightly longer melting time. The effect of relative humidity on the melting time of snowflakes was studied by Matsuo and Sasyo (1982b and c). Our data shown in Figs. 34 and 35 are, however, not sufficient to check the effect.

3.3.2 Regression analysis

There are 7 groups of snowflake melting data which are useful for the regression analysis to describe the time evolution of snowflake behaviors. The conditions of the temperature and relative humidity of each group are listed in Table 6, along with the intitial area and initial diameter determinted by the regression analysis.

Table 6 Environmental and initial snowflake conditions used for regression analysis of snowflake melting.

Group	T (°C)	RH (%)	A_0 (mm^2)	d_0 (mm)
A	2	100	33.23	6.51
B	2	100	22.38	5.34
C	2	100	17.7	4.75
D	3	100	17.51	4.72
E	3	100	40.2	7.15
F	4	100	14.19	4.23
G	4	100	8.38	3.16

For groups A, B and C, the regression lines of the change of area, and fall velocity with respect to time are plotted in Figs. 30 and 26, respectively. For groups D and E, same plots are shown in Figs. 31 and 27. For groups F and G, they are shown in Figs. 32 and 27.

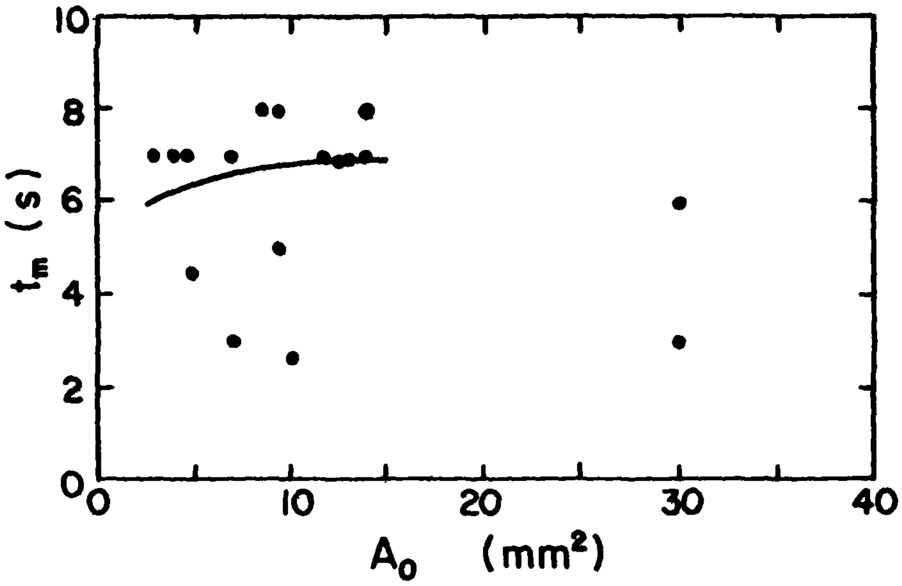

Fig. 34. Melting time t_m vs initial horizontal cross-sectional area A_o at 90% RH.

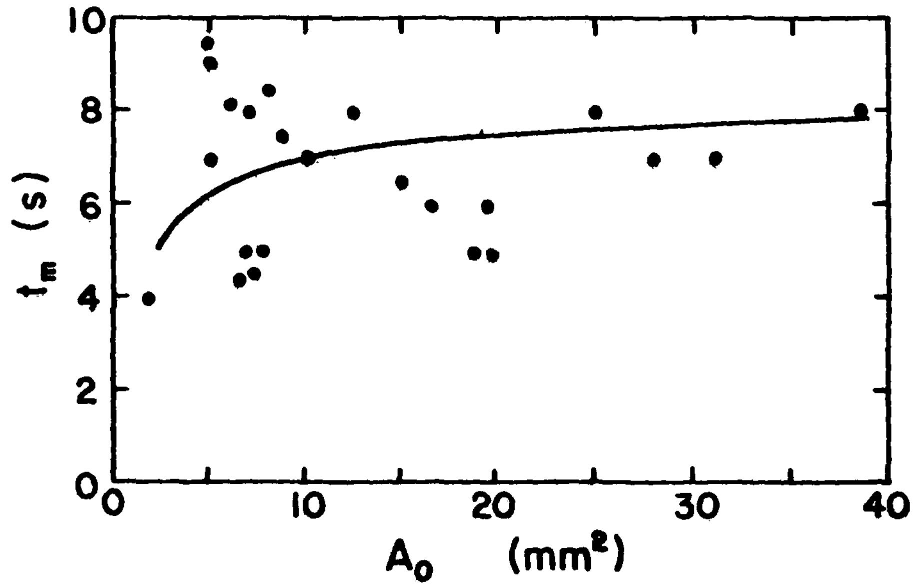

Fig. 35. Melting time t_m vs initial horizontal cross-sectional area A_o at 100% RH.

Assuming that the surface of snowflake is spherical, we can express the cross-sectional area $A = \frac{\pi}{4}d^2$, where d is the diameter. The regression equations describing the time variation of diameter and fall velocity of the snowflakes, therefore, are expressed as:

$$d = d_0\ (1 + C_1 t + C_2 t^2 + C_3 t^3 + C_4 t^4 + C_5 t^5), \tag{7}$$

and

$$v = d_0\ (v_0 + v_1 t), \tag{8}$$

where d_0 is the initial diameter. The constants in (7) and (8) are listed in Tables 7 and 8.

Table 7 Constants for the regression equation describing the diameter of snowflakes at different temperature and relative humidity.

T (°C)	RH (%)	C_1 (s^{-1})	C_2 (s^{-2})	C_3 (s^{-3})	C_4 (s^{-4})	C_5 (s^{-5})
2	100	-0.13	0.62×10^{-2}	0.25×10^{-2}	0.58×10^{-3}	-0.33×10^{-4}
3	100	-0.16	0.16×10^{-1}	0.6×10^{-2}	-0.41×10^{-3}	0.29×10^{-5}
4	100	-0.12	-0.55×10^{-2}	0.13×10^{-2}	-0.64×10^{-4}	0.46×10^{-5}

Furthermore, we can generalize these equations considering the effect of environmental temperature:

$$d = d_0\ (1 + \alpha_1 \Delta T t + \alpha_2 \Delta T t^2 + \alpha_3 \Delta T t^3 + \alpha_4 \Delta T t^4 + \alpha_5 \Delta T t^5), \tag{9}$$

and

$$v = d_0\ (\beta_0 + \beta_1 \Delta T + \beta_2 \Delta T t), \tag{10}$$

Table 8 Constants for the regression equation describing the fall velocity of snowflakes at different temperature and relative humidity.

T (°C)	RH (%)	V_0 (s^{-1})	V_1 (s^{-2})
2	100	16.91	1.7
3	100	18.64	1.59
4	100	29.23	2.47

to describe the evolution of melting snowflakes under constant temperature ΔT (°C) and 100% RH. The constants in (9) and (10) are given in Tables 9 and 10. It is clear that when ΔT = 0°C, the snowflake will keep its size with constant fall velocity.

Table 9 Constants for the generalized equation describing the diameter of melting snowflakes.

RH (%)	α_1 ($°C^{-1}s^{-1}$)	α_2 ($°C^{-1}s^{-2}$)	α_3 ($°C^{-1}s^{-3}$)	α_4 ($°C^{-1}s^{-4}$)	α_5 ($°C^{-1}s^{-5}$)
100	-0.042	-0.2×10^{-2}	0.63×10^{-3}	-0.11×10^{-4}	-0.13×10^{-5}

Table 10 Constants for the generalized equation describing the fall velocity of melting snowflakes.

RH (%)	β_0 (s^{-1})	β_1 ($°C^{-1}s^{-1}$)	β_2 ($°C^{-1}s^{-2}$)
100	21.59	0.43	0.62

3.3.3 Factor ε

For the melting of snowflakes, it may be assumed that the heat transfer rate to the surface of snowflake, dQ/dt, is equal to the sensible heat conduction from the environment and the latent heat transfer by condensing water vapor on the surface. For a spherical snowflake,

$$\frac{dQ}{dt} = 4\pi r(f_h K \Delta T + L_c f_v D \Delta\rho), \tag{11}$$

where

- r: radius
- f_h: ventilation coefficient of snowflakes for heat diffusion
- K: thermal conductivity of air
- ΔT: temperature difference between the environment and snowflake ($\Delta T = T_\infty - T_w$)
- L_c: latent heat of condensation of water vapor
- f_v: ventilation coefficient of snowflakes for water vapor diffusion
- D: coefficient of molecular diffusion of water vapor in air
- $\Delta\rho$: difference between water vapor density in environment and equilibrium water vapor density at snowflake surface. ($\Delta\rho = \rho_\infty - \rho_{w,sat}$)

It should be pointed out that the thermal conductivity of water is more than 20 times larger than that of the air, and the thickness of water layer is much smaller than that of air layer through which heat conduction proceeds. Therefore, we assume that $T_w = 0°C$ and $\rho_{w,sat} = \rho_0$, where ρ_0 is the saturation vapor density at $T = 0°C$. Furthermore, we assume that for a non-spherical snowflake, (11) is appliable with a factor ε on the right-hand side where ε is the factor comprising all the effects due to the non-spherical shape.

Also, we may assume that the total amount of heat transferred from the

air stream for given time interval Δt, is totally consumed by melting the ice existing in the surface layer of Δr thickness. Therefore, (11) is transformed to

$$-L_f 4\pi r^2 \rho_i \Delta r = 4\pi r \varepsilon (f_h K \Delta T + L_c f_v D \Delta \rho)\ \Delta t, \qquad (12)$$

where

L_f: latent heat of fusion
ρ_i: density of ice skeleton.

As $\Delta t \to 0$, (12) can be rewritten as

$$-r\frac{dr}{dt} = \frac{\varepsilon}{L_f \rho_i} (f_h K \Delta T + L_c f_v D \Delta \rho). \qquad (13)$$

Therefore, ε can be determined from (13), with the ventilation coefficients being expressed as

$$f = f_h = f_v = 1 + 0.24\ Re^{\frac{1}{2}}, \qquad (14)$$

(Matsuo and Sasyo, 1981), where Re is the Reynolds number.

Obviously, (14) indicates that the value of ε changes with time. Hence, applying the regression equations about diameter and fall velocity described earlier, we may obtain

$$\varepsilon = d_o\ (\varepsilon_o + \varepsilon_1 t^1 + \varepsilon_2 t^2 + \varepsilon_3 t^3 + \varepsilon_4 t^4 + \varepsilon_5 t^5). \qquad (15)$$

The constants in (15) for snowflakes are listed in Table 11.

Further, we may generalize the equation

$$\varepsilon = d_0\ \Delta T\ (b_0 + b_1 t + b_2 t^2 + b_3 t^3 + b_4 t^4 + b_5 t^5), \qquad (16)$$

for describing the change of ε of the snowflake melting with constant temperature ΔT (°C) and 100% Relative Humidity. The constants in (16) are given in Table 12.

Table 11 Constants in equation (15) for describing the ε of snowflakes.

T (°C)	RH (%)	ε_0 (mm^{-1})	ε_1 ($mm^{-1}s^{-1}$)	ε_2 ($mm^{-1}s^{-2}$)	ε_3 ($mm^{-1}s^{-3}$)	ε_4 ($mm^{-1}s^{-4}$)	ε_5 ($mm^{-1}s^{-5}$)
2	100	4.09	-0.45	-0.19×10^{-1}	-0.16×10^{-2}	-0.59×10^{-3}	0.99×10^{-4}
3	100	3.45	-0.16	-0.9	0.11×10^{-1}	0.34×10^{-2}	-0.3×10^{-3}
4	100	1.52	-0.17	0.7×10^{-2}	-0.61×10^{-3}	-0.65×10^{-3}	0.74×10^{-4}

Table 12 Constants in equation (16) for the generalized description of ε.

RH (%)	b_0 $(mm°C)^{-1}$	b_1 $(mm°Cs)^{-1}$	b_2 $(mm°Cs^2)^{-1}$	b_3 $(mm°Cs^3)^{-1}$	b_4 $(mm°Cs^4)^{-1}$	b_5 $(mm°Cs^5)^{-1}$
100	0.85	-0.71×10^{-1}	-0.2×10^{-1}	0.99×10^{-3}	0.22×10^{-3}	-0.14×10^{-4}

4. Theories of Ice Crystal and Snowflake Melting

When ice melts, the latent heat of fusion is absorbed by the ice and the heat is normally supplied from outside. So, melting proceeds inwards from the outer edges and surfaces of the ice.

In melting of snow crystals and snow flakes during their fall through zones of temperature higher than 0°C, the manner the heat is supplied to the ice surfaces controls the melting. Heat may be transported to the ice surfaces through the air normally in the following three mechanisms; radiative

transfer, sensible heat conduction and latent heat transfer by water vapor diffusion. While the atmospheric ice melting proceeds, the cloud above and the falling melted crystals below the melting layer sustain a radiative balance in the zone. Under such a balance at a temperature as low as 0°C, the radiative heat transfer to the melting layer may be ignored. The heat transfer to the surface of melting ice in the atmosphere may therefore be described by two other mechanisms, i.e., sensible and latent heat transfers.

If an ice crystal is placed in quiescent warm air without fall, a temperature field will establish around the crystal and sensible heat conduction occurs from the environment to the crystal through the field. The latent heat transfer takes place in an identical manner but the direction depends on the condition of the environment. If the environment is dry, heat removal takes place due to evaporation cooling. These processes are reasonably well understood with respect to ice crystal growth under supercooled environment although their directions may be partially or totally reversed.

Ice melting in the atmosphere takes place while ice crystals fall. The fall results in sheared air motions (convection) around the crystals, thereby deforming the temperature and water vapor fields of quiescent air. The fall motion of an ice crystal modifies the field most extensively at the distal points if the crystal shape were plate-like or prism-like. The distal points are for this reason the zones of fastest ice crystal melting. As ice melting proceeds, formed water should show a tendency of taking a shape of smaller surface area. Since the shape that takes the smallest surface area for a given volume is a sphere, the ice crystal shrinks from the distal points. This shape change of ice crystal during the melting leads to an increase in the fall speed. The fall speed increase in turn

alters the convective air motion around the crystal and further modifies the accompanied temperature and vapor fields.

The fall speed change during the melting, although it is beyond the scope of present study, will provide important leads to estimation of ice and water content variation as a function of altitude and to interpretation of radar reflectivity data in the bright band.

We shall next attempt formulation of this atmospheric ice melting process first with single crystals and then with snowflakes.

4.1 Single ice crystal melting

4.1.1 Description of the problem and the approach

There are two basic shapes of atmospheric single ice crystals, i.e., plate and prism. In order to permit a smooth theoretical treatment of various factors in atmospheric ice melting, it is necessary to simulate the two basic ice crystal shapes with simple geometrical bodies. A common practice in this regard is to use rotational spheroids, oblate for plate crystal and prolate for prism crystal. For simplicity, from now on we shall discuss oblate spheroid only. Treatment with a prolate spheroid can be easily obtained in an identical manner as we shall discuss below.

First of all, it is possible to treat the problems of heat conduction and vapor diffusion to and from the ice crystal in quiescent air environment, and then to add the effect of convective motion of air around the crystal which is caused by the fall. In stationary air, the heat conduction and vapor diffusion around the rotational oblate spheroid can be conveniently expressed by a spheroidal coordinate as shown in Fig. 36. Since the effects of condensation and thermal accommodation coefficients are negligible for the

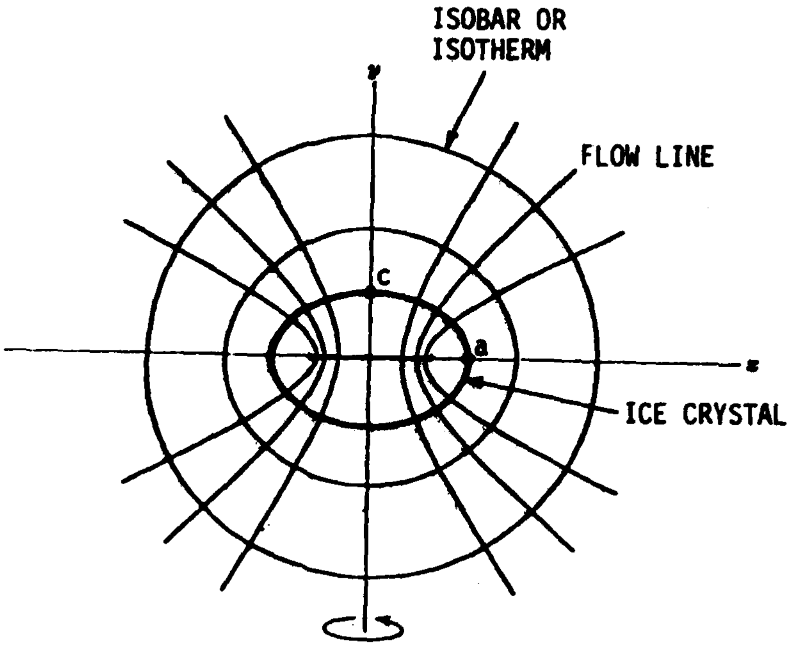

Fig. 36. Rotational oblate coordinate for heat conduction and vapor diffusion around a stationary ice crystal in air.

ice crystal size in question, the isotherms of heat conduction and the isobars of vapor diffusion correspond to the set of confocal spheroids outside the ice crystal. Similarly, the flow lines of heat and vapor are included in the set of confocal hyperboloids of two sheets. Since the coordinate is an orthogonal system, the set of spheroids and the set of hyperboloids cross each other at right angle. An analytic solution for heat or water vapor flux at an arbitrary point of this crystal surface is available.

The thermal flux at the distal points of ice spheroid is the largest and as the crystal melts, the surface tension forces the formed water to gather mostly at proximal areas, and let the water lenses sandwich the crystal (see Fig. 37). Under such a double system, the heat transfer by the sensible and latent heat fluxes suddenly becomes complex. There exists a clear need of proper simplification for the process. By examining the thermal conductivity in air (K_a), that in ice (K_i) and that in water (K_w);

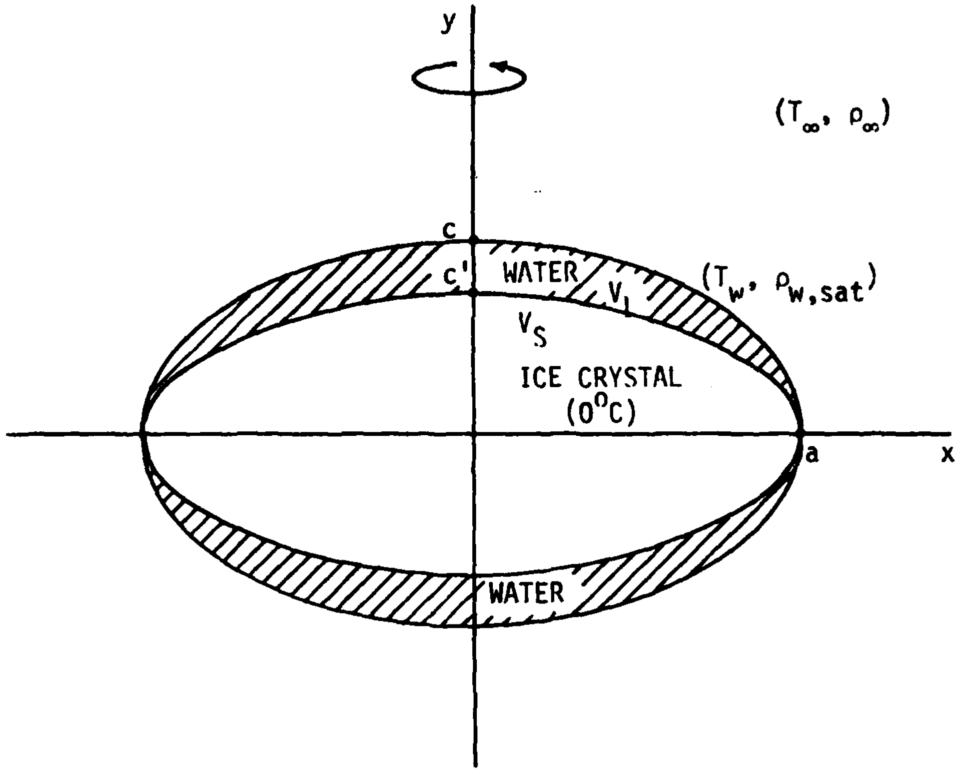

Fig. 37. A double rotational oblate spheroid model for partially melted ice crystal. Both water and ice spheroids are in contact at the distal point due to the surface tension effect of water.

$K_a = 5.73 \times 10^{-5}$ cal (cm · s · °K)$^{-1}$ (0°C)

$K_i = 4.99 \times 10^{-3}$ " " "

$K_w = 1.40 \times 10^{-3}$ " " (20°C)

1.52×10^{-3} " " (50°C)

it may be seen that $K_w > 20\ K_a$ at 0°C. This is to say that the heat conduction is slower in air under steady state than in water. So, in addition to simulating water lenses sandwiching melted ice with a rotational oblate spheroid (see Fig. 37), we assume that this double spheroid consisting of water and ice spheroids behaves in the same manner as an identical ice spheroid as far as heat and water vapor fields of the surrounding air are concerned.

When this crystal falls, the convective air motion further changes the heat conduction to the spheroid. However, the overall effect of this air ventilation is known. It is clear that the ventilation effect is zero at the proximal points and is largest at the distal points. For this reason, we proceed to assume that the ventilation effect is proportional to the heat flux at the distal points.

With these assumptions, we shall attempt to estimate the rates of changes of major semiaxis a, and minor semiaxis of water spheroid c and that of ice spheroid c' (see Fig. 37).

4.1.2 Melting of plate-like ice crystal

(a) Formulation of the theory

When an ice crystal melts, the rate of heat absorption relates to the rate of melting in the following manner

$$\frac{dQ}{dt} = L_f \left(\frac{dm}{dt}\right), \tag{17}$$

where Q is the heat, t the time, L_f the latent heat of fusion and m the mass of melted ice. Since the heat is supplied by two mechanisms, i.e., sensible and latent heat (vapor diffusion) transfers,

$$\frac{dQ}{dt} = \frac{1}{dt} (dQ_s + dQ_1), \tag{18}$$

where subscript s stands for sensible and 1 for latent. Using analogy to the electrostatic field around a conductor condensor of oblate shape, (analogy was also used for the temperature and vapor fields of a growing ice crystal in a quiescent air environment), we have

$$\frac{dQ}{dt} = 4\pi C \left[K_a (T_\infty - T_w) + DL_c (\rho_\infty - \rho_{w,sat}) \right], \tag{19}$$

where C is the electrostic capacitance of the outer water oblate spheroid enveloping the inner oblate ice spheroid, being given as

$$C = \frac{ae}{\sin^{-1}e}, \tag{20}$$

where

$$e = (1 - c^2/a^2)^{\frac{1}{2}}.$$

Since T_w and $\rho_{w,sat}$ are not known, (19) is, strictly speaking, not a solution. However, as we have examined above, the thermal conductivity of water is more than 20 times larger than that of air. Furthermore, the thickness of the water layer is much smaller than that of the air layer through which heat conduction must proceed. So, it may be reasonable to assume that

$$T_w = T_o, \text{ and } \rho_{w,sat} = \rho_o, \tag{21}$$

where ρ_o is the saturation vapor density at $T = T_o$ and T_o is the melting point of ice or 0°C. Since ice melting normally takes place in air whose temperature is not far above 0°C and whose relative humidity is high, and air flow condition around the falling and melting ice crystals is gentle, this assumption is not expected to create a large amount of error.

So far, we have obtained the expression for heat flux which is used for ice melting when the ice-containing oblate water spheroid is placed in quiescent air. When the spheroid falls through the air, the air motion changes the thermal and vapor fields around it (see Fig. 38). This ventilation affects the fields differently but there are reasons to believe the difference is small and the normal practice is to set both corrections same. Let us describe the ventilation correction by f. Then, we can modify (19) to obtain

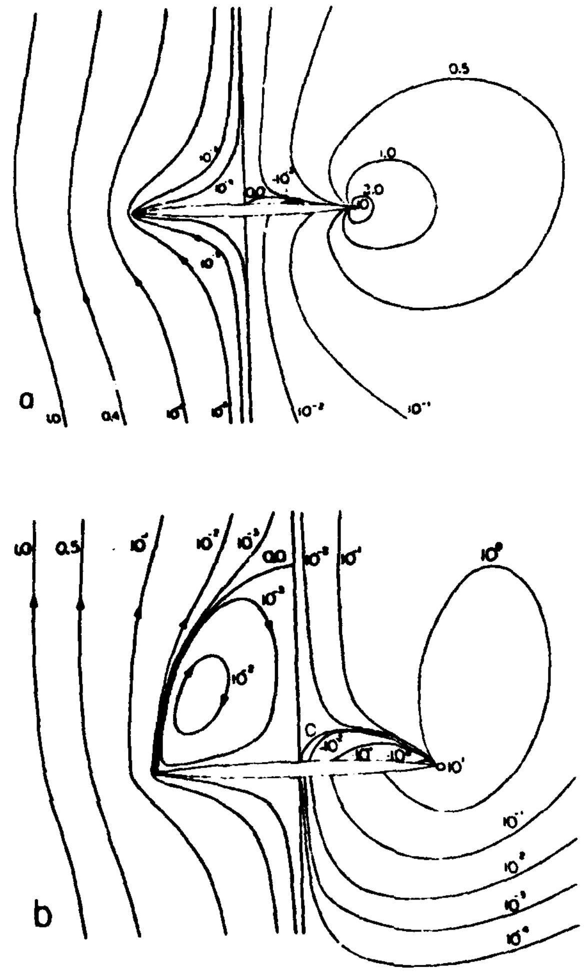

Fig. 38. Numerically computed stream function and vorticity distribution around an oblate speroid of $c/a = 0.05$ at (a) $Re = 1.0$ and (b) $Re = 20$ (Pruppacher and Klett, 1978).

$$\frac{dQ}{dt} = 4\pi C\ f\left[K_a\ (T_\infty - T_0) + DL_c\ (\rho_\infty - \rho_0)\right]. \tag{22}$$

The above equation already includes $T_w = T_0$, $\rho_x = \rho_0$ approximation, and consists of known quantities only.

The above treatment has clarified heat transfer to a ventilated water spheroid containing a melting ice spheroid. Now, we try to understand the shape change inside the water spheroid during the melting. The righthand term of (17) may be expressed as

$$L_f\frac{dm}{dt} = L_f\rho_L\frac{dV_L}{dt}, \tag{23}$$

where V_L and ρ_L are respectively the volume and the density of liquid water. If we can ignore evaporation loss of water, the volume of the outer water spheroid

$$V = V_L + V_S, \tag{24}$$

where V_S is the volume of the ice spheroid, and

$$V = \frac{4}{3}\pi a^2 c, \tag{25}$$

and

$$V_S = \frac{4}{3}\pi a^2 c', \tag{26}$$

(see Fig. 37). Then from eqs. (24), (25) and (26)

$$V_L = V - V_S = \frac{4}{3}\pi a^2(c - c'). \tag{27}$$

Then

$$dV_L = dV - dV_S = \frac{4}{3}\pi\left[2a(c - c')\ da + a^2(dc - dc')\right]. \tag{28}$$

From mass conservation ignoring the mass loss by evaporation,

$$\rho_L V_L + \rho_S V_S = m_0, \tag{29}$$

where m_0 is the mass of ice crystal before melting.

It is known that the sensible heat flux to the surface of a stationary spheroid has the following relationship

$$\frac{\text{(Heat flux on the a-axis)}}{\text{(Heat flux on the c-axis)}} = \frac{a}{c} .$$

An identical relationship holds for the latent heat transfer by vapor diffusion. Therefore the above relationship is valid for the net heat flux. Since these heat fluxes are used to melt ice crystal at corresponding positions,

$$\frac{\text{(Net heat flux on the a-axis)}}{\text{(Net heat flux on the c-axis)}} = \frac{a}{c} = \frac{da}{dc'} . \tag{30}$$

Note that although da corresponds to the change on the a-axis, dc′, not dc, does that on the c-axis because c′ represents a dimension of the ice crystal spheroid.

With the convective air motion around the falling ice crystal, the ventilation effect enhances the melting. As discussed above, the ventilation effect is assumed to be same for both sensible and latent heat (vapor diffusion) conductions. The factor f relates the total effect of ventilation to the stationary heat and vapor fields. It is clear that there is no ventilation effect on the c-axis but the effect is at its maximum on the a-axis. The effect on the a-axis must be proportional to $(f - 1)$. Taking a proportionality constant A_1, (30) may be modified to

$$\frac{da}{dc'} = \frac{a}{c}\left[A_1 (f - 1) + 1 \right]. \quad (31)$$

In this treatment, we leave A_1 determination for experiments.

We now have three relationships for variation of a, c, and c´, i.e., eqs. (28), (29) and (30). Eq. (22) adds the heat flux effect or introduces time variation to the quantities involved. So, we shall solve for da, dc and dc´ using eqs. (28), (29) and (30), applying a fixed time interval Δt to incorporate the net heat flux effect. In order to solve these equations, we convert (29) into the following form,

$$\rho_L dV_L + \rho_S dV_S = 0,$$

or inserting (28) and the differential form of (10), we have

$$2a \left[- (\rho_L - \rho_S)c' + c\rho_L \right] da + a^2 \rho_L dc - a^2 (\rho_L - \rho_S) dc' = 0. \quad (32)$$

The dV_L term in (28) is caused by the net heat flux in (22). So

$$dV_L = \frac{1}{\rho_L L_f} dQ, \quad (33)$$

and from (22)

$$dQ = A_2 Cf, \quad (34)$$

where

$$A_2 = 4\pi \left[K_a (T_\infty - T_o) + DL_c (\rho_\infty - \rho_o) \right] \Delta t. \quad (35)$$

In other words, dQ is the amount of heat used to melt the ice crystal in Δt time. This introduction of time interval Δt permits numerical computation as a function of time allowing incorporation of effects of time dependent variables. Eq. (28) becomes

$$\frac{A_2 C f}{\rho_L\, L_f} = \frac{4}{3}\pi \left[2a(c - c')da + a^2 dc - a^2 dc' \right]. \tag{36}$$

Using eqs. (31), (32) and (36) we can solve for da, dc and dc';

$$da = -\frac{3}{4\pi ac}\,\frac{A_2 A_3 C}{L_f\,\rho_S}\left[A_1(f-1) - 1\right], \tag{37}$$

where

$$A_3 = \frac{f}{\frac{2c'}{c}\,A_1(f-1) + 1 - 1}, \tag{38}$$

$$dc = \frac{3}{4\pi a^2}\,\frac{A_2 A_3 C}{L_f \rho_L \rho_S}\left\{\frac{2}{c}\left[-(\rho_L - \rho_S)c' + c\rho_L\right]\left[A_1(f-1) + 1\right] - (\rho_L - \rho_S)\right\}, \tag{39}$$

and

$$dc' = \frac{-3}{4\pi a^2}\,\frac{A_2 A_3 C}{L_f\,\rho_S}. \tag{40}$$

(b) Computation scheme

With these equations, it is now possible to compute melting of an ice crystal with the shape of rotational oblate spheroid falling in air with vertical temperature and relative humidity distributions.

COMPUTATION SCHEME

INITIAL CONDITIONS

$$a = a_0,\ c = c_0,\ c' = c_0,\ T = T_0,\ p,\ \rho_\infty,\ v,\ m_0$$

ASSOCIATED CONDITIONS

$$f,\ C,\ \rho_S,\ K_a,\ L_c,\ L_f,\ D,\ A_I$$

$$\downarrow$$

$$dQ \quad (34)$$

$$\downarrow$$

$$da\ (37),\ dc\ (39),\ dc'\ (40)$$

$$\downarrow$$

NEXT
TIME
STEP

$$a(= a_o + da),\ c(= c_o + dc),\ c'(= c_o + dc')$$

$$\downarrow$$

$$V + dV_L,\ V_S + dV_S,\ V + dV$$

$$\downarrow$$

$$\pi(a + da)(c + dc),\ \pi(a + da)(c' + dc'),\ \pi(a + da)^2$$

$$\downarrow$$

$$V + dV$$

4.1.3 Ventilation coefficient of vapor diffusion and heat conduction

According to Pruppacher and Klett (1978), the simplified ventilation coefficient for oblate crystal, f, is given as

$$f = 1 + 0.142X^2 + 0.054X^4 \ln(0.893X^2), \tag{41}$$

where

$$X = (N_{Sc})^{1/3} (Re)^{1/2} \leq 0.71 \text{ or } Re \leq 0.63 \text{ with } N_{Sc} = 0.71,$$

where N_{Sc} is the Schmidt number given as

$$N_{Sc} = \frac{\nu}{D} = (\nu;\ \text{kinematic viscosity}),$$

and Re is the Reynolds number given as

$$Re = \frac{2va}{\nu},$$

and

$$f = 0.937 + 0.178X, \tag{42}$$

for $X \geq 0.71$ or $Re \geq 0.63$.

When $X \geq 1$, f varies linearly with X, and in our present model, X is expected to fall in this range. These authors state that for $Re \leq 100$,

$$f = 0.86 + 0.28X \quad (X \geq 1.0), \tag{43}$$

agrees with experimental data to within 8%. So, (43) appears to be our best choice for the ventilation coefficient.

For the terminal velocities of oblate spheroid ice crystals, Pruppacher and Klett (1978) list the following empirical relationship; for $c/a = 0.2$,

$$\log Re = B_o + B_1 X + B_2 X^2, \tag{44}$$

where $X = \log (C_D\ Re^2)$ and $B_o = 1.3300$, $B_1 = 1.0217$, $B_2 = -0.049018$, and C_D is the hydrodynamic drag force coefficient, and for $c/a = 0.5$,

$$\log Re = B_o + B_1 X + B_2 X^2 + B_3 X^3, \tag{45}$$

where $B_o = -1.3247$, $B_1 = 1.0396$, $B_2 = -0.047556$, $B_3 = -0.002327$. For an oblate spheroid,

$$C_D\,Re^2 = \frac{32a^2c\,(\rho_S - \rho_a)\rho_a g}{3\eta} = \frac{8m_o\rho_a g}{\pi\eta^2}\ , \tag{46}$$

where ρ_a is the density of air, g the gravity acceleration and η the dynamic viscosity of air. They indicate that these equations are applicable for $Re \leq 100$, and beyond this level of the Reynolds number oscilliations will occur and eventually becomes a gliding-tumbling motion.

4.2 Snowflake melting

Snowflake melting problem has been recently tackled by Matso and Sasyo (1981a). Considering uncertainties involved in the process, their theory appears to be the best one we can choose at this moment. So, we briefly review it below.

The rate of heat transfer by the sensible heat conduction and vapor diffusion (latent heat transfer) can be expressed as, similar to (22)

$$\frac{dQ}{dt} = 4\pi r f \varepsilon \left[K_a (T_\infty - T_w) - DL_c\,(\rho_\infty - \rho_{w,sat}) \right]\ , \tag{47}$$

where r is the radius of snowflake, ε a factor involving the effects of various physical properties of the snowflake on the heat transfer rate. ε is assumed to be constant. For the Reynolds number between 10 and 1800

$$f = 1 + 0.275\, N_{Pr}^{\frac{1}{3}}\ Re^{\frac{1}{2}}, \tag{48}$$

where N_{Pr} is the Prandtl number being given as

$$N_{Pr} = \nu/K_a\ . \tag{49}$$

Since $N_{Pr}^{\frac{1}{3}}$ does not vary much in our range of atmospheric conditions, it is taken to be 0.87. This reduces (48) to

$$f = 1 + 0.24\, Re^{\frac{1}{2}}\ . \tag{50}$$

According to Matsuo and Sasho, during the melting of a snowflake, the water penetrates inwards leaving the surface uncovered with water. The flux of the sensible heat and that of the latent heat match the rate of heat absorption by ice melting, or

$$- L_f 4\pi r^2 \rho_i dr = 4\pi r \varepsilon f(K_a \Delta T + DL_c \Delta\rho)\Delta t, \tag{51}$$

where ρ_i is the density of ice-skeleton. Eq. (51) with simplifications discussed above reads

$$- \frac{dr}{dt} = \frac{K\Delta T}{L_f \rho_i} \frac{1}{r} \varepsilon \left[1 + 0.24(\frac{2rv}{\nu})^{\frac{1}{2}}\right], \tag{52}$$

They report the solution of (52) as

$$t = \frac{2L_f \rho_i}{\alpha^4 K\Delta T} \frac{1}{\varepsilon} \left[\frac{1}{3}\alpha^3 (r_o{}^{3/2} - r^{3/2}) - \frac{1}{2}\alpha^2 (r_o - r) + \alpha(r_o^{\frac{1}{2}} - r^{\frac{1}{2}}) - \ln\left(\frac{1 + r_o^{\frac{1}{2}}}{1 + r^{\frac{1}{2}}}\right)\right], \tag{53}$$

where $\alpha = 0.24\ (2v/\nu)^{\frac{1}{2}}$ and r_o is the initial snowflake radius. Their integration was carried out under the condition v = const., but in our case, v is coupled with r and this consideration is necessary when integration of (52) is performed.

In the range $10^{-2} \leq Re \leq 300$, the following empirical expression may be used to relate the fall velocity to the size (Pruppacher and Klett, 1978)

$$Y = B_o + B_1 X + \ldots B_6 X^6 , \tag{54}$$

where $B_o = -0.318657 \times 10^1$, $B_1 = +0.992696$, $B_2 = -0.153193 \times 10^{-2}$, $B_3 = -0.987059 \times 10^{-3}$, $B_4 = -0.578878 \times 10^{-3}$, $B_5 = +0.855176 \times 10^{-4}$, $B_6 = -0.327815 \times 10^{-5}$ and $X = \ell n\ (C_d\ Re^2)$ and $\ell n\ Re = Y$.

5. Mechanism of Bright Band Formation

Our vertical wind tunnel studies have produced some information about variation of microphysical parameters during the melting and they are now represented by the regression equation as discussed above. Although our knowledge is still limited, it may now be worthwhile to apply it to a realistic atmospheric condition to see the contribution of isolated melting particles to the radar reflectivity. Taking this as a stepping stone and comparing it with observed bright band data, we can then estimate the degree of contribution from other factors. Remembering the uncertainties and limitation associated with our data and present radar meteorology in general, we shall proceed with modeling of melting layer by making suitable approximations.

5.1 Model of melting snowflake

In order to estimate the backscattering from a melting snowflake, Ryde (1946) considered that during the melting process, it consisted of a homogeneous mixture of ice and water. Austin and Bemis (1950) applied the method to melting snowflakes to compute the radar reflectivity in the melting zone. However, the treatment is considered to be questionable (Battan, 1973). Clearly the effect of water skin on the melting ice has to be considered. Whereas, considering the wavelengths of microwave commonly used in radar and the thickness of the skeletal structure, the outer dimension of a melting snowflake cannot be equivalent to that of solid ice under melting.

The effect of water skin existing on melting spherical ice particles was estimated by Langleben and Gunn (Battan, 1973) based on the work by Aden and Kerker (1951). However, the effect on melting snowflakes is not available and its exact computation is beyond the scope of the present study.

There are uncertainty and variability in microphysical and environmental conditions as well as limitation on our knowledge about radar backscattering from melting hydrometeors. Considering this position, we have introduced the following simplified melting snowflake model (see Fig. 39).

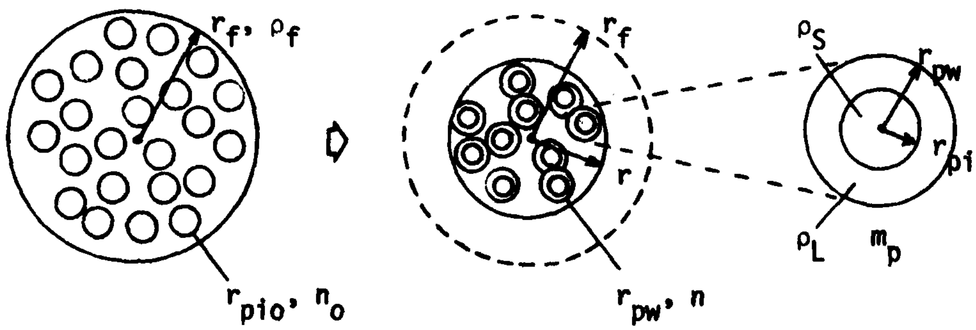

Fig. 39. Melting snowflake model involving melting ice particles whose positions are fixed with the space coordinate.

The model assumes a spherical shape. Initially, it has a radius r_f and an apparent density ρ_f, and consists of n_o number of ice spheres with radius r_{pio}. The ice spheres are fixed with the space coordinate so that they cannot change the positions. As the melting proceeds, the snowflake melts from outside as well as inside and allows the outer ice particles to disappear. The water formed by melting is assumed to distribute equally in the skin of remaining inner ice particles. No mass exchange is considered between the snowflake and the environment. This assumption should be reasonable in view of the fact that melting takes place normally in a nearly saturated environment close to 0°C isotherm.

The ice particles are assumed to change the radii according to the relation

$$r_{pi} = r_{pio}F, \tag{55}$$

where

$$F = \frac{r - r_w}{r_f - r_w}, \tag{56}$$

and r the snowflake radius and r_w the radius of formed water drop at the end of melting.

From the mass conservation assumption, the mass of an ice particle with water skin

$$\begin{aligned} m_p &= \frac{4}{3}\pi r_f^3 \rho_f / n \\ &= \frac{4}{3}\pi r_{pi}^3 \rho_S + \frac{4}{3}\pi (r_{pw}^3 - r_{pi}^3)\rho_L, \end{aligned} \tag{57}$$

where n is the number of remaining ice particles in the snowflake and r_{pi} and r_{pw} the radius of the ice particle and that of water-covered ice particle, respectively. Eq. (57) reduces to

$$n r_{pw}^3 = \frac{\rho_f}{\rho_L} r_f^3 - n \frac{(\rho_S - \rho_L)}{\rho_L} r_{pi}^3, \tag{58}$$

Snowflake melting from outside with ice particle position fixed leads to

$$n/n_o = \frac{4}{3}\pi r^3 / \frac{4}{3}\pi r_f^3 = r^3/r_f^3. \tag{59}$$

Whereas, the initial condition is

$$n_o \frac{4}{3}\pi r_{pio}^3 \rho_S = \frac{4}{3}\pi r_f^3 \rho_f,$$

or

$$r_{pio}^3 = \frac{1}{n_o}\frac{\rho_f}{\rho_S} r_f^3 . \tag{60}$$

Combination of eqs. (55), (58), (59) and (60) yields

$$nr_{pw}^{3} = \frac{\rho_f}{\rho_L} r_f^3 - \frac{\rho_f(\rho_S - \rho_L)}{\rho_L \rho_S} r^3 F(r)^3 . \tag{61}$$

To incorporate the effect of the water skin on melting ice particles, we assume

$$\sigma = \sigma_i - (\sigma_i - \sigma_w) G(r), \tag{62}$$

where σ is the backscattering cross section of a single particle and

$$G(r) = \frac{r_f^j - r^j}{r_f^j - r_w^j} , \tag{63}$$

where j is the number to be determined from the computation made by Langleben and Gunn. The estimation by Langleben and Gunn was for ice particle radius of 0.6 mm and the wavelength of microwave of 3 cm. It is rather insensitive to the wavelength range of commonly used radar. This permits us to apply their results to particle radii around 0.6 mm. For constant outer radius of water-coated ice particle,

$$\sigma \propto |K|^2,$$

where

$$|K|^2 = \left|\frac{m^2 - 1}{m^2 + 2}\right| , \tag{64}$$

m being the complex index of refraction. This leads to the relationship

$$|K|^2 = |K_i|^2 - (|K_i|^2 - |K_w|^2)\, G(r). \tag{65}$$

Then, since the radar reflectivity

$$\eta \propto |K|^2 V^2 N, \tag{66}$$

where V is the volume and N the number concentration of snowflakes, from eqs. (61), (65) and (66)

$$\eta \propto \left[|K_i|^2 - (|K_i|^2 - |K_w|^2)\, G(r)\right]\left[r_f^3 - \frac{(\rho_S - \rho_L)}{\rho_S} r^3 F(r)^3\right]\frac{1}{v}, \quad (67)$$

where v is the fall velocity of snowflake.

5.2 Numerical simulation of the melting of snowflakes in a realistic environment

Assuming the existence of a realistic atmospheric environment, we may numerically simulate the melting of either snowflakes or ice crystals in it, as they fall through the region where the air temperature is higher than ice. Under the process, the change of the size of snowflakes or ice crystal, and the change of its fall velocity may be calculated according to the generalized expressions derived from data obtained in the vertical wind tunnel under constant temperatures. We shall outline the details of this numerical simulation below.

5.2.1. The environmental condition

The atmospheric condition assumed for our numerical simulation of melting layer is that the temperature field satisfies the dry adibiatic lapse rate from the surface to the 5°C level and from the 5°C level to the 0°C level, the temperature field satisfies the moist adiabatic lapse rate with 100% RH with respect to water. We selected a case for surface pressure p_s = 1000 mb and temperature T_s = 10°C.

5.2.2. The computation

The generalized expressions of the change of the size (eqs. (5) and (9)) and the fall velocity (eqs. (6) and (10)) of snowflakes or ice crystal under constant temperatures are used. Under the atmospheric condition we have

chosen, we assume that within a thin layer with thickness $\Delta z = 25$ cm the temperature may be regarded as having a constant value $\overline{\Delta T}$. Then, when a snowflake or ice crystal reaches the top of this thin layer with the diameter d_T and fall velocity v_T, it melts and falls under this temperature. Therefore, based on equations for d and v, we may obtain the initial size $d_0{}^*$ and time t*, such that a snowflake or ice crystal with initial diameter $d_0{}^*$ falling into this chamber with constant $\overline{\Delta T}$ temperature and traveling t* for a period of time will reach a level where they are now d_T and v_T. Then, we may integrate (6) or (8) to obtain the time interval Δt required for the snowflake or ice crystal to travel through this thin layer of $\Delta z = 25$ cm, and eventually from eqs. (5), (6), (9) and (10) to obtain the size and fall velocity when it reaches the bottom of this thin layer.

Based on the calculation described above, we may then follow the change of snowflakes or ice crystals sequentially downward until it melts completely to become droplets. In our calculation, we assume that the mass is conserved, therefore

$$\frac{\text{Final density}}{\text{Initial density}} = \left(\frac{\text{Initial diameter}}{\text{final diameter}}\right)^3.$$

As the final density of water droplet is 1 g/cm^3, while the initial density of snowflakes or ice crystal is taken as 0.036 g/cm^3. Hence,

$$\frac{\text{Final diameter}}{\text{Initial diameter}} = 0.33.$$

Figs. 40 and 41 describe the change of the diameter of snowflakes and ice crystals as a function of altitude and Figs. 42 and 43 show the fall velocity variation with the altitude. It should be pointed out that our fall velocity profiles are quite different from that Austin and Bemis (1950) guessed.

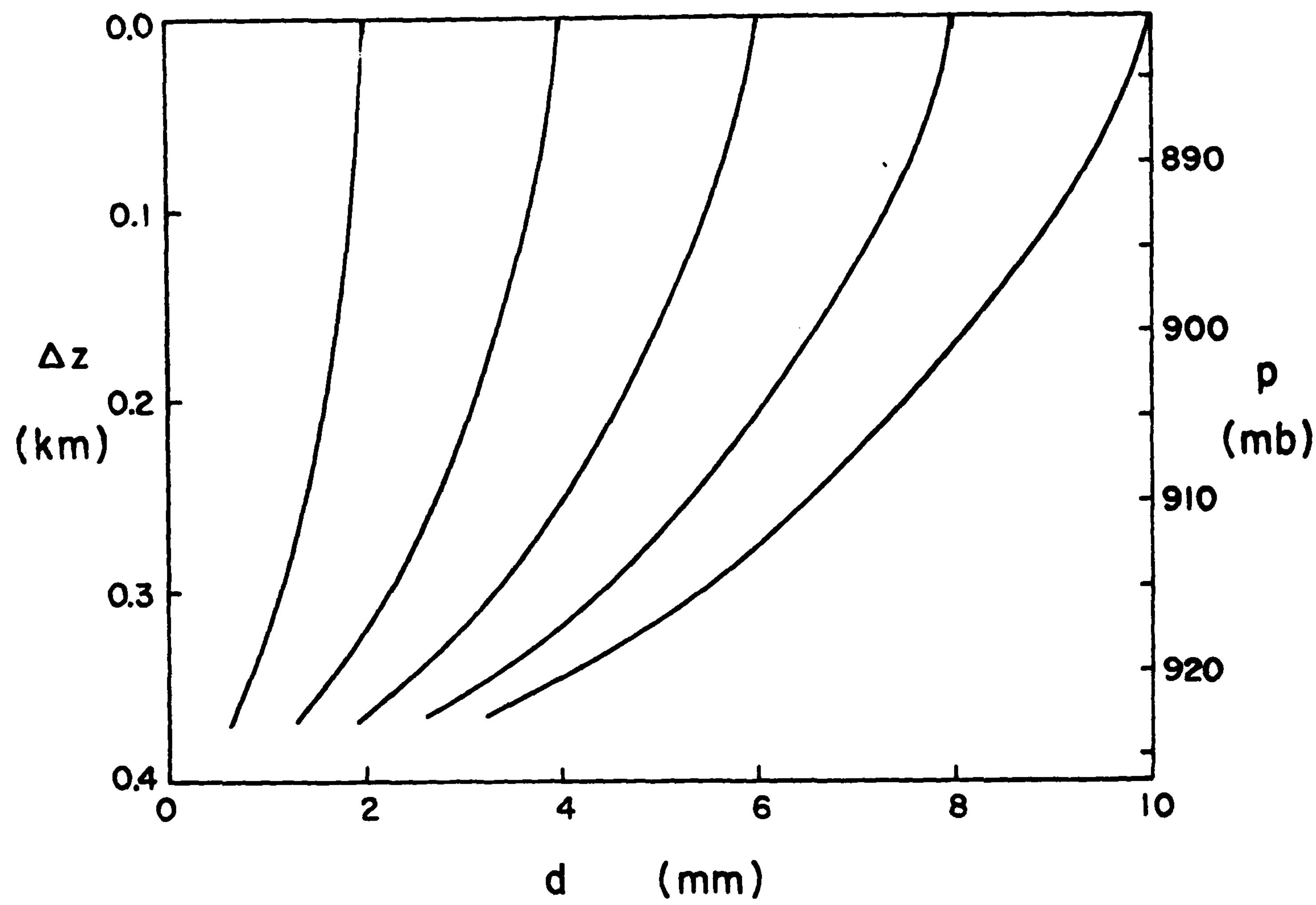

Fig. 40. Computed snowflake diamter d vs distance from the $0^{o}C$ isotherm Δz.

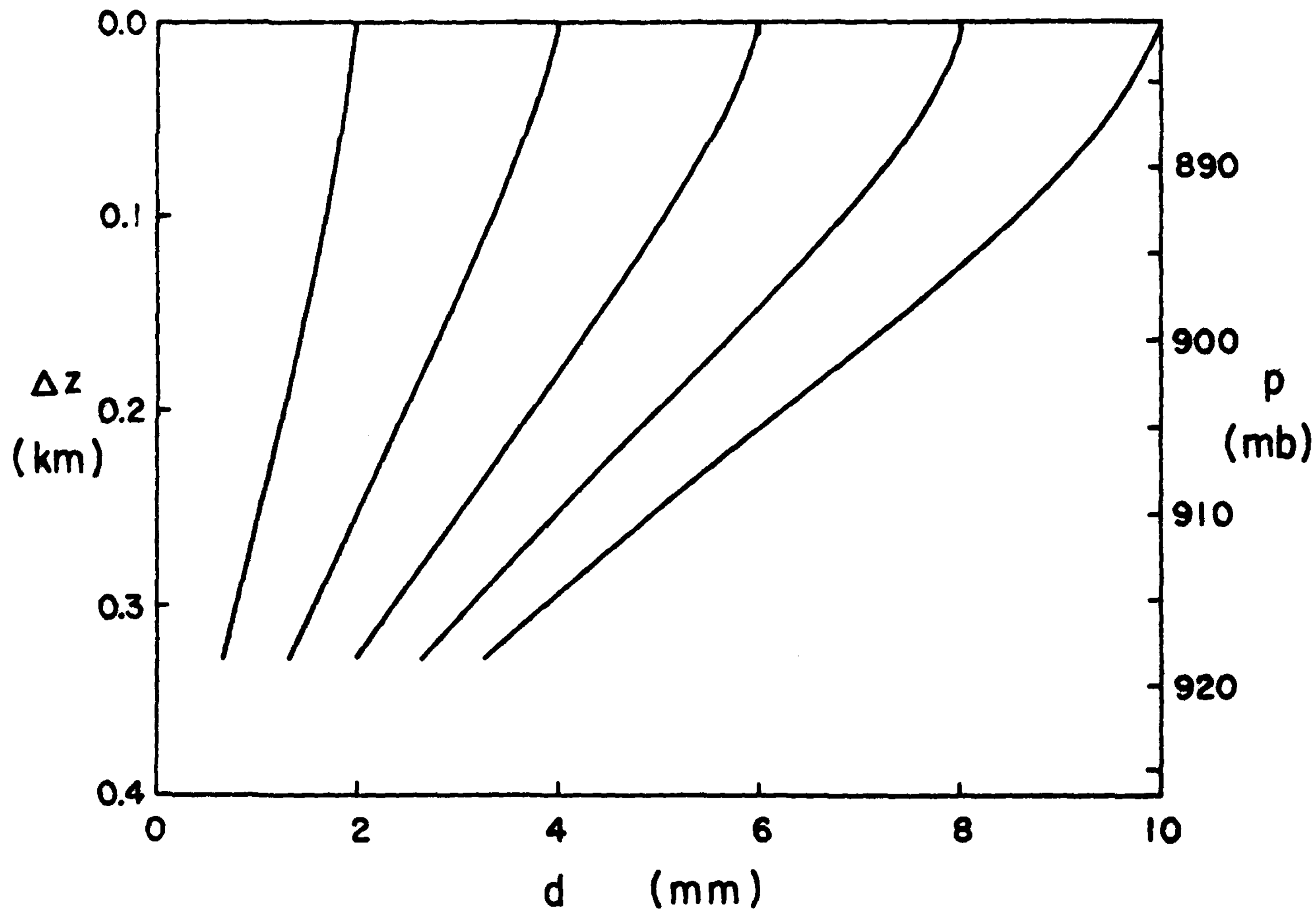

Fig. 41. Computed single ice crystal diameter d vs distance from the $0^{o}C$ isotherm Δz.

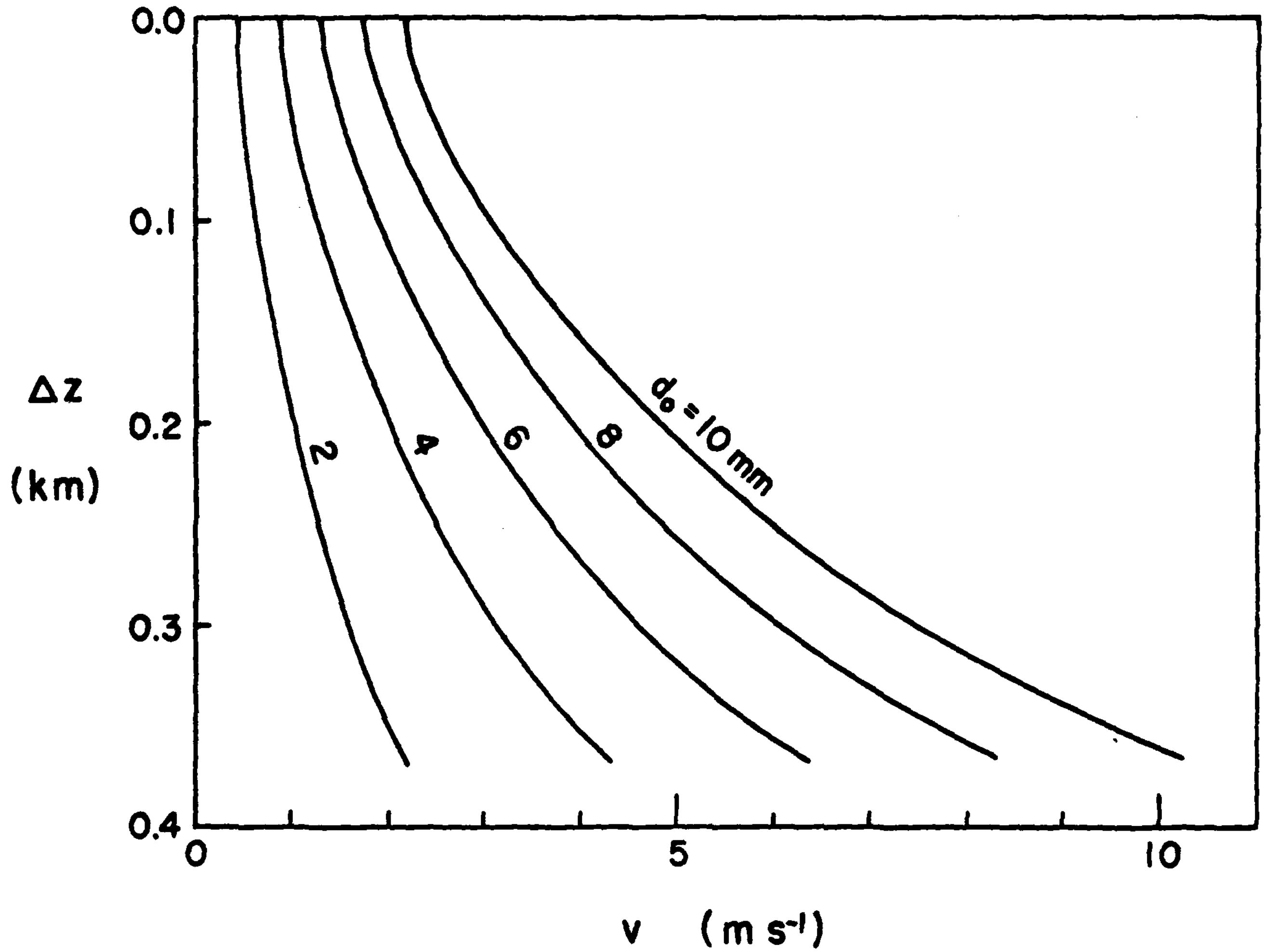

Fig. 42. Computed snowflake fall velocity v vs distance from the 0°C isotherm Δz.

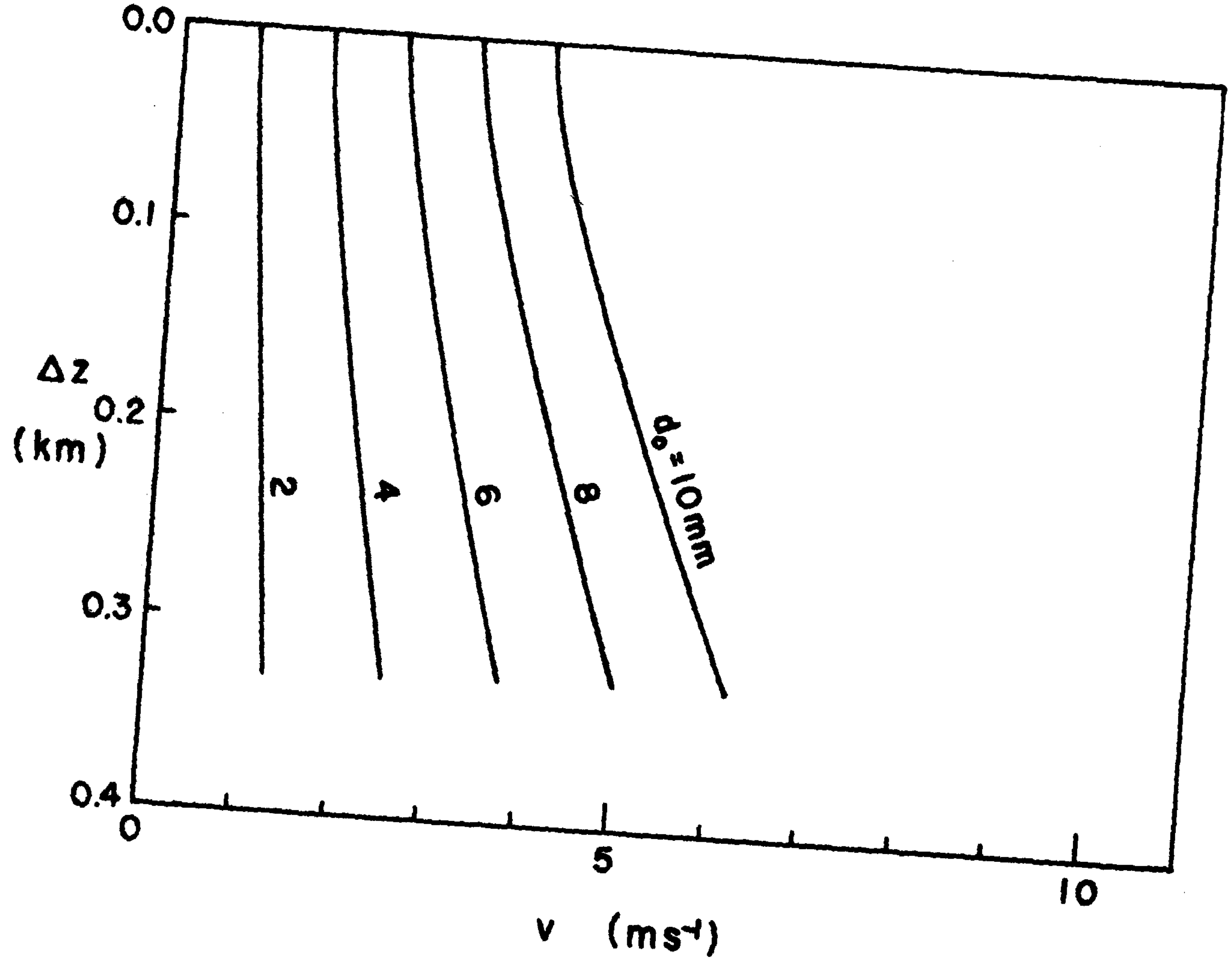

Fig. 43. Computed fall velocity of single ice crystals v vs distance from the $0^{o}C$ isotherm Δz.

Instead of the rapid variation toward later stages of melting in the work of Austin and Bemis, the fall velocities we estimated vary with the lowered altitude in the entire range.

5.3. Discussion

Fig. 44 shows the factor G computed in comparison with the work by Langleben and Gunn with the determined value of j being 32.2. Fig. 45 describes the radar reflectivity computed from (67) with $r_f = 5$ mm and normalized to that at the 0°C isotherm. In the computation it is assumed that snowflakes are spheres with 10 mm diameter and obey the size and the fall velocity the regression equations give. There is no aggregation taking place simulataneously. Also shown is the result with $|K|^2$ value for homogeneous mixture of water and ice with all other conditions being the same. From the figure, it is clear that the homogeneous mixture treatment gives a much lower value of radar reflectivity maximum compared with that of our model. Secondly, the position of the maximum reflectivity in our model is only about 40 m below the 0°C isotherm with the maximum 4 times larger than that at 0°C level. The maximum reflectivity position Austin and Bemis obtained in their model at about 300 m below the 0°C isotherm is due to the combined effect of several factors, such as (i) rather sudden increase in the assumed fall velocity toward the end of melting, (ii) the gradual $|K|^2$ increase due to the homogeneous mixture computation and (iii) the continuing effect of aggregation.

As mentioned in the introduction, the radar reflectivity in the center of the bright band normalized with respect to that at 0°C isotherm is normally between 15 and 30 with extremes as high as 100 and as low as 2 or 3. Since the homogeneous mixture model is incompatible with the computed results of Langleben and Gunn, we compare our spherical snowflake model without aggregation with these observations.

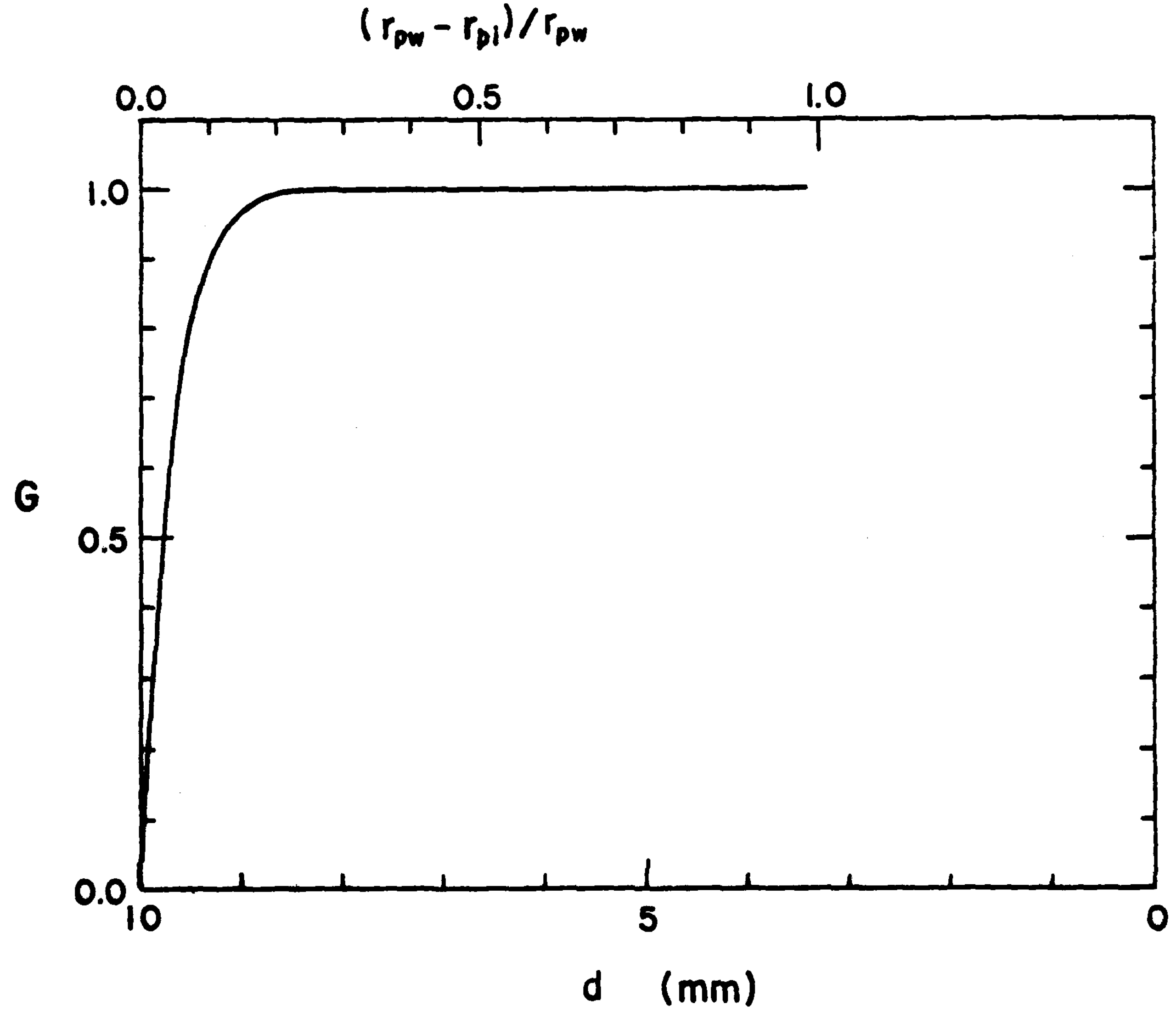

Fig. 44. Variation of the factor G with the snowflake diameter d.

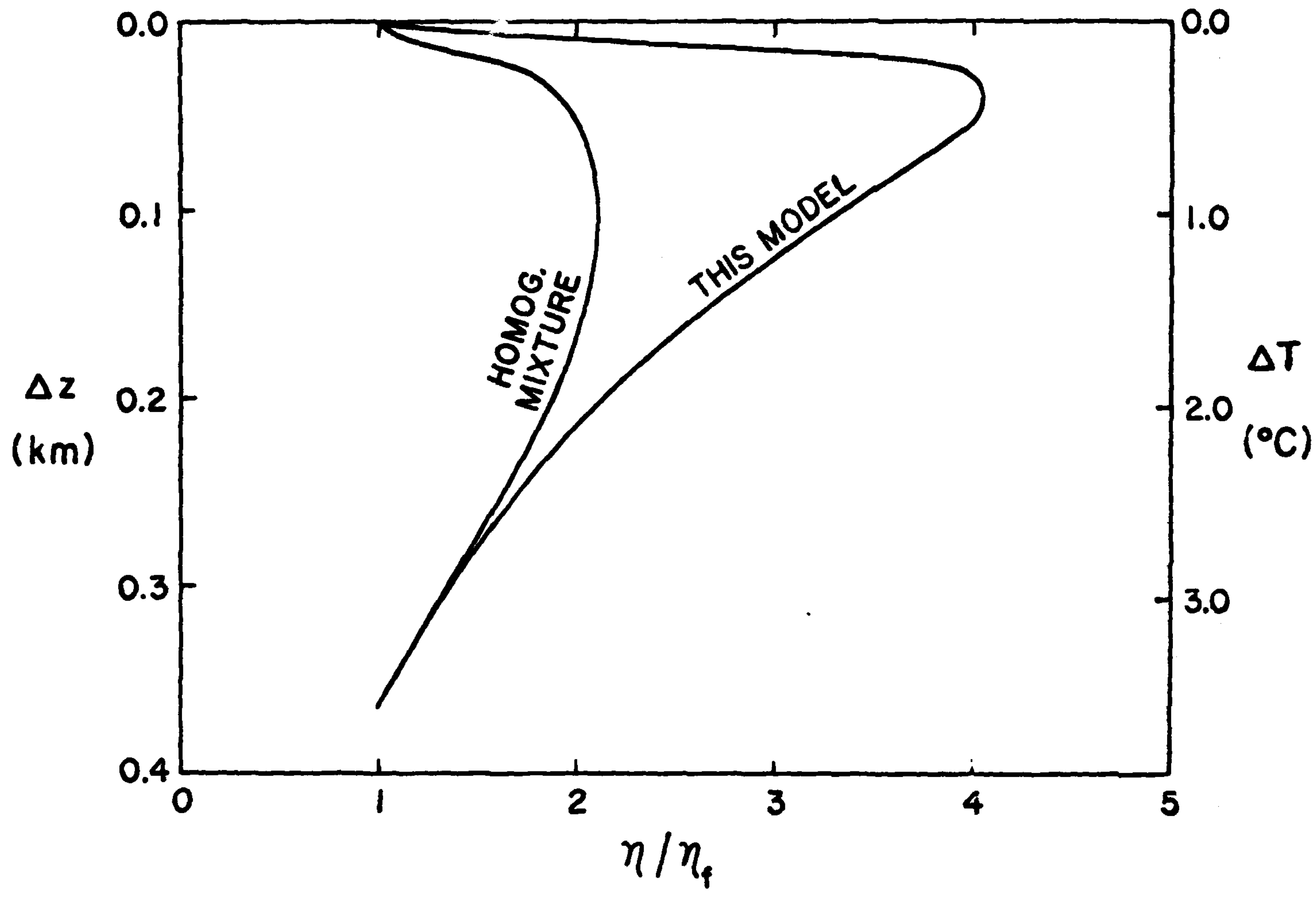

Fig. 45. The computed radar reflectivity of snowflakes normalized to that at the $0^{o}C$ isotherm η/η_f plotted as a function of distance (temperature) from the isotherm Δz (ΔT). Snowflakes are assumed to be spherical with a 10 mm diameter.

There are at least three more factors to be considered starting from our model in order to account for the natural variation of the bright band conditions. (i) According to Atlas et al. (1953), a partially melted ice spheroid gives a considerably stronger backscattering compared with a partially melted ice sphere of the same volume. It is possible to expect a similar effect with snowflakes. Aggregation of snowflakes is expected to take place more easily among partially melted snowflakes leading to (ii) shape development and (iii) size increase. (ii) and (iii) are expected to continue for some time after the spherical snowflake reflectivity has reached its maximum. If three spherical snowflakes form a linear aggregate at say 200 m below the 0°C isotherm, it will increase the reflectivity by a factor of 3 from the developed shape, by a factor of 9 from the V^2 term and by a factor of 1/3 from the number concentration, provided that the fall velocity remains the same. This will lead to an overall gain of reflectivity by a factor of 9. Multiplying this factor to the normalized reflectivity of 2 already existing at the level, we can expect the normalized reflectivity reaching to 18. It will be interesting to see if the reflectivity maximum is larger and the position lowered when the snowfall intensity or precipitation rate is high and vice versa.

6. Concluding Remarks

The present study includes the development of snow melting apparatus, the field measurement, the data analysis, the theoretical development, and interpretation of the bright band mechanism based on the theoretical and

experimental knowledge obtained. Main features and findings are as follows.

The apparatus development phase is highlighted with the following main features:

(i) An air conditioning system to control the temperature and relative humidity of air passing through the wind tunnel.

(ii) A valve mechanism to control the air velocity in the tunnel while maintaining the same temperature and humidity in it.

(ii) A new vertically diverging wind tunnel with proper design and combination of screens and a honeycomb to suspend snowflakes and snow crystals while melting.

(iv) A trap door mechanism for sample snow introduction into the tunnel without causing turbulence.

(v) A method to remove static electricity on the tunnel wall.

The main findings from snow melting measurements are:

(i) The observed melting time of snowflakes and snow crystals increased with size, but rather gently, suggesting internal melting.

(ii) Snow crystal disruption was observed and recognized as a dominant factor during the melting.

(iii) The vertical stability of suspended snowflake and snow crystals appeared to be dependent upon their size and shape. Small crystals, less than 1 mm in diameter, were the most stable.

(iv) Helicoptering, or the rotation of a crystal around its vertical axis, was observed in crystals 1-3 mm in diameter. They developed orbital motion with increasing radius during the last portion of their melting process.

(v) Crystals less than 1 mm in diameter jumped violently at the end of their melting process. The jump was upwards or to the side, but seldom downwards.

(vi) Large symmetrical dendrites appeared to melt from the outside in forming a drop in the final stages of melting. However, they too became unstable in the final stages of melting. There was no disruption of these type crystals.

Data analysis has produced sets of regression equations for fall velocity and size as functions of time and temperature.

The theoretical development carried out features with melting of non-spherical single ice crystals and spherical snowflakes.

A simple model of melting spherical snowflake has been developed in which the snowflake is represented by melting ice particles fixed with the space coordinate in the snowflake and the snowflake is assumed to melt from outside to shrink as well as from inside to incorporate the effect of water skin for the microwave backscattering. Comparison of this model under the changes of fall velocity and diameter predicted by the regression equations has revealed that shape and aggregation, i.e. size, of snowflakes during the melting stage appear to account for the observed increase of the radar reflectivity at the center of the bright band relative to that at the 0°C isotherm and the altitude. From this consideration, a relationship is predicted between the height of the center of the bright band and the snowfall intensity, i.e., the lower the center altitude, the stronger the snowfall intensity.

REFERENCES

Aden, A. L. and M. Kerker, 1951: Scattering of electromagnetic waves from two concentric spheres, J. Appl. Phys., 22, 1242-1246.

Atlas, D., M. Kerker and W. Hitschfeld, 1953: Scattering and attenuation by non-spherical atmospheric particles. J. Atmos. Terrest. Phys., 3, 108-119.

Austin, P. M. and A. C. Bemis, 1950: A quantitative study of the "bright band" in radar precipitation echoes. J. Meteor., 7, 145-151.

Bailey, I. H., and W. C. Macklin, 1968: Heat transfer from artificial hailstones. Quart. J. Roy. Meteor. Soc., 94, 93-98.

Battan, L. J., 1973: Radar Observation of the Atmosphere. The University of Chicago Press, 324 pp.

Beard, K. V., and H. R. Pruppacher, 1969: A determination of the terminal velocity and drag of a small drop by means of a wind tunnel. J. Atmos. Sci., 26, 1066-1072.

Cotton, W. R., and W. R. Gokhale, 1967: Collision, coalescence and breakup of large water drops in a vertical wind tunnel. J. Geophys. Res., 72, 4041-4049.

Donovan, G. J., 1982: Melting of natural snowflakes suspended in a vertical wind tunnel. Master Thesis, University of Utah.

Drake, J. C., and B. J. Mason, 1966: The melting of small ice spheres and cones. Quart. J. Roy. Meteor. Soc., 42, 500-509.

Fukuta, N., M. W. Kowa and N. H. Gong, 1982: Determination of ice crystal growth parameters in a new supercooled cloud tunnel. Preprints, Conf. on Cloud Phys., Chicago, Ill., 15-17 Nov., 1982. 325-328.

Fukuta, N., L. R. Neubauer, and D. D. Erickson, 1979: Laboratory studies of organic ice nuclei smoke under simulated seeding conditions: ice crystal growth. Final report to NSF under Grant No. ENV 77-15346, January 1979.

Hoffer, T. E., and S. C. Mallen, 1968: A vertical wind tunnel for small droplet studies. J. Appl. Meteor., 7, 290-292.

Hooper, J. E. N. and A. A. Kipax, 1950: The bright band: A phenomenon associated with radar echoes from falling rain. Quart. J. Roy. Meteor. Soc., 76, 125-131.

Iribarne, J. V., and M. Klemes, 1970: Electrification associated with breakup of drops of terminal velocity in air. J. Atmos. Sci., 27, 927-936.

Kinzer, G. D., and R. Gunn, 1951: The evaporation, temperature, and thermal relaxation-time of freely falling water drops. J. Meteor., 8, 71-83.

Kinzer, G. D., and W. E. Cobb, 1956: Laboratory measurements of the growth and collection efficiency of raindrops. J. Meteor., 13, 295-301.

_________, 1958: Laboratory measurements and analysis of the growth and collection efficiency of cloud droplets. J. Meteor. 15, 138-148.

Kowa, M., 1981: Determination of ice crystal growth parameters in a supercooled cloud tunnel. Masters thesis, University of Utah.

List, R., 1959: Design and operation of the Swiss hail tunnel. Geo-Phys. Monograph , 5, 310-316.

Macklin, W.C., 1963: Heat transfer from hailstones. Quart. J. Roy. Meteor. Soc., 89, 360-369.

Mason, B. J., 1956: On the melting of hailstones. Quart. J. Roy. Meteor. Soc., 82, 209-216.

Matsuo, T., and Y. Sasyo, 1981a: Empherical formula for the melting rate of snowflakes. J. Meteor. Soc. Japan, 59, 1-8.

_________, 1981b: Melting of snowflakes below freezing level in the atmosphere. J. Meteor. Soc. Japan, 59, 16-24.

_________, 1981c: Non-melting phenomena of snowflakes observed in sus-saturated air below freezing level. J. Meteor. Soc. Japan, 59, 26-32.

Matsuo, T. and Y. Sasyo, 1982: Melting of snow pellets in the atmosphere. Pap. Met. Geophys., 33, 55-64.

Pankhurst, R. C., and D. W. Holder, 1952: Wind Tunnel Technique. London: Sir Isaac Pittman and Sons, LTD.

Pflaum, J. C., and H. R. Pruppacher, 1979: A wind tunnel investigation of the growth of graupel initiated from frozen drops. J. Atmos. Sci., 36, 680-688.

Pitter, R. L, and H. R. Pruppacher, 1973: A wind tunnel investigation of freezing of small drops falling at terminal velocity in air. Quart. J. Roy. Meteor. Soc., 99, 540-555.

Pope, A., 1954: Wind-Tunnel Testing. New York: John Wiley & Sons.

Pope, A., and J. J. Harper, 1966: Low Speed Wind Tunnel Testing. New York: John Wiley & Sons, Inc.

Pruppacher, H. R. and J. D. Klett, 1978: Microphysics of Clouds and Precipitation. D. Reidel Publ. Co., Boston, 714 pp.

Pruppacher, H. R., and M. Neiburger, 1968: The UCLA cloud tunnel. Proc. Intl. Conf. Cloud Physics, Toronto. 389-392.

Pruppacher, H. R., and K. V. Beard, 1975: A wind tunnel investigation of the internal circulation and shape of water drops falling at terminal velocity in air. Quart. J. Roy. Meteor. Soc., 96, 247-256.

Pruppacher, H. T., and R. Rasmussen, 1979: A wind tunnel investigation of the rate of evaporation of large water drops falling at terminal velocity in air. J. Atmos. Sci., 36, 1255-1260.

Ryde, J. W., 1946: The attenuation and radar echoes produced at centimeter wavelengths by various meteorological phenomena. Meteorlogical Factors in Radio Wave Propagation, Physical Society, London, 169-188.

Savage, R. C., 1982: Melting of natural ice crystals in a vertical wind tunnel. Master Thesis, University of Utah.

Telford, J. W., N. S. Thorndike, and E. G. Bowen, 1955: The coalescence between small water drops. Quart. J. Roy. Meteor. Soc., 81, 241 - 250.

Zikmunda, J., and G. Vali, 1972: Fall patterns and fall velocities of rimed ice crystals. J. Atmos. Sci., 29, 1334 - 1335.